AWARD NUMBER: W81XWH-16-1-0057

TITLE: Regulation of Programmed Necrosis and Bone Marrow Failure

PRINCIPAL INVESTIGATOR: Sandra Zinkel

CONTRACTING ORGANIZATION: Vanderbilt University Medical Center
Nashville, TN 37203

REPORT DATE: JUNE 2018

TYPE OF REPORT: FINAL

PREPARED FOR: U.S. Army Medical Research and Materiel Command
Fort Detrick, Maryland 21702-5012

REPORT DOCUMENTATION PAGE

Form Approved
OMB No. 0704-0188

1. REPORT DATE	2. REPORT TYPE	3. DATES COVERED
JUNE 2018	FINAL	03/01/2016–02/28/2018

4. TITLE AND SUBTITLE
Regulation of Programmed Necrosis and Bone Marrow Failure

5a. CONTRACT NUMBER
W81XWH–16–1–0057

5b. GRANT NUMBER
BM150095

5c. PROGRAM ELEMENT NUMBER

6. AUTHOR(S)
Sandra S. Zinkel

E-Mail:Sandra.zinkel@vanderbilt.edu

5d. PROJECT NUMBER
0010804027

5e. TASK NUMBER

5f. WORK UNIT NUMBER

7. PERFORMING ORGANIZATION NAME(S) AND ADDRESS(ES)

Vanderbilt University Medical
Center
3319 West End Ave., STE 970
Nashville, TN 37203

8. PERFORMING ORGANIZATION REPORT NUMBER

9. SPONSORING / MONITORING AGENCY NAME(S) AND ADDRESS(ES)

U.S. Army Medical Research and Materiel Command
Fort Detrick, Maryland 21702-5012

10. SPONSOR/MONITOR'S ACRONYM(S)

11. SPONSOR/MONITOR'S REPORT NUMBER(S)

12. DISTRIBUTION / AVAILABILITY STATEMENT

Approved for Public Release; Distribution Unlimited

13. SUPPLEMENTARY NOTES

14. ABSTRACT

Blood cell production is a highly dynamic process, designed to respond to stresses such as infection or bleeding over the entire lifespan of a person or animal. During normal conditions, there is a careful balance between blood cells made and blood cells removed due to aging or damage. A highly regulated process called programmed cell death removes cells, and bone marrow failure occurs when more cells are removed than can be replaced. There are two major pathways of programmed cell death: apoptosis and necrosis. Simply described, apoptotic cells implode in an immune silent process, and necrotic cells explode, activating an inflammatory response. In bone marrow failure disorders, necrotic death of bone marrow cells increases normal bone marrow damage by amplifying the pathological inflammatory response. We hypothesize that increased necrotic cell death initiates a feed forward inflammatory process that kills normal bone marrow, and that targeting this programmed necrotic cell death could be used for therapeutic benefit. This proposal is focused on 1) determining how necrotic cell death impacts the surrounding normal bone marrow, and 2) determining whether inhibiting necrosis can rescue bone marrow failure in mouse models of MDS.

15. SUBJECT TERMS

Nothing listed

16. SECURITY CLASSIFICATION OF:			17. LIMITATION OF ABSTRACT	18. NUMBER OF PAGES	19a. NAME OF RESPONSIBLE PERSON
a. REPORT	b. ABSTRACT	c. THIS PAGE			USAMRMC
Unclassified	Unclassified	Unclassified	Unclassified	74	19b. TELEPHONE NUMBER *(include area code)*

Progress report CDMRP Idea Award

Table of Contents

1. **Introduction**----------1
2. **Keywords**---------- 2
3. **Accomplishments**----------2
4. **Summary and Impact**----------5
5. **Changes/problems**----------6
6. **Products**----------6
7. **Participants and other collaborating organizations**----------7
8. **Special reporting requirements**----------8
9. **Appendices**----------8

1. Introduction

Normal bone marrow function requires stringent control of production of new cells (proliferation) and removal of aging or damaged cells (programmed cell death). Patients with bone marrow failure disorders such as Myelodysplastic syndrome (MDS) have increased bone marrow programmed cell death, and increased levels of death-inducing cytokines such as TNFα. Discoveries in the last several years have demonstrated that in addition to apoptosis, TNFα also activates a novel form of cell death, programmed necrosis. Apoptotic cells implode in caspase-driven and immune silent process, whereas necrotic cells explode in a Rip kinase-driven process, releasing cellular contents (DAMPS) and eliciting an immune response. We find increased Rip1 kinase expression in 70% of MDS patient samples tested suggesting that necroptosis is activated in MDS. We also find that bone marrow from mouse models harboring known genetic mutations found in MDS (Asxl1-/-, Asxl1-/-Tet2-/-) display increased Rip1 kinase, suggesting that MDS genetic/epigenetic alterations result in increased necroptosis signaling that contributes to bone marrow cell death.

Substantial data demonstrate that MDS is a clonal stem cell disorder(Graubert et al., 2012; Walter et al., 2011; Walter et al., 2012; Walter et al., 2013). Recent data has also identified a rare population of bone marrow cells as the MDS-propagating population in patients with low to intermediate-risk MDS, and these MDS-propagating cells are expanded, representing 94% of the total HSC pool (Woll et al., 2014). A paradox inherent in MDS is that although the MDS-propagating clone has increased competitive ability, its expansion ultimately results in bone marrow failure. The presence of MDS stem cells and dying progenitor cells confers decreased function to the coexisting normal stem cells, suggesting that MDS stem and progenitor cells create a bone marrow environment that is killing normal hematopoietic stem cells. In our mouse model with unrestrained hematopoietic necrosis, mice die of bone marrow failure with the majority of the features of human MDS. Furthermore, bone marrow from these mice displayed increased competitive repopulating ability against wild type bone marrow. Transplanted mice die of bone marrow failure at four months despite the persistence of wild type bone marrow, suggesting that these necrotic HSC and progenitor cells can kill wild type HSCs to cause bone marrow failure. Our mice thus shed light on how an MDS clone can cause bone marrow failure:

Our overarching hypothesis is that programmed necrosis in MDS cells triggers an inflammatory response that kills normal hematopoietic stem cells. This in term enables mutant stem and progenitor cells to expand and take over the bone marrow, thus driving bone marrow failure. Interrupting the cell death signaling pathway or altering the inflammatory signaling pathway has

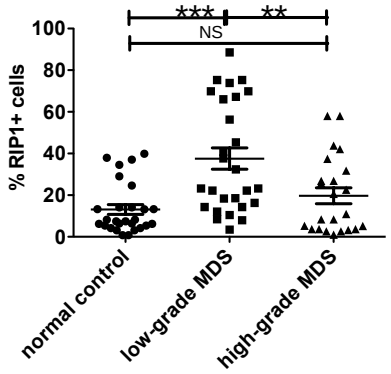

Figure 1: *Human MDS patient bone marrow samples display increased RipK1 staining relative to normal control bone marrow.*
FFPE sections from 37 de novo MDS cases and 36 normal control cases were stained with antibodies to Ripk1 and pMLKL as necroptosis markers and cleaved Caspase 3 as an apoptosis marker.
The MDS specimens included 20 cases of lower-grade MDS and 17 cases of higher-grade MDS. All cases were reviewed, and the diagnosis confirmed by board-certified hematopathologist.
Whole slide images were obtained using Aperio Versa 200 (Leica Microsystems). We developed a pipeline for statistical analysis to evaluate the immunofluorescence of stained and scanned images using CellProfiler (Broad Institute) image analysis software. For each data point, (slide) over 10,000 cells were analyzed.

the potential to prevent cell death and re-establish bone marrow homeostasis for therapeutic benefit.

Study design: we propose to use mouse models of both genetic mutations found in MDS and unrestrained necroptosis to characterize the death and inflammatory pathways, cytokines elicited by necrotic cell death, and dynamics of cell proliferation in HSC and progenitor populations using multiplex cytokine arrays and intracellular flow cytometry. We will then inhibit key pathways to determine the impact on hematopoietic homeostasis and determine whether we can prevent bone marrow failure.

Impact: The goal is to identify how HSCs and progenitor cells harboring MDS mutations execute cell death, and how they kill normal HSCs, and determine whether interrupting this cell death can rescue bone marrow function. As most MDS patients die of cytopenias, this therapy, if successful, will directly address the major morbidity of this disease through targeted therapeutic treatments. We acknowledge that one potential side effect of our strategy, may be accelerated transformation to leukemia, thus we will initially test our hypotheses in mouse models. However, we postulate that expansion of the MDS clone potentiates the acquisition of additional mutations that allow progression to AML, and that intervening in the signaling that expands this clone may actually increase the latency to transformation.

2. Keywords

Programmed cell death, hematopoiesis, hematopoietic stem cell, inflammation, bone marrow failure, Myelodysplastic syndrome, necroptosis, apoptosis, electron microscopy, RipK1 kinase

3. Accomplishments

The accomplishments for the first year of this grant are outlined below and in the attached manuscript that has been submitted to *Blood.* We have revised the manuscript to address all reviewer concerns and are ready to resubmit it for consideration for publication.
Goals:

1. Obtain regulatory approval- completed
2. Define cell death signaling of HSC and progenitor cells
3. Determine how cells die in competitive repopulation
4. Determine cytokine profile of bone marrow
5. Determine the effects of pharmacologic inhibition
6. Determine the effect of inhibition of inflammation on competitive repopulation
7. Determine the effects of inhibition of inflammation on cytokine production

Major activities:

The major activity has been characterization of the mouse models outlined in the original proposal

Specific objectives:

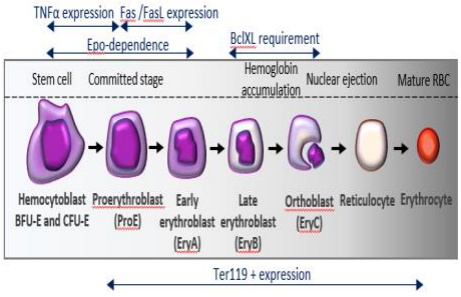

Figure 2: Schematic of erythropoiesis. Erythropoietin responsive early erythroid progenitor cell numbers are responsive to TNFα and Fas death receptor signaling

Aim 1: Define cell signaling of HSC and progenitor cells in mouse models of unrestrained cell death

Characterize cell death in mouse models of unrestrained necrosis

We have created a mouse model in which we have activated necrosis signaling in the hematopoietic system. Deletion of the pro-apoptotic Bcl-2 family members, *Bax* and *Bak* inhibits bone marrow programmed cell death (PCD). Further deletion of the BH3-only member Bid, to generate *BaxBakBid* TKO mice, leads to unrestrained bone marrow necroptosis.

During the initial funding period of the CDMRP award, we have characterized the cell death signaling and cytokine production in hematopoietic stem and progenitor cells in normal and *BaxBakBid TKO* (TKO) mice. (Aim 1, task 1-4) We find that the hematopoietic stem cells in TKO mice are expanded, and display increased proliferation, consistent with resistance to cell death despite increased necroptosis signaling. In contrast, hematopoietic progenitor cells display dramatically reduced cell numbers and reduced proliferation, consistent with increased cell death (attached manuscript, figures 4A-E). Immunofluorescence of bone marrow from TKO mice displays increased Rip1 staining, but no increased activated Caspase 3 staining, consistent with increased programmed necroptosis and inconsistent with apoptosis (attached manuscript, figures 2E-G). Of note, in a parallel study in human MDS patient samples (funded from an independent agency (VA MERIT award), and not funded by this DOD award), we have demonstrated increased RipK1 and not increased cleaved Caspase 3 staining. Transmission Electron Microscopy of bone marrow as well as myeloid progenitor cells from TKO mice displays increased necrosis morphology (attached manuscript, (Figures 2A, C and 3B, respectively). We then performed primary and secondary competitive repopulation experiments of wild type and TKO bone marrow. Consistent with protection of HSCs from cell death, TKO mice display increased competitive repopulating ability in primary transplants (attached manuscript, Figures 5 A). However, transplanted TKO mice develop progressive cytopenias and bone marrow failure (attached manuscript, Figures 5B-D). Consistent with the progressive cytopenias observed in primary transplants, TKO bone marrow fails to repopulate in secondary transplantation experiments (attached manuscript, Figure 5G). These results are consistent with a model in which increased necroptotic cell death in progenitor cells results in an inflammatory microenvironment. The initial response of the bone marrow is increased proliferation of HSCs. Ultimately, the increased proliferation and inflammatory microenvironment result in Hematopoietic stem cell exhaustion with failure to reconstitute in secondary transplantation.

As programmed necrosis results in release of DAMPS that create an inflammatory microenvironment, we hypothesized that our TKO bone marrow would display increased cytokine production. We therefore proceeded to

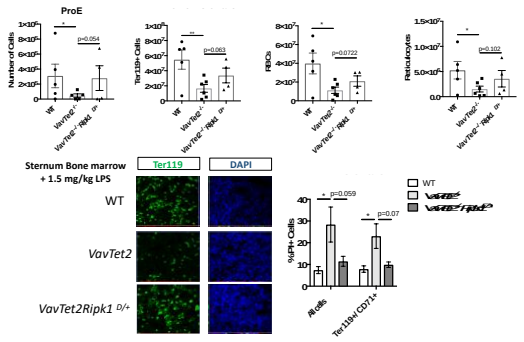

Figure 4: VavTet2 mouse bone marrow erythroid progenitors are highly sensitive to LPS-mediated inflammation. Loss of RIPK1 kinase activity can improve erythroid numbers.

evaluate cytokine production in wild type and TKO LSK and progenitor cells by intracellular cytokine staining. We find that TKO LSK but not progenitor cells display increased TNF alpha and IL-6 production. Both TKO LSK and Progenitor cells display increased IL1-beta production (Attached manuscript, figure 6A-C).

Aim 2: Determine whether inhibiting inflammatory signaling or necrosis signaling can reset hematopoiesis and prevent bone marrow failure

We have demonstrated that our mouse model in which we activated necrosis signaling in the bone marrow develops bone marrow failure that results from altered hematopoietic homeostasis with increased progenitor cell death, resulting in HSC exhaustion. We further demonstrate increased cytokine production in the bone marrow of these mice. We hypothesized that normal bone marrow homeostasis and normal hematopoiesis may be restored by either inhibiting programmed necrosis, or by inhibiting the inflammatory response.
Bone marrow failure disorders such as MDS as well as aplastic anemia display increased TNF alpha production. To inhibit the excess TNFα observed in our mice, we treated TKO mice with Enbrel. We are able to partially restore myeloid progenitor cell numbers and proliferation in our TKO mice and partially restore peripheral blood. To inhibit programmed necrosis, we undertook to approaches: pharmacologic inhibition with an inhibitor of RipK1 kinase (7N-1), and genetic inhibition by crossing our mice with a mouse expressing a kinase inactive form of RIPK1.
We found that the pharmacologic inhibition of RipK1 was complicated by toxicity. Despite careful titration of 7N-1, we were not able to arrive at a therapeutic dose (data not shown but available upon request). Genetic inhibition of RipK1 required a complicated cross (5 alleles) and was time intensive. However, we were able to demonstrate a complete rescue of normal peripheral blood counts in TKO mice with 1 allele of kinase inactive RipK1 (Attached manuscript, Figure 4I). Furthermore, we were able to partially rescue normal myeloid progenitor cell numbers (Attached manuscript, Figure 4 G, H). As we completely rescued peripheral blood counts, with only partial rescue of progenitor cell numbers. As erythropoiesis is known to be regulated by programmed cell death (Figure 2) we further investigated erythrocyte precursors. We were able to fully rescue erythroid progenitor cell numbers. TKO mice develop extramedullary hematopoiesis with a markedly increased spleen size. We were able to prevent the development of splenomegaly and extramedullary hematopoiesis in TKO mice with one allele of kinase inactive RipK1. We have hypothesized that the increased inflammatory cytokines noted in TKO mice were a result of necroptotic cell death. We therefore predict that inhibition of necroptosis will prevent cytokine production. We are able to prevent TNF alpha and IL-1 beta production in TKO bone marrow with one allele of kinase in active RipK1 (Figure 6 D, E). Our TKO mice with increased necroptosis closely resemble human MDS, and we have demonstrated increased necroptosis signaling in human MDS patient samples.

VavTet2 sternum bone marrow has increased TNFα staining and decreased Ter119+ staining. Ter119+ and TNF+Ter119+ cells are restored upon crossing to Rip1-kinase dead mice

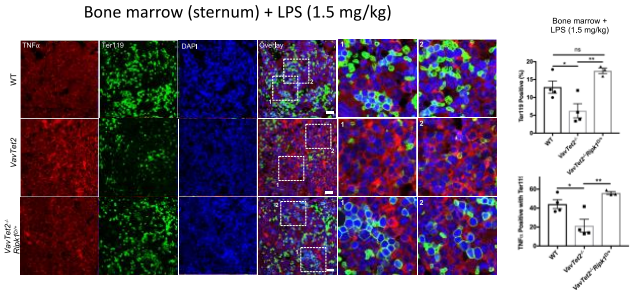

Figure 5: Loss of RIPK1 kinase function improves erythropoiesis and inhibits TNFα in *VavTet2F/F* bone marrow following LPS.

Next generation sequencing efforts have identified recurrent mutations in MDS, including Asxl1 and Tet2. Despite the

identification of these mutations, the mechanism whereby these mutations result in bone marrow failure has not been identified. We have obtained mice harboring these mutations and crossed them with kinase inactive RipK1. We find that *VavTet2F/F* erythroid precursors are sensitive to LPS treatment. Loss of 1 allele of RIPK1 or loss of the kinase function of RIPK1 improves erythroid progenitor cell numbers (Figure 4). We further evaluated the impact of genetically inhibiting RIPK1 on cytokine production in *VavTet2F/F* bone marrow. We find that VavTet2F/F bone marrow displays increased TNFα and decreased Ter119+ cells following LPS. Loss of RIPK1 kinase function restores Ter119+ cells. A manuscript reporting these results has been submitted and is now being revised.
The experiments investigating the impact of necroptosis on hematopoiesis in our TKO mice was published in *Blood* (manuscript attached). The manuscript was featured as a plenary paper, and our immunofluorescence image of pMLKL staining in human MDS was the cover image for *Blood.*

Opportunities for training and professional development

The above work has provided the opportunity for training in hematopoiesis for a graduate student and research associate in my laboratory.

Dissemination to communities of interest

I had the opportunity to present this work at the Edward P Evans Foundation symposium in 2016, comprised of investigators involved in investigation related to MDS.
In addition, I have presented this work at the Gordon Conference for Programmed cell death in 2016. I was an invited speaker and presented this work at the VA-sponsored symposium on inflammation and cancer in honor of Dr. Ann Richmond this fall at Vanderbilt University. I presented the work on necroptosis in erythropoiesis in our *TKO* mice modeling unrestrained necroptosis and *VavTet2* mice at the TNF meeting in 2019 as well as the Gordon conference for Programmed Cell Death in 2019.

Goals Accomplished

The experiments investigating the impact of necroptosis on hematopoiesis in our TKO mice was published in *Blood* (manuscript attached). The manuscript was featured as a plenary paper, and our immunofluorescence image of pMLKL staining in human MDS was the cover image for *Blood.* We continued the analysis of mouse models of MDS mutations. We completed the initial analysis on the role of necroptosis in erythropoiesis in our mouse model of unrestrained necroptosis as well as our mouse models harboring MDS mutations (*VavTet2)* during the period of this grant. We were able to leverage these initial results to apply for funding from the NHLBI and VA MERIT review. We have now submitted a manuscript for publication and are currently completing the substantial revisions requested by reviewers.

4. Summary and impact:

Hematopoiesis is a dynamic system that requires careful balance between cell division, differentiation, and cell death. The two major modes of programmed cell death (PCD), apoptosis and recently recognized necroptosis, share molecular machinery, but diverge in outcome with important implications for the microenvironment: apoptotic cells implode and are removed in an immune silent process, whereas necroptotic cells leak cellular contents that incite inflammation. Given the importance of cytokine directed cues for hematopoietic cell survival and differentiation, the potential impact of biasing cell death fate to necroptosis on hematopoietic

homeostasis is substantial and poorly understood. Here we present a mouse model with increased bone marrow necroptosis: deletion of the pro-apoptotic Bcl-2 family members, Bax and Bak inhibits bone marrow PCD, further deletion of the BH3-only member Bid, to generate BaxBakBid TKO mice, leads to unrestrained bone marrow necroptosis. TKO mice display loss of progenitor cells leading to increased stem cell proliferation and stem cell exhaustion, and increased cytokine production, culminating in bone marrow failure (BMF). Importantly, genetic inactivation of Rip1 kinase restores normal cytokine production, normal hematopoiesis, and normal erythropoiesis in TKO mice as well as mice harboring deletion of the MDS-associated gene*Tet2.* To our knowledge, this is the first demonstration of rescue of hematopoiesis by a defined genetic pathway in a mouse model of MDS. TKO bone marrow is hyper cellular with abnormal differentiation, resembling the human disorder Myelodysplastic syndrome (MDS), and we demonstrate increased necroptosis in MDS bone marrow. Finally, we show that Bid impacts necroptotic signaling through modulation of Caspase-8-mediated Rip1 degradation. We thus demonstrate that dysregulated necroptosis in hematopoiesis promotes bone marrow progenitor cell death that incites inflammation, impairs hematopoietic stem cells, and recapitulates the salient features of the bone marrow failure disorder, MDS.
We have accomplished the first step on the way to our goal to provide proof of concept that necrosis and/or inflammatory signaling can be targeted for therapeutic benefit in bone marrow failure syndromes such as MDS with the long-term goal of improving patients cytopenias and preventing disease progression to benefit MDS patients.

5. Changes/problems

As noted above, despite a careful titration, we were unable to rescue hematopoiesis using the Rip1 kinase inhibitor 7N-1. We have therefore proceeded to cross our mice to the Rip1 kinase inactive knock in mice developed by Michelle Kelliher as well as GSK with promising results. We would note that the cross involved 5 alleles to inactivate Rip1 kinase in our mouse model of increased necroptosis, resulting in some significant delay and additional expenditures on mouse costs. We do feel that this has been a highly productive cross that has given significant insight into bone marrow failure regulated by necroptosis as well as mouse models of MDS as evidenced by the publication of our initial work as a plenary paper.
In addition, we uncovered an unanticipated finding in erythropoiesis that is highly relevant to MDS as a number of the major morbidities of this disease are due to anemia. Furthermore, understanding the cell death pathways that drive anemia will be highly relevant to a number of other disorders that are prevalent in older individuals.

Changes to the use or care of animals, biohazards

None

Changes to care of human subjects

N/A

6. Products

Journal publications:
Plenary paper in *Blood* (manuscript attached).
Manuscript in progress on the role of necroptosis in erythropoiesis in mouse models of unrestrained necroptosis as well as mouse models harboring MDS mutations (*VavTet2).*

Presentations

2016	Invited Speaker: Gordon Research Conference. New concepts in Cell Death research: From Basic Mechanisms to Clinical Opportunities (Girona, Spain)
2016	Invited speaker, Edward P Evans Foundation Symposium Necrosis regulation of bone marrow function (Nashville, TN)
2017	Invited speaker: Center for Mitochondrial and Epigenomic Medicine Full length Bid maintains mitochondrial cristae structure and function – Integrating a gene-based PheWAS (PrediXcan) approach and mouse models to probe roles in human disease (Philadelphia, PA)
2017	Invited Speaker: Third National Veterans Health Affairs Research Conference: Cancer Immunotherapy: Advances and Challenges Necrosis regulation of bone marrow function (Nashville, TN)
2019	Platform presentation: TNF Meeting (Monterey, CA) RIPK1 dependent necroptosis drives bone marrow failure and anemia
2019	Platform presentation, CSHL meeting on Programmed Cell Death (CSHL, NY) RIPK1 dependent necroptosis drives bone marrow failure and anemia
2019	American Society of Hematology Myeloid Workshop Orlando FLA.

Technology or Techniques

None

Inventions, patent applications, and/or licenses

Invention disclosure (VU20042) Targeting the necroptosis pathway in anemias and other hematologic disorders.

Other products

None

7. Participants and other collaborating organizations

NAME	SANDRA ZINKEL	QIONG SHI	YULIYA HASSAN
PROJECT ROLE	**PI**	**Senior research scientist**	**Research Assistant II**
RESEARCH IDENTIFIER			
NEAREST PERSON MONTHS WORKED	**1.8**	**4**	**2.4**

CONTRIBUTION TO PROJECT	**Dr. Zinkel designs experiments, oversees execution of experiments, analyzes data and writes papers**	**Qiong Shi executes experiments with minimal supervision. She participated in the analysis of TKO mice**	**Yuliya Hassan maintains the mouse colony, manages animal husbandry, genotypes animals and performs analysis of mouse models**
FUNDING SUPPORT	**DOD, VA MERIT**	**DOD, VA MERIT**	**DOD, VA MERIT**

There has been no change in active support of the above individuals since the original reporting period

Other organizations involved as partners

None

8.Special reporting requirements:

None

9.Appendices

Manuscript published in *Blood.* This paper was featured as a plenary paper.

https://doi.org/10.1182/blood-2018-05-847335

Figure 5: Cover image. pMLKL staining of human MDS from Wagner et al.

Increased Ripk1-mediated bone marrow necroptosis leads to myelodysplasia and bone marrow failure in mice

Running Title: Bid restrains necroptosis to preserve HSPC function

Patrice N. Wagner[1], Qiong Shi[2], Christi T. Salisbury-Ruf[1], Jing Zou[2], Michael R. Savona[2], Yuri Fedoriw[3], Sandra S. Zinkel[1, 2*]
[1] Department of Cell and Developmental Biology, Vanderbilt University, 2220 Pierce Avenue, Nashville, TN 37232
[2] Department of Medicine, Vanderbilt University School of Medicine, 2220 Pierce Avenue, Nashville, TN 37232
[3] Department of Pathology and Laboratory Medicine, University of North Carolina School of Medicine, CB #7290 715 Mary Ellen Jones Bldg., Chapel Hill, NC 27599
*Correspondence: sandra.zinkel@vanderbilt.edu

Sandra S. Zinkel
Mailing Address: 2220 Pierce Avenue
548 Preston Research Building
Nashville, TN 37232

Fax Number: (615) 936-3857
Telephone number: (615) 936-1801
Email: Sandra.Zinkel@Vanderbilt.edu

Abstract Word Count: 249

Text Word Count: 3950

Number of Figures: 7

Number of References: 36

Scientific Category

Hematopoiesis and stem cells

Key Points: Unrestrained bone marrow necroptosis promotes inflammatory cytokine production that impairs HSPC function.
A new role for a recognized pro-apoptotic protein in programmed cell death fate linking hematopoietic necroptosis to bone marrow failure.

Abstract

Hematopoiesis is a dynamic system that requires balanced cell division, differentiation, and death. The two major modes of programmed cell death (PCD), apoptosis and necroptosis, share molecular machinery, but diverge in outcome with important implications for the microenvironment: apoptotic cells are removed in an immune silent process, whereas necroptotic cells leak cellular contents that incite inflammation. Given the importance of cytokine directed cues for hematopoietic cell survival and differentiation, the impact on hematopoietic homeostasis of biasing cell death fate to necroptosis is substantial and poorly understood. Here we present a mouse model with increased bone marrow necroptosis. Deletion of the pro-apoptotic Bcl-2 family members Bax and Bak inhibits bone marrow apoptosis. Further deletion of the BH3-only member Bid, to generate *VavCreBaxBakBid* TKO mice, leads to unrestrained bone marrow necroptosis driven by increased Rip1 kinase (Ripk1). TKO mice display loss of progenitor cells leading to increased cytokine production and increased stem cell proliferation and exhaustion, culminating in bone marrow failure (BMF). Genetically restoring Ripk1 to wild type levels restores peripheral red cell counts as well as normal cytokine production. TKO bone marrow is hyper cellular with abnormal differentiation, resembling the

human disorder Myelodysplastic syndrome (MDS), and we demonstrate increased necroptosis in MDS bone marrow. Finally, we show that Bid impacts necroptotic signaling through modulation of Caspase-8-mediated Ripk1 degradation. Thus, we demonstrate that dysregulated necroptosis in hematopoiesis promotes bone marrow progenitor cell death that incites inflammation, impairs hematopoietic stem cells, and recapitulates the salient features of the bone marrow failure disorder, MDS.

Manuscript in progress:

"RipK1-mediated inflammation impairs erythropoiesis in Tet2-loss: phenomics, human genetics and mice"

This work was initiated during the course of this award and the initial draft was completed subsequently. It is currently being revised for publication.

blood®
Plenary Paper

HEMATOPOIESIS AND STEM CELLS

Increased Ripk1-mediated bone marrow necroptosis leads to myelodysplasia and bone marrow failure in mice

Patrice N. Wagner,[1] Qiong Shi,[2] Christi T. Salisbury-Ruf,[1] Jing Zou,[2] Michael R. Savona,[2] Yuri Fedoriw,[3] and Sandra S. Zinkel[1,2]

[1]Department of Cell and Developmental Biology, Vanderbilt University, Nashville, TN; [2]Department of Medicine, Vanderbilt University Medical Center, Nashville, TN; and [3]Department of Pathology and Laboratory Medicine, University of North Carolina School of Medicine, Chapel Hill, NC

KEY POINTS

- **Unrestrained bone marrow necroptosis promotes inflammatory cytokine production that impairs HSPC function.**

Hematopoiesis is a dynamic system that requires balanced cell division, differentiation, and death. The 2 major modes of programmed cell death, apoptosis and necroptosis, share molecular machinery but diverge in outcome with important implications for the microenvironment; apoptotic cells are removed in an immune silent process, whereas necroptotic cells leak cellular contents that incite inflammation. Given the importance of cytokine-directed cues for hematopoietic cell survival and differentiation, the impact on hematopoietic homeostasis of biasing cell death fate to necroptosis is substantial and poorly understood. Here, we present a mouse model with increased bone marrow necroptosis. Deletion of the proapoptotic Bcl-2 family members Bax and Bak inhibits bone marrow apoptosis. Further deletion of the BH3-only member Bid (to generate *VavCreBaxBakBid* triple-knockout [TKO] mice) leads to unrestrained bone marrow necroptosis driven by increased Rip1 kinase (Ripk1). TKO mice display loss of progenitor cells, leading to increased cytokine production and increased stem cell proliferation and exhaustion and culminating in bone marrow failure. Genetically restoring Ripk1 to wild-type levels restores peripheral red cell counts as well as normal cytokine production. TKO bone marrow is hypercellular with abnormal differentiation, resembling the human disorder myelodysplastic syndrome (MDS), and we demonstrate increased necroptosis in MDS bone marrow. Finally, we show that Bid impacts necroptotic signaling through modulation of caspase-8–mediated Ripk1 degradation. Thus, we demonstrate that dysregulated necroptosis in hematopoiesis promotes bone marrow progenitor cell death that incites inflammation, impairs hematopoietic stem cells, and recapitulates the salient features of the bone marrow failure disorder MDS. (*Blood*. 2019;133(2):107-120)

Introduction

Programmed cell death (PCD) is required to maintain homeostasis in dynamic systems such as hematopoiesis. The two main forms of PCD, apoptosis and necroptosis, result in markedly different outcomes with important implications for the cellular microenvironment. Whereas apoptosis is predominantly immune silent, necroptosis promotes inflammation through release of endogenous molecules such as DNA or membrane lipids, known as damage-associated molecular patterns (DAMPS).[1]

The process of necroptosis has the potential to amplify both cell death and inflammation within the bone marrow. Hematopoietic and stromal cells can respond to necroptosis-released DAMPS to produce cytokines such as tumor necrosis factor α (TNF-α) that also act as death receptor ligands. In the bone marrow microenvironment, cytokines such as TNF-α provide cues to maintain homeostasis.[2-4] In addition, TNF-α as well as interferon can impair hematopoietic stem cell colony formation and the ability to sustain multilineage differentiation.[5] The impact of necroptotic cell death on hematopoietic homeostasis is therefore potentially substantial and not well understood.

Seminal results from genetic mouse models demonstrate that the upstream activators of apoptosis, Fas-associated protein with death domain (FADD) and caspase-8, act as key inhibitors of necroptotic cell death during embryonic development.[6-12] Situated at this central decision point of cell death fate, the Bcl-2 (B-cell lymphoma) family functions downstream of death receptor signaling before activation of executioner caspases. In particular, the BH3-only family member Bid acts as a sensor and amplifier of death receptor signaling. Upon activation of death receptors (TNF receptor [TNFR] and Fas), Bid is cleaved by caspase-8[13] and activates Bax/Bak to initiate the release of cytochrome *c* and the execution of apoptosis.[14] The interaction of Bid with caspase-8 and Bid's role in early activation of apoptosis are therefore well established. Bid has been shown to function in a prosurvival role, independent of apoptosis, in certain contexts,[15,16] raising the possibility that Bid's prosurvival function may extend to necroptosis.

We have developed a series of mouse models in which we alter the mechanism of cell death in hematopoiesis. Bone marrow in wild-type (WT) mice undergoes predominantly apoptotic cell

death. As necroptosis is known to occur in situations where apoptosis is inhibited,[17] we constructed a mouse in which intrinsic apoptosis is blocked in hematopoiesis: germline deletion of *Bak* and conditional deletion of *Bax* within the hematopoietic system with *VavCre* (DKO mice) completely blocks apoptotic cell death but is not sufficient to initiate necroptotic cell death. Further deletion of *Bid* (to create *BaxBakBid* triple-knockout [TKO] mice) leads to robust activation of necroptosis. While protection from programmed cell death leads to leukemia (double-knockout [DKO] mice), increased necroptotic cell death (TKO) leads to decreased survival due to bone marrow failure (BMF). Importantly, restoring WT levels of Ripk1 through genetic knockdown of 1 allele of *Ripk1* fully restores peripheral blood counts and substantially increases progenitor cell percentages and proliferation as measured by 5-bromo-2′-deoxyuridine (BrdU) incorporation, establishing that TKO BMF is driven by Ripk1.

As a consequence of necroptosis, TKO mice display increased bone marrow cytokine production. This cytokine production is significantly diminished by genetically restoring normal levels of Ripk1 in TKO mice. Furthermore, blocking TNF-α in TKO mice with the decoy TNFR etanercept (Enbrel) partially restores TKO progenitor cells, anemia, and thrombocytopenia. Lastly, in samples from patients with the BMF disorder myelodysplastic syndrome (MDS), we observe prominent Ripk1 and phospho-mixed lineage kinase domain-like pseudokinase (pMLKL) immunofluorescence staining and necroptotic morphology by electron microscopy. Thus, we propose that uncontrolled necroptosis-mediated cell death leads to BMF that is in part due to inflammation and resembles MDS.

Methods

Additional details are included in supplemental Methods (available on the *Blood* Web site).

Mice

VavCreBaxBak mice were developed by crossing $Bax^{F/F}$ $Bak^{-/-}$ mice with $VavCre^{+}$ mice. $VavCreBax^{F/F}Bak^{-/-}$ mice were further crossed to $Bid^{-/-}$ mice to generate $VavCre$ $Bax^{F/F}Bak^{-/-}Bid^{-/-}$ mice (TKO). *VavCreBaxBakBid* mice were also crossed with $Ripk1^{K45A}$ mice, which harbor *loxP* sites flanking exon 3 of *Ripk1* (from Peter Gough).[18] Mice were backcrossed 9 generations with C57BL/6J mice from The Jackson Laboratory.

Flow cytometry

Cells from peripheral blood and bone marrow were stained and analyzed on a BD LSR Fortessa according to previously described protocols.[16]

Immunoblotting and immunofluorescence

Formalin-fixed paraffin-embedded samples were stained and imaged on a Nikon AZ100 microscope, and images were captured using a Nikon DS-Ri1 color camera or a Zeiss Axioplan microscope using a Hamamatsu ORCA-ER monochrome digital camera. Details of the staining protocols and antibodies used can be found in supplemental Methods.

Competitive reconstitution

Lethally irradiated (900-cGy split dose) B6 CD45.1 mice were transplanted with a 1×10^6 bone marrow cells with a 1:1 ratio of test (CD45.2) to control (CD45.1) cells according to previously described protocols.[16] The Vanderbilt University Institutional Animal Care and Use Committee approved all experiments (M16000037).

Methylcellulose culture

Whole bone marrow from competitive reconstitution studies was isolated 3 months after reconstitution. Cells were stained with anti-CD45.1 and CD45.2 antibodies and sorted on a BD FACSAria III instrument. Cells were plated according to previously described protocols.[16] Colonies were counted 10 days after plating.

Results

VavCreBaxBakBid TKO mice die of BMF

To create a mouse model with increased bone marrow necroptosis, we first blocked intrinsic apoptotic execution in hematopoiesis by creating $VavCreBax^{F/F}Bak^{-/-}$ DKO mice (Figure 1A).[19] We then crossed DKO mice with mice harboring germline deletion of *Bid*,[20] resulting in $VavCreBax^{F/F}BakBid$ TKO mice. *VavCre* efficiently deletes *Bax* in the bone marrow and spleen of DKO and TKO mice (Figure 1B-C; supplemental Figure 1A).

DKO mice die predominantly of leukemia (89%) that can be transferred to recipient mice, with a median survival of 10 months, consistent with loss of mitochondrial-mediated death (Figure 1D-F).[21] In contrast, TKO mice develop significant cytopenias (Figure 1G); 66% die of BMF, and 22% die of leukemia (Figure 1D-E), with a median survival of 5.5 months. Morphologically, TKO marrow harbors dysplastic myeloid cells, including neutrophil hypersegmentation, megakaryocyte hypolobulation, and erythroid precursor binucleation and intrachromosomal bridging (Figure 1H).[22] Thus, hematopoietic loss of *Bax* and *Bak* prevents apoptosis and promotes leukemia. Further loss of *Bid* results in BMF.

TKO bone marrow displays necrotic morphology and increased Rip1 kinase

We examined cellular morphology, a defining feature of both apoptosis (eg, pyknotic nuclei, cell membrane and organelle shrinkage) and necroptosis (eg, membrane integrity loss, cell membrane and organelle swelling) by transmission electron microscopy (TEM). TKO bone marrow cells displayed significantly increased necrotic morphology compared with $Bid^{+/+}$ bone marrow cells (25% vs 7% [of 100 cells], respectively) (Figure 2A-B). Furthermore, cells undergoing necrotic death have recently been reported to display bubbles at the membrane by TEM as a consequence of phospho-MLKL (pMLKL) activation and translocation.[23] We observe an increase in the number of these bubbles in TKO bone marrow compared with $Bid^{+/+}$ marrow (Figure 2C-D), consistent with activated pMLKL.

Consistent with the observed cellular morphology, Ripk1 levels are increased in TKO bone marrow, but not $Bid^{+/+}$, $Bid^{-/-}$, or DKO bone marrow (Figure 2E). Minimal cleaved caspase-3 was observed in $Bid^{+/+}$, TKO (Figure 2F), $Bid^{-/-}$, and DKO bone marrow (supplemental Figure 2A). A strong cleaved caspase-3 signal was observed in $Bid^{+/+}$ Fas-treated livers, validating our antibody and staining technique (Figure 2G). Ripk1 staining of WT cells, but not $Ripk1^{-/-}$ 3T3 cells, validated specificity of Ripk1 staining (supplemental Figure 2B-C). Only in the context of transformation from BMF to leukemia do we observe decreased Ripk1 (supplemental Figure 2D). Overall, these results are consistent with

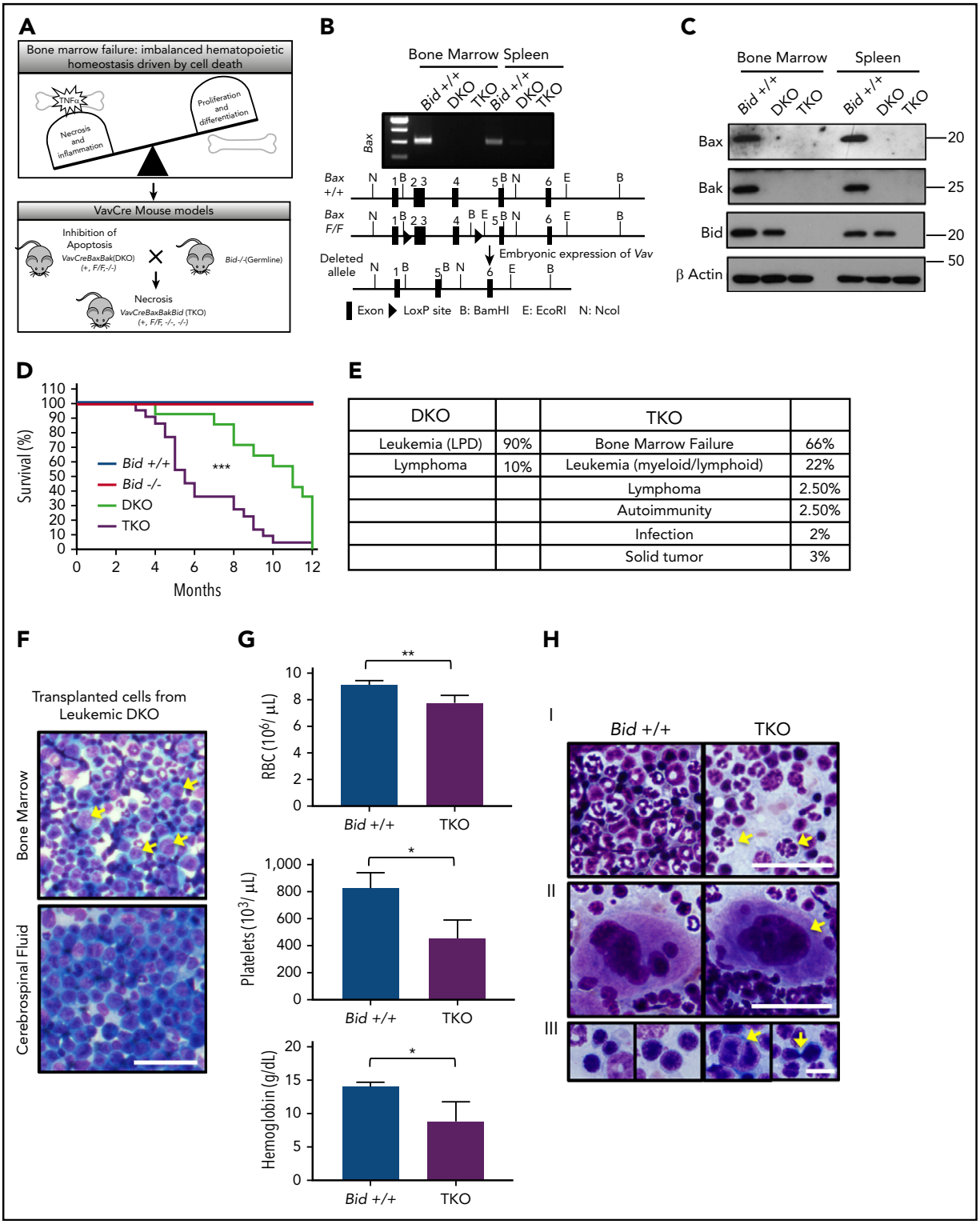

DKO		TKO	
Leukemia (LPD)	90%	Bone Marrow Failure	66%
Lymphoma	10%	Leukemia (myeloid/lymphoid)	22%
		Lymphoma	2.50%
		Autoimmunity	2.50%
		Infection	2%
		Solid tumor	3%

Figure 1. *VavCreBaxBakBid* TKO mice die of BMF. (A) Schematic of hematopoietic homeostasis and BMF and development of *VavCre* transgenic mouse models to study the role of cell death. (B) Deletion of *Bax* in bone marrow and spleen determined by reverse-transcription polymerase chain reaction (top), and diagram of highlighting Cre-Lox recombination with *loxP* sites flanking exons 2 to 4 of the *Bax* gene (bottom). (C) Immunoblot examining the expression of Bax, Bak, and Bid in WT ($Bid^{+/+}$), *VavCreBaxBak* (DKO), and *VavCreBaxBakBid* (TKO) mice. (D) Survival curves of $Bid^{+/+}$, $Bid^{-/-}$, DKO, and TKO mice. Statistics demonstrate differences between DKO and TKO animals. $Bid^{+/+}$ n = 4, $Bid^{-/-}$ n = 4, DKO n = 14, TKO n = 22. (E) Cause of death in DKO and TKO mice determined at time of necropsy. (F) Bone marrow and cerebrospinal fluid from $Bid^{+/+}$ mice transplanted with leukemic DKO bone marrow after sublethal irradiation. Arrows indicate leukemic blasts. Scale bar, 50 μm. (G) Complete blood counts, including RBCs (top; 10^6/μL), platelet counts (middle; 10^6/μL), and hemoglobin (bottom; g/dL); n = 3 and 4 $Bid^{+/+}$ and TKO mice, respectively. (H) Cytospins from bone marrow $Bid^{+/+}$ and TKO mouse bone marrow mice denoting neutrophils (I), megakaryocytes (II), and erythroid precursors (III). Arrows indicate hypersegmentation (I), hypolobulation (II), and binucleation and intrachromosomal bridging (III). Scale bars, 10 μm. *$P < .05$, ***$P < .001$. Data represent mean ± standard error of the mean (SEM). LDP, lymphoproliferative disorder.

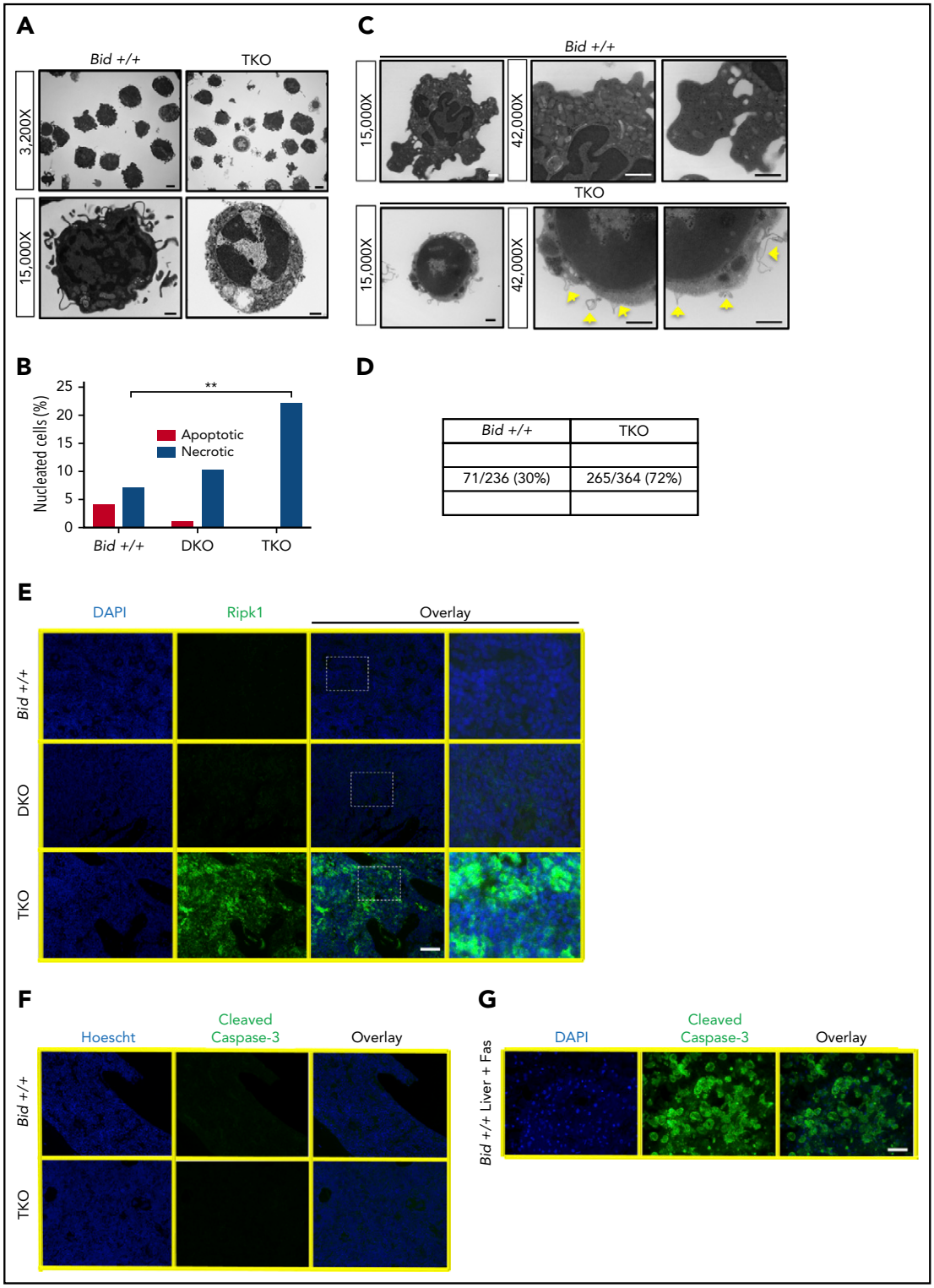

Figure 2. TKO bone marrow dies by necrosis. (A) Representative TEM images from *Bid*$^{+/+}$ and TKO mice (top: original magnification ×3200; scale bar, 2 μm; bottom: original magnification ×15 000; scale bar, 500 nm). (B) Quantitation of apoptotic and necrotic cells from *Bid*$^{+/+}$, DKO, and TKO TEM. A total of 100 cells with a nucleus from lower-magnification images were scored based on cell and organelle morphology (see supplemental Methods for quantitation details). (C) TEM images of bone marrow from *Bid*$^{+/+}$ and TKO mice analyzed for membrane bubble. Images of the whole cell are original magnification ×15 000, and zoomed images of the cell membrane are original magnification ×42 000 (scale bars, 500 nm). (D) Quantitation of the number of bubbles show in panel C. (E) Ripk1 fluorescent immunohistochemistry as a marker for necrotic cell death on paraffin-embedded bone marrow sections from *Bid*$^{+/+}$, DKO, and TKO mice. Staining was performed 3 independent times (scale bar, 50 μm). Zoomed-in images (250%) are of the indicated boxed area. (F) Fluorescent immunohistochemistry for cleaved caspase-3 as a marker of apoptotic cell death on *Bid*$^{+/+}$ and TKO bone marrow sections as in panel C. (G) Fluorescent immunohistochemistry for *Bid*$^{+/+}$ liver after tail vein injection with Fas ligand as a positive control for cleaved caspase-3 staining. $^{**}P < .01$. Data represent mean ± SEM. DAPI, 4′,6-diamidino-2-phenylindole.

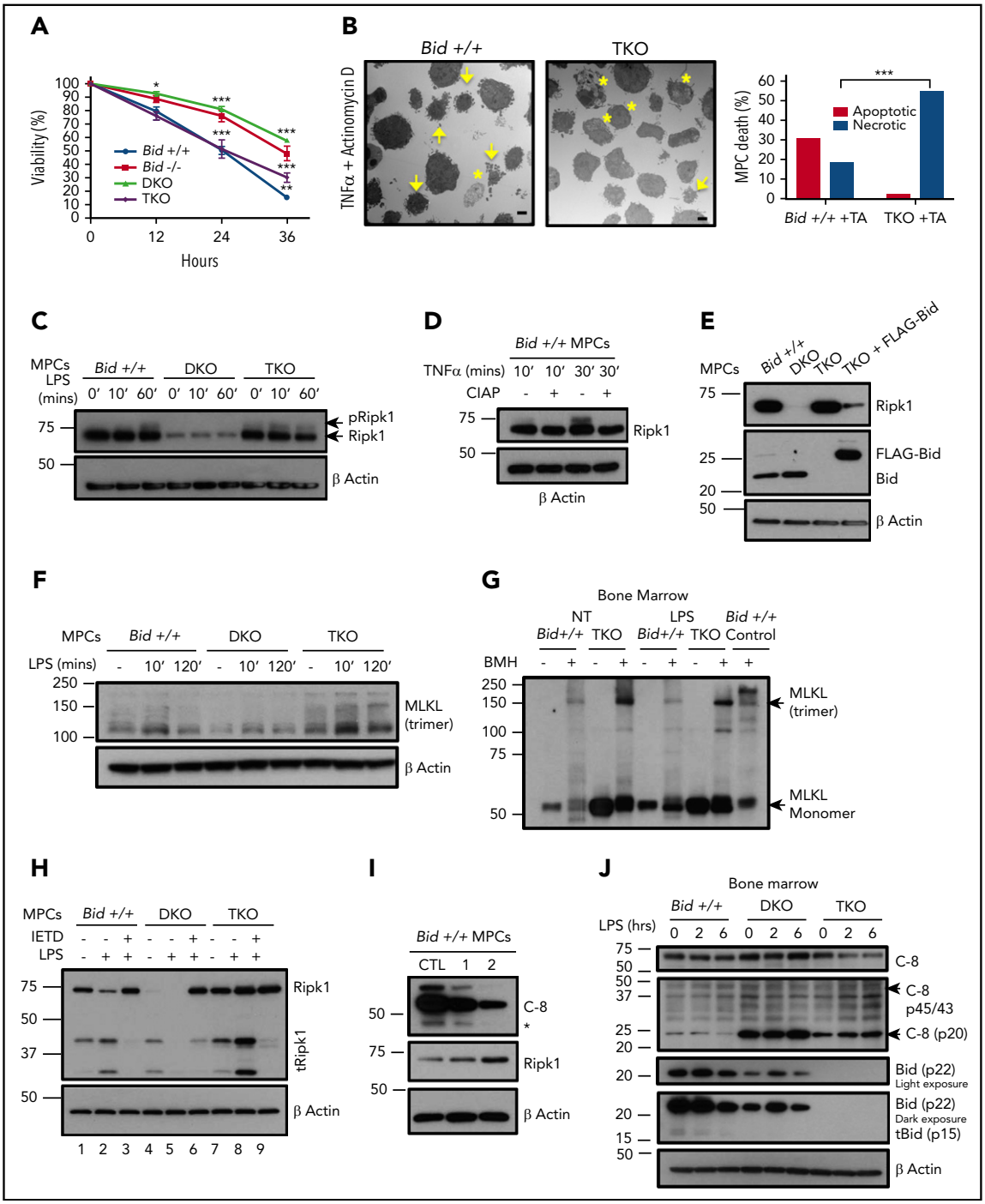

Figure 3. Bid modulates Ripk1 signaling in MPCs in a caspase-8–dependent manner. (A) Examination of death in MPCs. MPCs were treated with 25 ng/mL TNF-α + 50 ng/mL ActD. Viability was determined by Annexin V/propidium iodide staining. The experiment was performed three independent times. Statistics indicate differences between *Bid*$^{+/+}$ vs *Bid*$^{-/-}$, DKO, and TKO. (B) *Bid*$^{+/+}$ and TKO MPCs treated with TNF-α/ActD were examined by TEM. A total of 50 cells with a nucleus were examined and characterized as being apoptotic or necrotic. Arrows indicate apoptotic cells, and asterisks indicate necrotic cells (scale bars, 2 μm). Quantitation of cells is to the right of images. (C) MPCs unstimulated or stimulated with 250 ng/mL LPS for 10 minutes and 1 hour followed by immunoblot for Ripk1. pRipk1, phospho-Ripk1. The experiment was performed 4 times. (D) Immunoblot of *Bid*$^{+/+}$ MPCs treated with or without TNF-α in the presence or absence of calf intestinal alkaline phosphatase (CIAP). pRipk1 is lost in the presence of CIAP. (E) Immunoblot of Ripk1 in *Bid*$^{+/+}$, DKO, TKO, and TKO+ FLAG-Bid MPCs following LPS stimulation. The experiment was performed 2 independent times. (F) Immunoblot of MLKL trimerization in *Bid*$^{+/+}$, DKO, and TKO MPCs following stimulation with LPS. MLKL trimer is ~150 kDa. The experiment was performed 3 times. (G) Bone marrow from *Bid*$^{+/+}$ and TKO mice treated with or without LPS (250 ng/mL) for 4 hours followed by bismaleimidohexane (BMH) crosslinking and probed for MLKL. Control lane indicates *Bid*$^{+/+}$ bone marrow pretreated with zVAD (25 μM) followed by Smac mimetic (Birinapant [100 nM]) and TNF-α (25 ng/mL) for 4 hours as a positive control. The experiment was performed 2 independent times. NT, not treated. (H) Immunoblot of Ripk1 in *Bid*$^{+/+}$, DKO, and TKO MPCs following stimulation with 250 ng/mL LPS and pretreatment with 20 μM Z-IETD-FMK (an inhibitor of caspase-8). The experiment was performed 3 independent times. (I) Ripk1 levels by immunoblot after knockdown of caspase-8 utilizing the CRISPR-Cas9 system in *Bid*$^{+/+}$ MPCs. The experiment was performed 2 times. (J) Immunoblot of bone marrow from *Bid*$^{+/+}$, DKO, and TKO mice treated with LPS for the indicated times. The experiment was performed 3 independent times. $^{**}P < .01$, $^{***}P < .001$. Data represent mean ± SEM.

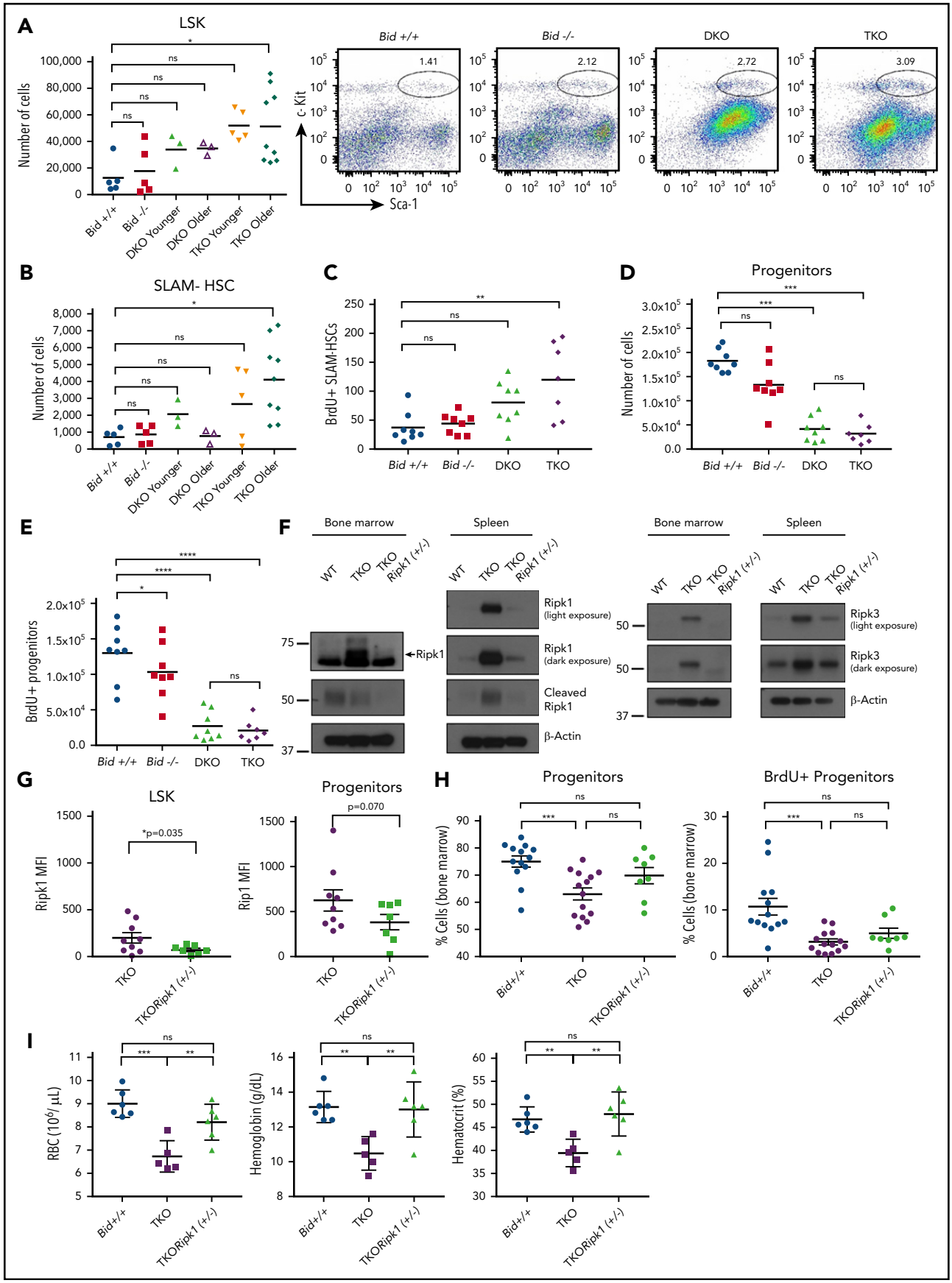

Figure 4.

abrogation of apoptosis in DKO bone marrow and increased necroptosis upon additional loss of *Bid* in TKO bone marrow under homeostatic conditions.

TKO myeloid progenitors die by necrosis

We next generated Hox11 immortalized myeloid progenitor cells (MPCs) from the bone marrow of $Bid^{+/+}$, DKO, and TKO mice.[15] We treated these MPCs with TNF-α plus actinomycin D (ActD) to activate TNFR cell death signaling. As expected, $Bid^{-/-}$ and DKO cells exhibited less death (by Annexin V^+/propidium $iodide^+$) in response to TNF-α/ActD.[24] TKO and $Bid^{+/+}$ cells display similar death kinetics (Figure 3A); however, $Bid^{+/+}$, but not TKO MPCs, displayed increased cleaved caspase-3 (supplemental Figure 3A). TEM of untreated MPCs reveals minimal cell death (supplemental Figure 3B). TEM of TNF-α/ActD-treated MPCs reveals predominantly apoptotic morphology in $Bid^{+/+}$ cells and predominantly necrotic cell morphology in TKO cells (Figure 3B). Canonical death receptor signaling is thus preserved in our MPCs. $Bid^{+/+}$ MPCs undergo apoptosis in response to TNF-α/ActD, and removal of *Bax* and *Bak* prevents cell death. Importantly, removal of *Bid* in addition to *Bax* and *Bak* results in necroptotic cell death, consistent with a novel role for Bid to restrain necroptosis.

TKO MPCs and bone marrow display increased necroptotic signaling

Phosphorylation of Ripk1 has been shown to stabilize its association with a pronecroptotic complex and activate necroptotic kinase activity.[25] TKO MPCs, but not $Bid^{+/+}$, $Bid^{-/-}$, or DKO MPCs, displayed constitutive and increased kinetics of Ripk1 phosphorylation manifested by a phosphatase-sensitive shifted band upon treatment with lipopolysaccharide (LPS)[26] or TNF-α (Figure 3C-D; supplemental Figure 3C-D). Furthermore, TKO bone marrow exhibits more total Ripk1 and phospho-Ripk1 (supplemental Figure 3D). Importantly, reintroduction of FLAG-tagged Bid into TKO MPCs by retroviral transduction results in decreased Ripk1 levels (Figure 3E), demonstrating that decreased Ripk1 observed in DKO MPCs is due to the presence of Bid.

In addition, TKO MPCs, but not $Bid^{+/+}$ or DKO MPCs, display increased MLKL trimerization with or without LPS stimulation (Figure 3F; supplemental Figure 3E).[27] Importantly, TKO bone marrow with and without LPS stimulation, displays increased MLKL monomers, trimers, and phospho-MLKL relative to $Bid^{+/+}$ bone marrow (Figure 3G; supplemental Figure 3F). These results suggest that loss of *Bid* in addition to *Bax* and *Bak* is sufficient to stimulate Ripk1 phosphorylation and MLKL trimerization, consistent with increased necroptotic signaling.

Bid regulates Ripk1 stability by modulating caspase-8 activity

The above studies reveal that Ripk1 levels vary markedly between genotypes, with decreased Ripk1 observed in DKO MPCs compared with both $Bid^{+/+}$ and TKO cells (Figure 3C).

Ripk1 can be cleaved by proteases such as caspase-8[28] and cathepsins[29] to generate truncated Ripk1 (tRipk1). Treatment with the caspase-8–specific inhibitor Z-IETD-FMK, but not MG132 (proteasome inhibitor) or Z-VAD-FMK (pan-caspase inhibitor), following LPS (Figure 3H; supplemental Figure 4A) completely recovered full-length Ripk1 in DKO MPCs and decreased tRipk1 in $Bid^{+/+}$ and TKO MPCs, indicating that a Z-IETD-FMK–inhibitable enzyme cleaves Ripk1. Similar recovery of a caspase-8 substrate, cylindromatosis, was also observed (supplemental Figure 4B). Furthermore, deletion of caspase-8 using CRISPR-Cas9 with 2 independent guide RNAs increased Ripk1 levels in $Bid^{+/+}$ MPCs proportional to the degree of caspase-8 knockdown (Figure 3I).

Treatment of $Bid^{+/+}$, DKO, and TKO bone marrow with LPS also revealed striking differences in caspase-8 levels. Both the p43/45 and p20 forms of active caspase-8 are elevated in DKO bone marrow. Despite this, only minimal cleaved Bid (tBid) can be observed in $Bid^{+/+}$, but not DKO, marrow (Figure 3J). This suggests that in the absence of Bax and Bak, caspase-8 preferentially cleaves Ripk1 over Bid. The above results are consistent with a role for caspase-8 in mediating Ripk1 levels.

Unrestrained bone marrow necroptosis disrupts hematopoietic homeostasis

To determine whether bone marrow necroptosis may impair hematopoietic homeostasis, we evaluated hematopoietic stem and progenitor cell (HSPC) populations. Immunophenotyping of HSPCs reveals that LSK ($Lin^-Sca1^+c\text{-}Kit^+$) cell populations are expanded in TKO mice, but not $Bid^{+/+}$, $Bid^{-/-}$, or DKO mice (Figure 4A). The signaling lymphocyte activating molecule hematopoietic stem cell (SLAM-HSC; LSK $Flt3^{Lo}CD48^-CD150^+$) population[30] continues to expand in TKO mice with age, whereas SLAM-HSC populations decline in aged DKO mice. Accordingly, TKO, but not DKO, SLAM-HSCs displayed increased numbers (Figure 4B; supplemental Figure 5A) as well as proliferation assessed by in vivo BrdU analysis (Figure 4C), consistent with an appropriate response to bone marrow stress. Long-term hematopoietic stem cell ($Lin^-Sca1^+c\text{-}Kit^+CD135^{Lo}$) populations were not significantly changed between genotypes (supplemental Figure 5B).

Figure 4. TKO mice have fewer myeloid progenitor cells and more hematopoietic stem cells (HSCs), which can be rescued with a genetic cross to *Ripk1*$^{(+/-)}$ heterozygous mice. (A) Flow cytometry analysis of bone marrow to examine LSK and (B) SLAM-HSC populations. Mice were examined before onset of sickness. Younger mice were 11 to 15 weeks old, and older mice were 15 to 20 weeks of age. $Bid^{+/+}$, n = 5; $Bid^{-/-}$, n = 5; DKO, n = 6; TKO younger, n = 5; and TKO older, n = 9. (C) Examination of the number of BrdU-positive SLAM-HSCs in bone marrow. Mice were injected with a total of 4 mg BrdU in 3 doses over 36 hours. Bone marrow was harvested, depleted for terminal lineages, and stained for flow cytometry. Mice were 18 to 20 weeks of age. (D) Numbers of myeloid progenitors ($Lin^-Sca\text{-}1^-c\text{-}Kit^+$) as in panel A. Mice were 18 to 20 weeks of age. (E) Number of BrdU-positive myeloid progenitors. Numbers of mice for panels C–E are as follows: $Bid^{+/+}$, n = 8; $Bid^{-/-}$, n = 7; DKO, n = 8; and TKO, n = 7. (F) Western blot of Ripk1, cleaved Ripk1, and Ripk3 expression in $Bid^{+/+}$, TKO, and TKO*Ripk1*$^{(+/-)}$ mouse bone marrow and spleen. (G) Intracellular flow cytometry analysis of LSK (left) and progenitor cell populations (right). TKO, n = 9; TKO*Ripk1*$^{(+/-)}$, n = 6 . (H) Percentage of MPCs from lineage-depleted bone marrow. $Bid^{+/+}$, n = 12; TKO, n = 14; and TKO*Ripk1*$^{(+/-)}$, n = 8. (I) Percentage of BrdU-positive myeloid progenitors from lineage-depleted bone marrow. $Bid^{+/+}$, n = 13; TKO, n = 15; and TKO*Ripk1*$^{(+/-)}$, n = 8. (I) RBCs ($10^6/\mu L$), hemoglobin (g/dL), and hematocrit (%) were measured in peripheral blood. $Bid^{+/+}$, n = 6; TKO, n = 6; and TKO*Ripk1*$^{(+/-)}$, n = 6. ns, not significant; $^*P < .05$, $^{**}P < .01$, $^{***}P < .001$, and $^{****}P < .0001$. Data represent mean ± SEM.

Given the apparent bone marrow stress observed in TKO SLAM-HSCs, we anticipated similar progenitor expansion. In contrast, we observed decreased TKO myeloid progenitor (Lin^- $Sca1^-c\text{-}Kit^+$) populations (Figure 4D) with decreased BrdU incorporation as compared with $Bid^{+/+}$ mice (Figure 4E), consistent with increased progenitor cell death with compensatory hematopoietic stem cell proliferation. Despite a similarly decreased progenitor cell population, DKO mice do not display increased SLAM-HSC proliferation (Figure 4B-C), suggesting a distinct defect in hematopoietic homeostasis in the setting of impaired apoptosis (DKO) vs increased necroptosis (TKO).

Consistent with the increased programmed cell death noted in myeloid cell lines, TKO mice, but not $Bid^{+/+}$, $Bid^{-/-}$, or DKO mice, display splenomegaly with increased $Ter119^+$ cells (erythroid), indicative of extramedullary hematopoiesis that is progressive with age (supplemental Figure 5C-D). Notably, B-cell and monocyte populations are not different between genotypes at necropsy, but DKO and TKO T-cell populations are expanded (supplemental Figure 5E).

Restoring normal Ripk1 levels rescues TKO red blood cells (RBCs) and bone marrow progenitors

To definitively establish whether the altered hematopoiesis observed in TKO mice was due to unrestrained necroptosis, we crossed *VavCre*TKO mice to mice in which exon 3 within the endogenous *Ripk1* gene locus is flanked by 2 *loxP* sites[18] to generate mice in which 1 allele of *Ripk1* was knocked out in hematopoietic tissues (TKO*Ripk1*$^{(+/-)}$) (supplemental Figure 6A-B). Deletion of 1 allele of *Ripk1* resulted in decreased Ripk1 and Ripk3 levels in TKO bone marrow and spleen, comparable to Ripk1and Ripk3 levels in $Bid^{+/+}$ mice (Figure 4F). Intracellular Ripk1 staining revealed increased Ripk1 expression at baseline in progenitor compared with LSK cells in TKO*Ripk1*$^{(+/-)}$ mice. Importantly, Ripk1 levels were decreased in TKO*Ripk1*$^{(+/-)}$ LSK and progenitor populations (Figure 4G; supplemental Figure 6C). Compared with TKO mice, TKO*Ripk1*$^{(+/-)}$ mice have a trend for increased total cell number in the marrow (supplemental Figure 6D), as well as increased progenitor cells and proliferation (Figure 4H). Strikingly, loss of 1 allele of *Ripk1* is sufficient to restore red cell peripheral counts, as indicated by the number of red blood cells, hemoglobin, and hematocrit (Figure 4I). Thus, we establish that increased Ripk1-mediated necroptosis drives the altered hematopoiesis observed in TKO mice.

TKO cells outcompete $Bid^{+/+}$ cells but fail to maintain hematopoiesis in competitive repopulation experiments

To evaluate TKO HSPC function, we performed a competitive repopulation of lethally irradiated congenic mice. Accordingly, we injected a 1:1 ratio of TKO ($Ly45.2^+$) to $Bid^{+/+}$ ($Ly45.1^+$) bone marrow into lethally irradiated $Bid^{+/+}$ (Ly5.1+) mice and evaluated peripheral blood for $Ly45.2^+$ and $Ly45.1^+$ mononuclear cells. Two additional cohorts of mice were examined in which a 1:1 ratio of $Bid^{+/+}$ ($Ly5.2^+$) or DKO ($Ly5.2^+$) to $Bid^{+/+}$ ($Ly5.1^+$) marrow was similarly transplanted. Both DKO and TKO bone marrow displayed increased repopulating ability relative to $Bid^{+/+}$ marrow (Figure 5A). However, peripheral blood counts reflected bone marrow stress in TKO mice, with decreased RBC counts (anemia) and platelets (thrombocytopenia) and increasing platelet size (Mean platelet volume) over time (Figure 5B-D; supplemental Figure 7A-B), consistent with BMF. Despite the presence of WT bone marrow, hematopoiesis was not maintained, suggesting a cell-extrinsic effect of TKO bone marrow on WT HSPCs.

Hematopoietic stem and progenitor compartments reflect a distinct phenotype of DKO and TKO HSPCs

To further explore how altered cell death mechanism impacts non–cell-autonomous interactions in the HSPC and progenitor compartment, we evaluated progenitor, LSK, and SLAM-HSC populations after 20 weeks in primary competitive repopulation experiments. Progenitor cell numbers were similar between DKO and TKO transplanted mice and untransplanted mice (Figure 5E; supplemental Figure 7C) and markedly decreased relative to $Bid^{+/+}$ transplanted mice. Interestingly, $Bid^{+/+}$ progenitors in TKO transplanted mice were decreased relative to $Bid^{+/+}$ progenitors in DKO transplanted mice, suggesting the possibility that the presence of dying TKO progenitors may impair cotransplanted $Bid^{+/+}$ progenitors. Strikingly, whereas DKO and $Bid^{+/+}$ LSK cell numbers are similar, TKO bone marrow displays a substantial increase in LSK cells (approximately sevenfold), with a highly significant difference between DKO and TKO LSK cell numbers (Figure 5E-F). There was a trend to increased TKO SLAM-HSC (approximately twofold) numbers and a relative decrease in TKO progenitor cells (supplemental Figure 7C). In contrast, DKO HSPCs displayed a trend to an approximately twofold decrease relative to $Bid^{+/+}$ HSPCs, consistent with bone marrow crowding due to increased mature cells (supplemental Figure 7C).

To further evaluate HSPC function and compare DKO and TKO bone marrow reserve, we performed a secondary transplant. DKO bone marrow continues to outcompete $Bid^{+/+}$ marrow even in secondary transplant conditions, indicating continued HSPC self-renewal capacity (Figure 5G). In contrast, TKO bone marrow displays strikingly decreased competitive repopulating ability, consistent with decreased HSPC self-renewal capacity (exhaustion) in secondary transplant conditions (Figure 5G). We thus demonstrate that increased necroptosis impairs long-term HSPC function, resulting in HSPC exhaustion.

To further explore the impact of TKO bone marrow on WT hematopoietic progenitor cell function, we isolated $CD45.1^+$ and $CD45.2^+$ cells from competitively repopulated mice by FACS sorting, cultured these cells in methylcellulose, and evaluated colony numbers 10 days after plating. Transplanted TKO cells display decreased colony-forming ability (Figure 5H) relative to transplanted $Bid^{+/+}$ cells. Strikingly, $Bid^{+/+}$ cells transplanted in the presence of TKO cells also displayed decreased colony-forming ability as measured by the ratio of $CD45.1^+$ cells transplanted with $Bid^{+/+}$ cells to $CD45.1^+$ cells transplanted with TKO cells (Figure 5I).

TKO bone marrow displays increased TNF-α and IL-1β production

TKO bone marrow displayed elevated TNF-α staining without treatment (supplemental Figure 7E). Examination of HSPCs revealed significantly increased TNF-α and interleukin-6 (IL-6) in LSK cells and IL-1β in both LSK and progenitors in TKO marrow compared with $Bid^{+/+}$ marrow, but not interferon-γ

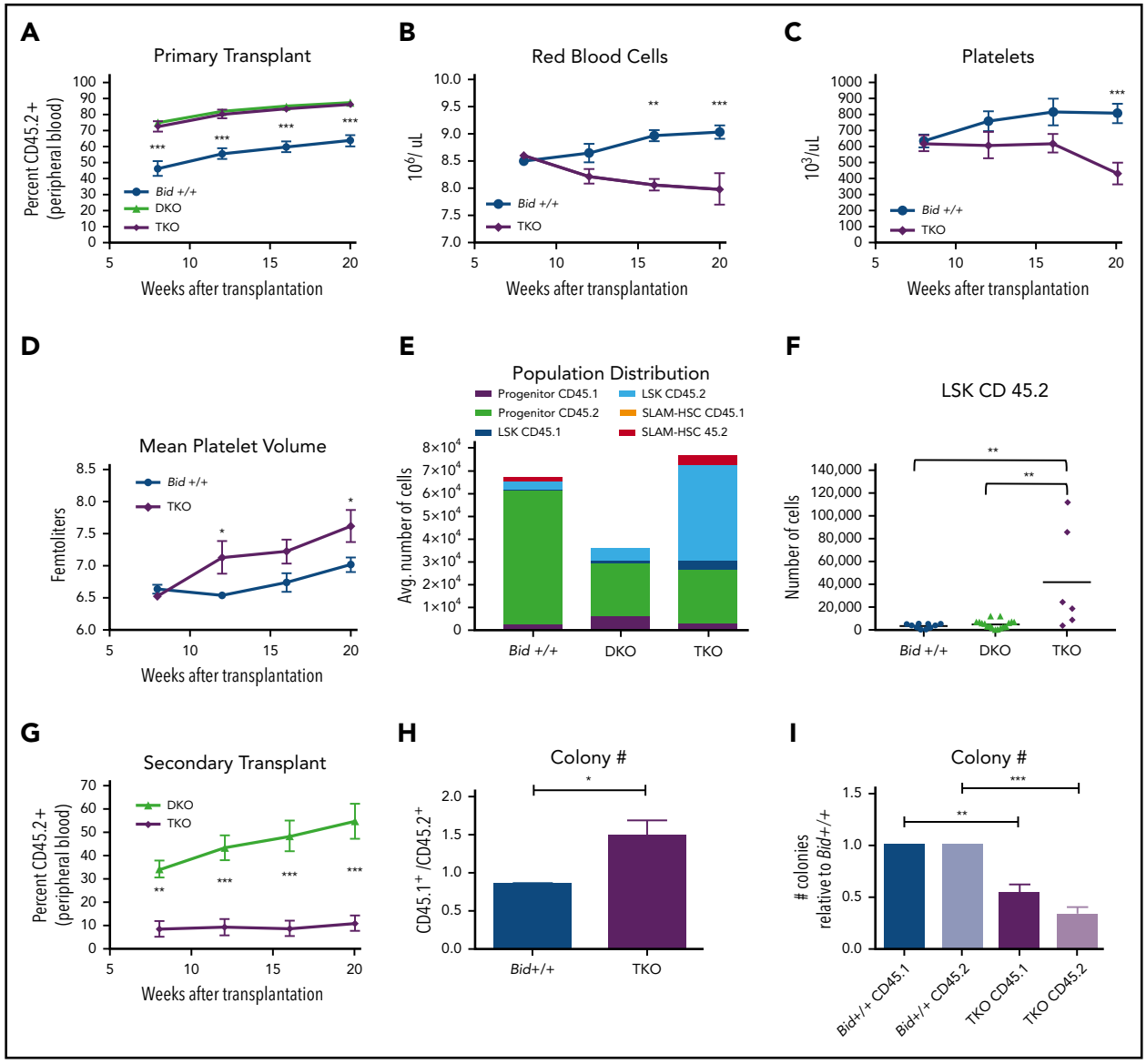

Figure 5. TKO bone marrow can reconstitute and outcompete *Bid*$^{+/+}$ bone marrow but is unable to maintain long-term hematopoiesis. (A) Percentage of CD45.2$^+$ cells in *Bid*$^{+/+}$, DKO, and TKO transplant mice at 8, 12, 16, and 20 weeks after transplantation. Mice were transplanted with experimental and control bone marrow at a 1:1 ratio. *Bid*$^{+/+}$, n = 7; DKO, n = 7; and TKO, n = 6. Statistics demonstrate differences between *Bid*$^{+/+}$ and TKO animals. (B-D) RBCs (10^6/μL; B), platelet counts (10^3/μl; C), and mean platelet volume (fL; D) in transplanted *Bid*$^{+/+}$ and TKO mice at 8, 12, 16, and 20 weeks after transplantation. *Bid*$^{+/+}$, n = 5; TKO, n = 8. Statistics demonstrate differences between *Bid*$^{+/+}$ and TKO animals. (E) Distribution of myeloid progenitor, LSK, and SLAM-HSC populations in *Bid*$^{+/+}$, DKO, and TKO transplanted mice. *Bid*$^{+/+}$, n = 5; DKO, n = 7; and TKO, n = 6. (F) CD45.2$^+$ LSK cells in transplanted mice. (G) Secondary transplantation of DKO and TKO bone marrow (primary transplant in a 1:1 ratio with *Bid*$^{+/+}$) to rigorously test hematopoietic stem cell function. DKO, n = 8; and TKO, n = 7. (H) Ratio of the colony-forming ability of CD45.1$^+$ to CD45.2$^+$ cells isolated from primary transplants. *Bid*$^{+/+}$ or TKO CD45.2$^+$ cells are transplanted in a 1:1 ratio with congenic CD45.1$^+$ *Bid*$^{+/+}$ cells. CD45.1$^+$ and CD45.2$^+$ bone marrow cells were sorted and cultured in methylcellulose in the presence of IL3, IL6, SCF, EPO. Colonies were counted at 10 days. The data are from 3 independent experiments. (I) Number of colonies for indicated bone marrow cells relative to *Bid*$^{+/+}$ colonies. Bid$^{+/+}$ CD45.1 denotes WT CD45.1 cells transplanted with Bid$^{+/+}$ CD45.2 cells. TKO CD45.1 denotes WT CD45.1 cells transplanted with TKO CD45.2 cells. ns, not significant; *$P < .05$ **$P < .01$, ***$P < .001$, and ****$P < .0001$. Data represent mean ± SEM.

(Figure 6A-C; supplemental Figure 7D). Bone marrow from TKO*Ripk1*($^{+/-}$) mice has significantly decreased TNF-α and IL-1β cytokine production (Figure 6D-E) relative to bone marrow from TKO mice. The above results are consistent with inflammation induced by necroptotic TKO cells.

Treatment with the TNF decoy receptor Enbrel restores MPCs and improves cytopenia in TKO mice

We next sought to determine whether inhibiting TNF-α could improve TKO cytopenia. We treated a cohort of *Bid*$^{+/+}$, DKO, and TKO mice with the TNFR decoy Enbrel. Enbrel treatment increased the number of TKO myeloid progenitor cells and BrdU$^+$ myeloid progenitor cells so that they were not significantly different from the corresponding *Bid*$^{+/+}$ cell numbers (Figure 6F-G). Enbrel treatment also improved RBC and platelet counts in TKO mice (Figure 6H-I), consistent with a role of necroptosis-induced TNF-α in TKO BMF.

We propose that our results suggest a model (Figure 6J) in which loss of Bax and Bak removes a feed-forward amplification of caspase activation and intrinsic apoptotic cell death. In a TKO mouse, further loss of Bid results in a change in caspase-8 activation,

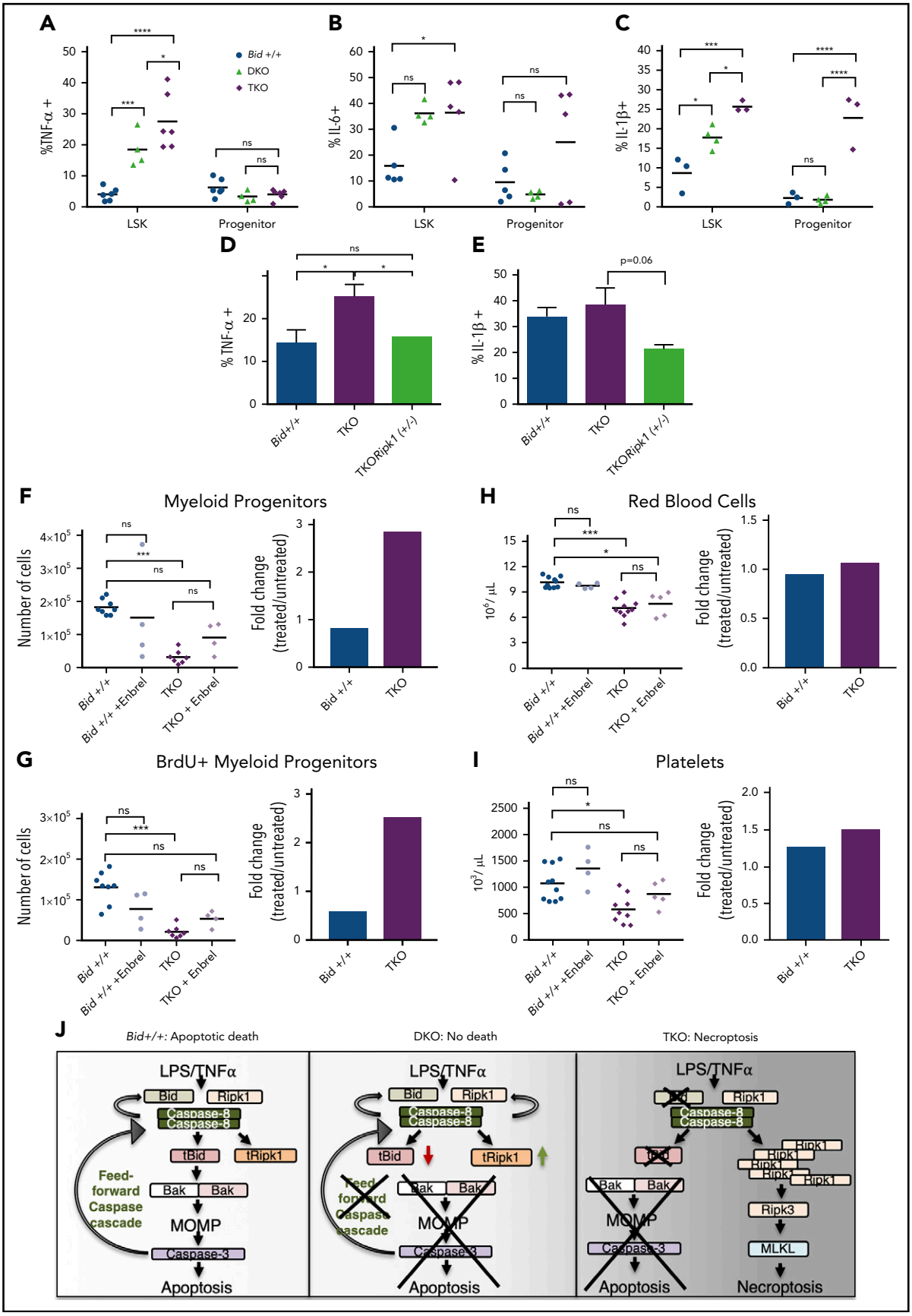

Figure 6.

resulting in decreased cleaved Ripk1 and increased necroptosis, consequently creating a highly inflammatory microenvironment in the marrow, leading to failure.

MDS demonstrates increased Ripk1 and pMLKL expression, suggesting increased necroptotic signaling

We have demonstrated that increased necroptosis in mouse bone marrow results in BMF with hypercellular marrow, prominent dysplasia, and a small frequency of transformation to leukemia, phenocopying the human BMF disorder MDS. Increased cell death in MDS bone marrow has been attributed to apoptosis based on techniques to measure cell death that do not distinguish between apoptotic and necroptotic cells,[31] including in situ end labeling, terminal deoxynucleotidyltransferase-mediated dUTP nick end labeling staining, or DNA laddering on gels.[32] Increased caspase-3 activity was seen in cultured MDS bone marrow,[33] but only in 10% of MDS samples measured directly ex vivo.[34]

To determine whether necroptotic cell death may play a role in MDS, we investigated necroptosis and apoptosis in MDS patient bone marrow samples. Immunofluorescence for Ripk1 (Figure 7A) and pMLKL (Figure 7B) revealed increased expression of these markers in all samples of refractory cytopenia with multilineage dysplasia and 50% of RAEB-1 and RAEB-2 subtypes of MDS in our 22-patient cohort (Figure 7C). Staining for cleaved caspase-3 reveals modest staining in only a few samples, including controls (Figure 7D). These findings are consistent with increased necroptosis signaling in MDS bone marrow. We also observed an inverse correlation between Ripk1 and Bid expression in several MDS, but not control, patient samples (supplemental Figure 8A).

We further obtained bone marrow from 3 patients with normal bone marrow, early MDS, and RAEB at the time of biopsy for TEM to minimize cell death artifacts. Early MDS cells show marked necrosis morphology relative to RAEB or control bone marrow (Figure 7E). While this study does not rule out a role for apoptosis in a subset of MDS patients, our study clearly implicates necroptosis signaling in MDS bone marrow cell death.

Discussion

The role of necroptosis in dynamic systems such as hematopoiesis and the impact on the microenvironment is not well understood. We have developed a novel set of mouse models tuned to undergo apoptosis (WT) or necroptosis (TKO) to explore the impact of necroptotic PCD on hematopoiesis. Using these models, we demonstrate that increased necroptotic cell death in the bone marrow leads to loss of the progenitor cell populations with compensatory expansion and proliferation of SLAM-HSCs (Figure 4), leading to an initial increase in repopulating ability in primary competitive repopulation studies; ultimately, this leads to stem cell exhaustion and BMF in secondary competitive repopulating experiments.

We further demonstrate in competitive repopulation experiments that necroptotic cells can cause cytopenias. This suggests that necroptotic cell death results in a cell extrinsic impairment of normal hematopoietic stem cells, mediated by the release of DAMPS, that promote release of inflammatory cytokines such as TNF-α that amplify cell death in a feed-forward manner (supplemental Figure 8B-C). Accordingly, while treatment of TKO mice with Enbrel partially restores TKO progenitor cells and peripheral cytopenias (Figure 6), loss of 1 allele of Rip1 kinase restores peripheral red cell counts and significantly improves progenitor numbers and proliferation. Our data demonstrate that the mechanism by which cells die can have a marked impact on bone marrow homeostasis. Skewing death to necroptosis results in BMF driven at least in part by necroptosis-induced TNF-α production.

Multiple lines of evidence have identified caspase-8 and the Rip kinases as central to the early signaling events that commit a cell to a given cell death fate. Leveraging cell lines from our mouse models and bone marrow and splenocytes taken directly from the mouse, we demonstrate that Bid restrains hematopoietic necroptosis through a Bid/caspase-8 axis, which cleaves and inactivates Ripk1 (Figure 3; supplemental Figures S3 and S4). This is consistent with a previous finding[6] that Ripk3 activates an apoptotic cell death pathway in settings where Ripk1 is blocked and also highlights a new, central role for Bid in the restraint of necroptosis.

Two recent studies demonstrate hematopoietic stem cell dysfunction in mice harboring genetic loss of *Ripk1* in hematopoietic cells. Roderick et al demonstrated that a hematopoietic specific deletion of *Ripk1* (*Vav-iCre-Ripk1*$^{F/F}$) resulted in BMF as a result of HSPC loss that is partially restored by loss of *Ripk3*.[35] Rickard et al demonstrated impaired engraftment of fetal liver cells from *Ripk1*$^{-/-}$ embryos that could be partially restored with a TNF blocking antibody.[36] These studies are both consistent with a requirement for signaling through Rip1 kinase to support proper HSC function. Our study, designed to interrogate increased necroptosis signaling, demonstrates an expanded HSC population with increased repopulating ability, in agreement with a role for Rip1 kinase signaling to support hematopoietic stem cell function. We further provide evidence that the level of Ripk1 kinase signaling is critical, as restoring normal Ripk1 levels in hematopoietic cells can restore normal peripheral blood counts.

Our results significantly contribute to our understanding of how necroptosis, through increased Ripk1-dependent inflammatory cytokines, impacts hematopoietic homeostasis and hematopoietic stem cell function leading to BMF. Significantly, the hematopoietic phenotype of our TKO mice phenocopies the human BMF disorder MDS. Substantial data have established

Figure 6. TKO mice display increased TNF-α, which can be rescued by a genetic cross with *Ripk1*$^{(+/-)}$ mice or the anti-inflammatory drug Enbrel. (A) TNF-α, (B) IL-6, and (C) IL-1β positivity in myeloid progenitor and LSK populations in *Bid*$^{+/+}$, DKO, and TKO mice. (D-E) Intracellular cytokine staining for TNF-α (D) and IL-1β (E) in *Bid*$^{+/+}$, TKO, and TKO*Ripk1*$^{(+/-)}$ mouse bone marrow after 5 hours of LPS stimulation (200 ng/mL) + Golgi Plug. *Bid*$^{+/+}$, n = 5; TKO, n = 7; and TKO*Ripk1*$^{(+/-)}$, n = 5. (F) Myeloid progenitor populations and corresponding fold change for *Bid*$^{+/+}$ and TKO mice before and after treatment with Enbrel (TNF decoy receptor). (G) Number of BrdU-positive myeloid progenitors and fold change as in panel F. (H-I) RBCs (10^6/μL; H, left) and platelet counts (10^3/μL; I, right) in *Bid*$^{+/+}$ and TKO mice with and without Enbrel and corresponding fold change. (J) Model diagram for cell death pathways in *Bid*$^{+/+}$, DKO, and TKO mice. In a TKO mouse, the absence of Bax and Bak inhibits the feed-forward caspase amplification, while further loss of Bid results in necrotic cell death. *Bid*$^{+/+}$, n = 4; and TKO, n = 4. *$P < .05$, ***$P < .001$, and ****$P < .0001$. Data represent mean ± SEM. MOMP, mitochondrial outer membrane permeabilization; ns, not significant.

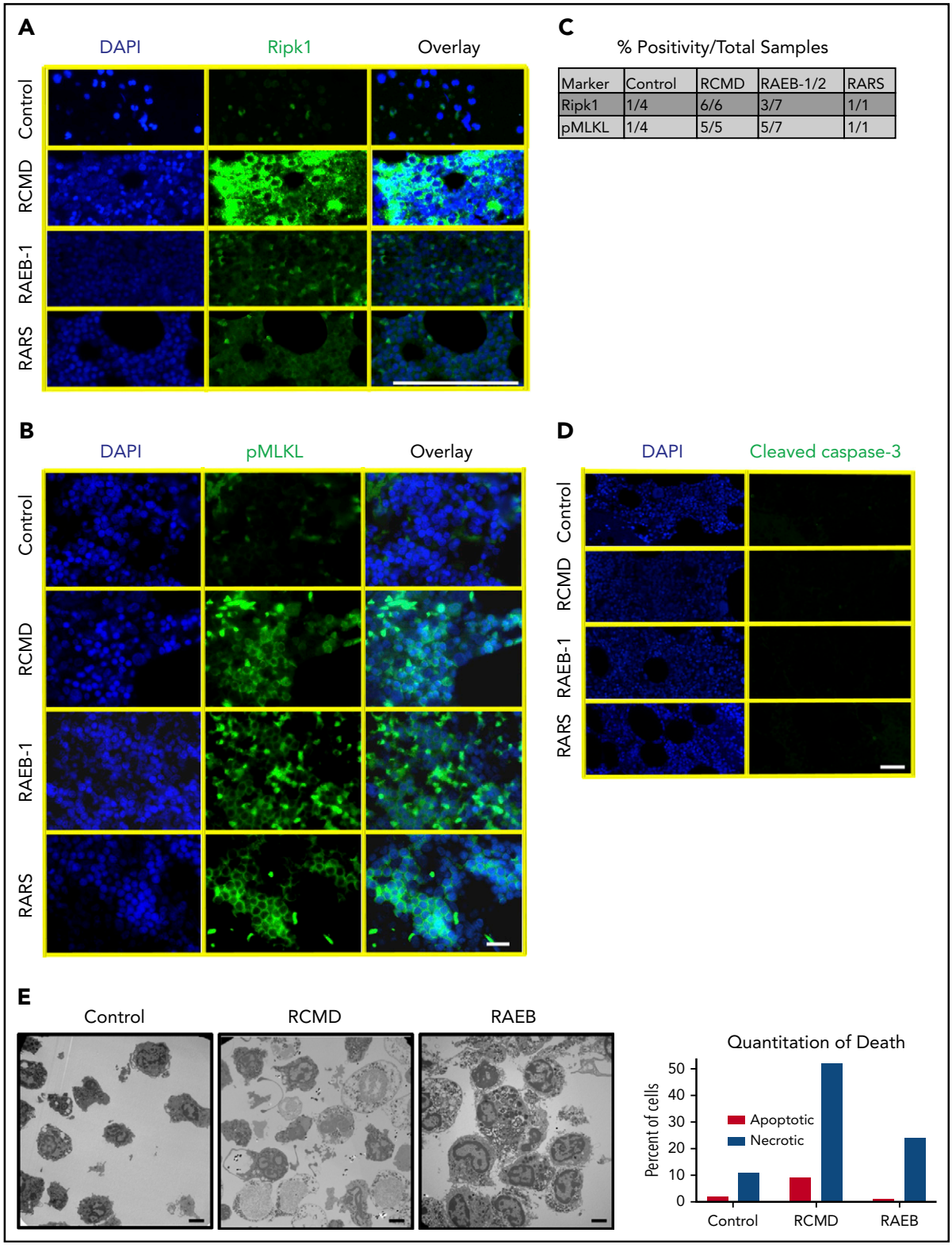

Figure 7. Bone marrow from patients with MDS displays increased Ripk1 and pMLKL and necrotic morphology on electron microscopy. (A) Ripk1 staining on paraffin-embedded human bone marrow aspirate for DAPI and Ripk1. MDS subtypes include (from top to bottom) refractory cytopenia with multilineage dysplasia (RCMD), refractory anemia with excess blasts (RAEB-1), and refractory anemia with ring sideroblasts (RARS). Scale bar, 100 μm. The experiment was performed 3 independent times. (B) Phospho-MLKL staining on paraffin-embedded human bone marrow aspirate. The experiment was performed 2 independent times. Scale bar, 50 μm. (C) Table demonstrating positivity of human samples for Ripk1 and pMLKL by subtype. (D) Cleaved caspase-3 staining on paraffin-embedded human bone marrow aspirate. The experiment was performed 3 independent times. Scale bar, 50 μm. (E) TEM of human bone marrow aspirate following RBC lysis from a normal control donor, an early MDS patient, and a RAEB patient. Scale bars, 2 μm; original magnification ×4400. Quantitation of apoptotic or necroptotic cell death for each patient represented in graph (right).

the presence of increased cell death and increased inflammation in MDS, and we now demonstrate increased necroptosis in MDS patient bone marrow. We show in mouse models that genetic loss of 1 allele of Ripk1 is sufficient to restore RBC peripheral counts and ameliorate excess cytokine production. Additional studies will be required to determine whether combining inhibition of both necroptosis and cytokines will provide added benefit.

Acknowledgments

The authors thank Jennifer Pietenpol and Scott Hiebert for helpful comments, Janice Williams and Mary Dawes for assistance with TEM, Heidi Chen for help with biostatistics, and Claudio Mosse and James Atkinson for assistance with mouse pathology.

This work was supported by the National Institutes of Health, National Heart, Lung, and Blood Institute (grants R01-HL088347 [S.S.Z.] and 5T32HL06976509 [P.N.W.], the American Society of Hematology (bridge grant) (S.S.Z.), the US Department of Veterans Affairs (merit award BX002250, CDMRP W81XWH-16-1-0057) (S.S.Z.), the Evans Foundation (S.S.Z.). Immunofluorescence and TEM experiments were performed in part through the Vanderbilt University Cell Imaging Shared Resource and supported by the National Institutes of Health, National Cancer Institute (grant CA68485), National Institute of Diabetes and Digestive and Kidney Diseases (grants DK20593, DK58404, DK59637), and National Eye Institute (grant EY08126). Flow cytometry experiments were performed at the Vanderbilt University Medical Center, Flow Cytometry Shared Resource, and Vanderbilt-Ingram Cancer Center and supported by the National Institutes of Health, National Cancer Institute (grant P30CA68485) and Vanderbilt Digestive Disease Research Center (DDRC), National Institute of Diabetes and Digestive and Kidney Diseases (grant DK058404).

Authorship

Contribution: P.N.W., Q.S., C.T.S.-R., S.S.Z., and J.Z. performed experiments; S.S.Z., P.N.W., and C.T.S.-R. designed experiments and analyzed experimental results; Y.F. and M.R.S. provided MDS patient samples; all authors analyzed and interpreted data; and P.N.W., S.S.Z., and C.T.S.-R. wrote the manuscript.

Conflict-of-interest disclosure: M.R.S. received grants, personal fees, and nonfinancial support from Astex, Incyte Corporation, Takeda, and TG Therapeutics; personal fees and other funds from Boehringer-Ingelheim, Celgene, and Gilead; personal fees, nonfinancial support, and other support from Karyopharm; and grants and personal fees from Sunesis. The remaining authors declare no competing financial interests.

Correspondence: Sandra S. Zinkel, 2220 Pierce Ave, 548 Preston Research Building, Nashville, TN 37232; e-mail: sandra.zinkel@vumc.org.

Footnotes

Submitted 17 May 2018; accepted 24 October 2018. Prepublished online as *Blood* First Edition paper, 9 November 2018; DOI 10.1182/blood-2018-05-847335.

The online version of this article contains a data supplement.

There is a *Blood* Commentary on this article in this issue.

The publication costs of this article were defrayed in part by page charge payment. Therefore, and solely to indicate this fact, this article is hereby marked "advertisement" in accordance with 18 USC section 1734.

REFERENCES

1. Kaczmarek A, Vandenabeele P, Krysko DV. Necroptosis: the release of damage-associated molecular patterns and its physiological relevance. *Immunity*. 2013;38(2):209-223.
2. Pasparakis M, Vandenabeele P. Necroptosis and its role in inflammation. *Nature*. 2015; 517(7534):311-320.
3. Socolovsky M, Murrell M, Liu Y, Pop R, Porpiglia E, Levchenko A. Negative autoregulation by FAS mediates robust fetal erythropoiesis. *PLoS Biol*. 2007;5(10):e252.
4. Koulnis M, Liu Y, Hallstrom K, Socolovsky M. Negative autoregulation by Fas stabilizes adult erythropoiesis and accelerates its stress response. *PLoS One*. 2011;6(7):e21192.
5. King KY, Goodell MA. Inflammatory modulation of HSCs: viewing the HSC as a foundation for the immune response. *Nat Rev Immunol*. 2011;11(10):685-692.
6. Dillon CP, Weinlich R, Rodriguez DA, et al. RIPK1 blocks early postnatal lethality mediated by caspase-8 and RIPK3. *Cell*. 2014; 157(5):1189-1202.
7. Rickard JA, Anderton H, Etemadi N, et al. TNFR1-dependent cell death drives inflammation in Sharpin-deficient mice. *eLife*. 2014;3:e03464.
8. Weng D, Marty-Roix R, Ganesan S, et al. Caspase-8 and RIP kinases regulate bacteria-induced innate immune responses and cell death. *Proc Natl Acad Sci USA*. 2014;111(20): 7391-7396.
9. Oberst A, Dillon CP, Weinlich R, et al. Catalytic activity of the caspase-8-FLIP(L) complex inhibits RIPK3-dependent necrosis. *Nature*. 2011;471(7338):363-367.
10. Dickens LS, Boyd RS, Jukes-Jones R, et al. A death effector domain chain DISC model reveals a crucial role for caspase-8 chain assembly in mediating apoptotic cell death. *Mol Cell*. 2012;47(2):291-305.
11. Weinlich R, Dillon CP, Green DR. Ripped to death. *Trends Cell Biol*. 2011;21(11):630-637.
12. Zhou W, Yuan J. Necroptosis in health and diseases. *Semin Cell Dev Biol*. 2014;35:14-23.
13. Li H, Zhu H, Xu CJ, Yuan J. Cleavage of BID by caspase 8 mediates the mitochondrial damage in the Fas pathway of apoptosis. *Cell*. 1998;94(4):491-501.
14. Danial NN, Korsmeyer SJ. Cell death: critical control points. *Cell*. 2004;116(2):205-219.
15. Zinkel SS, Hurov KE, Ong C, Abtahi FM, Gross A, Korsmeyer SJ. A role for proapoptotic BID in the DNA-damage response. *Cell*. 2005; 122(4):579-591.
16. Zinkel SS, Ong CC, Ferguson DO, et al. Proapoptotic BID is required for myeloid homeostasis and tumor suppression. *Genes Dev*. 2003;17(2):229-239.
17. Hitomi J, Christofferson DE, Ng A, et al. Identification of a molecular signaling network that regulates a cellular necrotic cell death pathway. *Cell*. 2008;135(7):1311-1323.
18. Berger SB, Kasparcova V, Hoffman S, et al. Cutting Edge: RIP1 kinase activity is dispensable for normal development but is a key regulator of inflammation in SHARPIN-deficient mice. *J Immunol*. 2014;192(12): 5476-5480.
19. Takeuchi O, Fisher J, Suh H, Harada H, Malynn BA, Korsmeyer SJ. Essential role of BAX,BAK in B cell homeostasis and prevention of autoimmune disease. *Proc Natl Acad Sci U S A*. 2005;102(32):11272-11277.
20. Yin XM, Wang K, Gross A, et al. Bid-deficient mice are resistant to Fas-induced hepatocellular apoptosis. *Nature*. 1999;400(6747): 886-891.
21. Biswas S, Shi Q, Matise L, Cleveland S, Dave U, Zinkel S. A role for proapoptotic Bax and Bak in T-cell differentiation and transformation. *Blood*. 2010;116(24): 5237-5246.
22. Zhou T, Kinney MC, Scott LM, Zinkel SS, Rebel VI. Revisiting the case for genetically engineered mouse models in human myelodysplastic syndrome research. *Blood*. 2015; 126(9):1057-1068.
23. Green DR. An Element of Life. *Cell*. 2018; 172(3):389-390.
24. Scaffidi C, Schmitz I, Zha J, Korsmeyer SJ, Krammer PH, Peter ME. Differential modulation of apoptosis sensitivity in CD95 type I and type II cells. *J Biol Chem*. 1999;274(32): 22532-22538.
25. Cho YS, Challa S, Moquin D, et al. Phosphorylation-driven assembly of the RIP1-RIP3 complex regulates programmed necrosis and virus-induced inflammation. *Cell*. 2009; 137(6):1112-1123.

26. Vanlangenakker N, Vanden Berghe T, Vandenabeele P. Many stimuli pull the necrotic trigger, an overview. *Cell Death Differ*. 2012;19(1):75-86.

27. Cai Z, Jitkaew S, Zhao J, et al. Plasma membrane translocation of trimerized MLKL protein is required for TNF-induced necroptosis [published correction appears in *Nat Cell Biol*. 2014;16(2):200]. *Nat Cell Biol*. 2014;16(1):55-65.

28. Lin Y, Devin A, Rodriguez Y, et al. Cleavage of the death domain kinase RIP by Caspase 8 prompts TNF-induced apoptosis. *Genes & Dev*. 1999;13(19):2514-2526.

29. McComb S, Shutinoski B, Thurston S, Cessford E, Kumar K, Sad S. Cathepsins limit macrophage necroptosis through cleavage of Rip1 kinase. *J Immunol*. 2014;192(12):5671-5678.

30. Kiel MJ, Yilmaz OH, Iwashita T, Yilmaz OH, Terhorst C, Morrison SJ. SLAM family receptors distinguish hematopoietic stem and progenitor cells and reveal endothelial niches for stem cells. *Cell*. 2005;121(7):1109-1121.

31. Galluzzi L, Vitale I, Aaronson SA, et al. Molecular mechanism of cell death: recommendations of the Nomenclature Committee on Cell Death 2018. *Cell Death Differ*. 2018;25(3):486-541.

32. Kerbauy DB, Deeg HJ. Apoptosis and antiapoptotic mechanisms in the progression of myelodysplastic syndrome. *Exp Hematol*. 2007;35(11):1739-1746.

33. Mundle SD, Reza S, Ali A, et al. Correlation of tumor necrosis factor alpha (TNF alpha) with high Caspase 3-like activity in myelodysplastic syndromes. *Cancer Lett*. 1999;140(1-2):201-207.

34. Spinelli E, Caporale R, Buchi F, et al. Distinct signal transduction abnormalities and erythropoietin response in bone marrow hematopoietic cell subpopulations of myelodysplastic syndrome patients. *Clin Cancer Res*. 2012;18(11):3079-3089.

35. Roderick JE, Hermance N, Zelic M, et al. Hematopoietic RIPK1 deficiency results in bone marrow failure caused by apoptosis and RIPK3-mediated necroptosis. *Proc Natl Acad Sci USA*. 2014;111(40):14436-14441.

36. Rickard JA, O'Donnell JA, Evans JM, et al. RIPK1 regulates RIPK3-MLKL-driven systemic inflammation and emergency hematopoiesis. *Cell*. 2014;157(5):1175-1188.

RIPK1-mediated inflammation impairs erythropoiesis in Tet2-loss: phenomics, human genetics and mice

Christi T Salisbury-Ruf[a], Teresa C Dugger[b], Eric R. Gamazon[d,e*], and Sandra S. Zinkel[a,b*]

Department of Cell and Developmental Biology[a]

Vanderbilt University, 2200 Pierce Avenue, Nashville, TN, 37232

Department of Medicine[b], Department of Biomedical Informatics[c], and Division of Genetic Medicine[d]

Vanderbilt University Medical Center, 1211 Medical Center Drive, Nashville, TN, USA, 37212

Clare Hall, University of Cambridge, Herschel Road, Cambridge, CB3 9AL, United Kingdom[e]

*Address correspondence to Sandra S. Zinkel, sandra.zinkel@vanderbilt.edu

*Address correspondence to Eric R. Gamazon, eric.gamazon@vanderbilt.edu

Character limit 20,000 (Intro & results), current characters: 19,993)

Abstract

An association between immune dysregulation and bone marrow failure disorders such as Myelodysplastic syndrome (MDS) is emerging. Inflammatory cytokines produced by innate immune stimulation can lead to disease. We have shown that inflammatory programmed cell death or necroptosis, mediated by Ripk1 can induce inflammation and bone marrow failure in mice and show increased Ripk1 in human myelodysplastic syndrome (MDS) bone marrow. How inflammation and increased RIPK1 may predispose to MDS in human disease and the impact of necroptosis on the erythroid compartment are not well-understood. We use an integrative approach combining phenomic studies in large-scale electronic health records (n>2.8 million), human genetic analysis (n>25,000), and mouse models. We find significant comorbidity

between anemias, including MDS, and inflammatory diseases (OR between 4.2 and 15.9). In two mouse models, *VavTet2* and TKO, erythrocytes were highly sensitive to inflammation mediated by LPS and necroptotic death, respectively. Lastly, we find significant epistatic interaction between TET2 and RIPK1 expression for effect on inflammatory diseases and hemolytic anemia. These results suggest that RipK1-mediated inflammation is detrimental to erythrocytes, particularly in TET2 deficiency, which may contribute to bone marrow failure progression.

Introduction (Current characters: 4,078 without spaces)

Myelodysplastic syndromes (MDS) are a group of bone marrow failure disorders, characterized by ineffective hematopoiesis resulting in cytopenias, particularly anemia. Inflammation within the MDS marrow microenvironment contributes to disease progression (Banerjee *et al.,* 2019; Sallman *et al.,* 2019). Necroptotic cell death mediated by Ripk1, most prominent in erythroid islands, contributes to MDS bone marrow inflammation through increased cytokine production, especially TNFα (Wagner *et al.,* 2018; Zou *et al.,* 2019).

Genetic mutations identified in clonal hematopoiesis of indeterminate potential (CHIP) and MDS, such as Ten-eleven translocation 2 (TET2), are also associated with dysfunctional erythropoiesis and inflammation (Busque *et al.,* 2012; Libby *et al.,* 2018). TET2 restrains inflammation through transcriptional regulation (Zhang *et al.*, 2015; Rauh *et al.*, 2017). TET2 loss impairs erythrocyte development, with compensatory increased colony forming unit-erythroid (CFU-E) formation. It is unknown, however, whether TET2 also confers increased susceptibility of erythrocytes to inflammatory stress.

In anemia of chronic disease (ACD), inflammation impairs iron utilization and proliferation of early RBC precursors, particularly burst-forming units-erythroid (BFU-E) and CFU-E (Weiss *et al.,* 2005). LPS injected mice display TNF-induced decreased erythropoietin (EPO) expression and colony formation (Rusten *et al.,* 1995; Tanyong *et al.,* 2015).

Red cells themselves can also impact inflammation. RBCs contain high concentrations of pro-inflammation cytokines, (Straat *et al.*, 2015; Karsten *et al.,* 2018) and release TLR9 bound DNA during necroptosis (Hotz *et al.*, 2018). In MDS, red cells have higher levels of reactive oxygen species (ROS), and abnormal cell membranes (Majumder *et al.*, 2006; Ghoti *et al.*, 2007). As anemia is an early symptom of MDS, and current therapies such as EPO alleviate symptoms, but fail to prevent progression (Cogle *et al.,* 2015), a better understanding of red cell defects in MDS warrants further study.

Here we investigate the impact of Ripk1-mediated inflammation on erythropoiesis in the context of bone marrow failure. We present a comprehensive approach (Salisbury-Ruf *et al.*, 2018) combining (a) phenomic studies of disease comorbidities using a large-scale electronic health records (EHR) database, (b) human genetic studies, including a phenome-wide association study of single nucleotide polymorphisms (SNPs) in the RIPK1 locus and analysis of genetic regulation of gene expression, and (c) functional studies in two different mouse models of bone marrow failure (Fig. 1 A).

Comorbidity analysis using EHR data reveals a significant pattern of disease co-occurrence of MDS and inflammatory diseases. We identify SNPs in the RIPK1 locus associated with several inflammatory conditions, most significantly with endocarditis, and MDS. Further,

PrediXcan analysis (Gamazon *et al.,* 2015) reveals anemia associated with increased genetically-determined necroptotic gene expression, particularly increased RIPK1.

PrediXcan analysis reveals that decreased TET2 expression significantly associates with inflammatory disease, and individuals expressing the lowest TET2 have significantly increased RIPK1 expression in hemolytic anemia. There is significant evidence for epistatic interaction between TET2 and RIPK1. ATAC-Seq analysis of mouse stem cells reveal altered chromatin accessibility in the *Ripk1* locus in the absence of *Tet2*, highlighting the impact of *Tet2* loss on *Ripk1* transcription.

Mouse studies of erythropoiesis demonstrate that early precursor erythrocytes from *VavCre^{+}Tet2$^{F/F}$* (*VavTet2$^{-/-}$)* mice (Moran-Crusio *et al.*, 2011) are extremely sensitive to acute treatment with LPS, which could be rescued by one allele of kinase-inactive *Ripk1*, (*Ripk1$^{D138N/+}$ $^{(D/+)}$*). The *Ripk1^{D138N}* mice are mutated in the proton acceptor region of the catalytic site of Ripk1, but maintain normal NFκB signaling (Polykratis *et al.*, 2014). We confirm increased CFU-E colonies (Qu *et al.,* 2018), which we rescue by genetic inhibition of Ripk1 function. Furthermore, *VavCre^{+}Bax $^{F/F}$Bak $^{-/-}$Bid $^{-/-}$* (TKO) mice, shown to have bone marrow failure driven by necroptosis (Wagner *et al.,* 2018) display decreased mature RBCs, which is partially rescued by crossing to *Ripk1(+/-)* (Berger *et al.*, 2014) mice as well as *Ripk1$^{D138N/D138N\ (D/D)}$* mice, indicating the importance of the necroptotic arm of Ripk1.

Lastly, we present a novel risk reduction model using EHR data. We find that individuals on anti-TNFα biologics, such as Humira or Enbrel, display significantly decreased MDS risk. These data suggest that alleviating inflammation mediated by Ripk1 may directly impact red cell homeostasis, and MDS progression.

Results and Discussion (Characters: 15,915 without spaces)

Phenomic analysis in large-scale electron health records reveals elevated risk between MDS and inflammatory diseases

To probe relevant disease mechanisms, we undertook a systematic analysis of disease comorbidities between anemias and inflammatory conditions. To confirm method validity, we first evaluated known disease associations with MDS, including aplastic anemia (Kim *et al.*, 2014; Kulasekararaj *et al.*, 2019), thrombocytopenia (Li *et al.*, 2016; Waisbren *et al.*, 2017), acute myeloid leukemia (AML) (Pfeilstocker *et al.*, 2016), and myelofibrosis (Marisavljevic *et al.*, 2004). In Vanderbilt University's Synthetic Derivative (SD) of 2.8 million de-identified EHR data, we identified 2,548 individuals diagnosed with MDS (of European ancestry, all ages, all sexes) (Fig. S1 A) (Roden *et al.*, 2008). Comorbidity analysis recapitulated the known association of thrombocytopenia and aplastic anemia with elevated risk of MDS (Fig. 1 B). Furthermore, we confirmed the association between MDS and AML (Odds Ratio [OR]=266.6, 95% CI [245.54-291.23]) and between MDS and myelofibrosis (OR=1090.1, 95% CI [937.13-1269.27]) (Fig. 1 C and Fig. S1, A and B).

We have recently shown that MDS is associated with inflammation driven by necroptotic cell death (Wagner *et al.,* 2019; Zou *et al.,* 2019). Additionally, several autoimmune diseases, particularly thyroiditis, increase MDS risk (Wolach and Stone, 2016; Montoro *et al.*, 2018). To elucidate how these associations are reflected in the disease phenome, we defined a "super-inflammatory" phenotype characterized by individuals with inflammatory etiologies such as autoimmunity to increase sample size and improve statistical power (Fig. S1, C-E). Compared to control phenotypes (including headache, acne, and the common cold) chosen at

the outset for their large sample size, ORs between all anemias and MDS and the "super-inflammatory" disease were substantially elevated (MDS OR=15.9, 95% CI [14.61-17.40]) (Fig. 1 C).

We evaluated infection as an additional driver of inflammation. As expected, there was a significant association between MDS and sepsis (OR=19.2, 95% CI [17.45-21.23]), consistent with compromised immunity of MDS patients (Dayyani *et al.*, 2010). We then evaluated infections driven by viruses such as Epstein-Barr and herpes, which are often acquired by young adults (Smatti *et al.*, 2018) and thus would potentially be predisposing. We found ORs of 5.8 (95% CI [4.75-7.06]) and 6.4 (95% CI [4.62-8.88]) for herpes virus and mononucleosis, respectively (Fig. 1 D and Fig. S1, C-G). Importantly, the associations were not driven by sample size (Fig. S1, E and G). Collectively, these results show a highly significant association between MDS and inflammation.

Human genetic analyses highlight RIPK1 effect on anemia and inflammation

Ripk1-mediated necroptosis results in inflammation in multiple organ systems in mice, including the colon and central nervous system (Vlantis *et al.*, 2016; Yuan J *et al.,* 2019). We have recently shown that necroptosis-driven inflammation in the bone marrow microenvironment impairs HSPC and erythrocyte function due to feed-forward activation of cytokines, resulting in bone marrow failure (Wagner *et al.,* 2018; Zou *et al.,* 2019).

We performed human genetic studies to characterize the phenotypic consequences of RIPK1 on erythropoiesis and inflammation. First, we leveraged the UK Biobank (n~500,000) to identify the phenome significantly associated with single-nucleotide polymorphisms (SNPs) in the RIPK1 gene locus (Bycroft *et al.*, 2018). The top SNP associations in the locus for "I38

Endocarditis" (Fig. 2 A) (rs114183703; p=1.9e-13), "K83.0 Cholangitis" (rs764727241; p=3.1e-12), and "D46.9 Myelodysplastic syndrome" (rs573478296; p=1.9e-10) indicate phenome-wide significant effects of the locus (after Bonferroni correction; see Methods) on inflammatory phenotypes and ineffective hematopoiesis (Fig. 2 B for additional associations with p<5e-08).

Next, we performed PrediXcan analysis (Fig. 2 C) (Gamazon *et al.,* 2015), which estimates the genetically-determined component of gene expression and evaluates its effect on phenotype. Testing a subset of hemolytic anemia cases and controls in Vanderbilt's EHR with whole-genome data (see Methods), we found a significant increase in the expression of RIPK1 and, in secondary analyses, additional necroptosis genes (Fig. 2 D), including MLKL, and a significant decrease in the apoptotic gene CASP8 among cases relative to controls, suggesting that germline, genetically-determined predisposition to necroptosis may be predisposing for anemia.

Increased RIPK1 expression was associated with increased predisposition to several inflammatory disorders (Fig. S1 H). Additional PrediXcan analysis shows that increased RIPK1 expression was associated with inflammatory bowel disease (IBD) and other gastroenteritis diseases ($p=9.4x10^{-3}$, cases=405, controls = 16,064). In two additional GWAS studies with much larger sample sizes (see Methods), increased RIPK1 was nominally associated with IBD (Fig. S1 I), demonstrating that the pattern of associations with inflammatory traits is not due to confounding variables present in EHR (Rioux *et al.*, 2007; Liu *et al.*, 2015).

Significant interaction between TET2 and RIPK1 expression for effect on inflammatory diseases and hemolytic anemia

158 TET2 has been associated with CHIP which predisposes to MDS. The factors that lead to
159 progression from CHIP to MDS are unknown. Loss of TET2 in mice increases stem cell renewal
160 and myeloproliferation, potentially contributing to transformation (Moran-Crusio *et al.*, 2011).
161 Inhibiting inflammatory signaling in *Tet2* mutant mouse pre-leukemic cells mitigates clonal
162 expansion, suggesting a role for inflammation (Cai *et al.*, 2018). TET2 is also important for
163 normal erythropoiesis, particularly the CFU-E compartment (Yan *et al.*, 2017; Qu *et al.*, 2018)
164 and for preventing atherosclerosis through inflammatory macrophages (Higgins *et al.*, 2014;
165 Saleheen *et al.*, 2017; Sano *et al.*, 2018).
166 In human genetic analysis, we found significant associations between TET2 genetically-
167 determined expression and inflammatory diseases, including chronic pericarditis, eosinophilic
168 esophagitis, and stomatitis and mucositis (ulcerative) (Fig. 2 E). Furthermore, decreased
169 genetically-determined TET2 expression was significantly associated with infectious
170 mononucleosis ($p=5.8x10^{-3}$). Consistent with this, comorbidity analysis indicated high OR for
171 MDS and mononucleosis (OR=6.4, 95% CI [4.62-8.88]) (Fig. 1 D) which is driven by EBV. These
172 data suggest that TET2 levels may contribute to susceptibility to infection, and consequently
173 inflammation and bone marrow failure risk.
174 Among individuals with the lowest TET2 expression (n=2,898, representing 12.5% of
175 samples), increased RIPK1 expression was significantly higher among non-autoimmune
176 hemolytic anemia cases than controls (Mann-Whitney U test $p<2.2x10^{-16}$) (Fig. 2, F and G).
177 These results suggest that in TET2 deficiency, increased RIPK1 genetically-determined
178 expression may be highly detrimental to the erythroid compartment. Notably, TET2 and RIPK1
179 expression show significant enrichment (p=0.01; see Methods) for interaction (statistical

180 epistasis) effects on inflammatory traits and hemolytic anemia, indicating that the expression of
181 one modifies the effect of the expression of the other on disease (Fig. 2 H).
182 To gain further insights into the observed interaction, we evaluated the effect of *Tet2*
183 loss on chromatin accessibility across the *Ripk1* locus. We analyzed ATAC-Seq data from WT
184 and *Tet2*$^{-/-}$ ES cells and observed altered chromatin accessibility in the *Ripk1* locus in the
185 absence of *Tet2* (Fig. 2 I) (Rasmussen *et al.*, 2019), indicating that *Tet2* loss was modifying the
186 local chromatin environment and thus, potentially, transcriptional regulation of *Ripk1*.
187
188 **Erythropoiesis in *VavTet2*$^{-/-}$ mice is highly sensitive to acute LPS due in part to necroptotic cell**
189 **death which can be rescued with *Ripk1*$^{D138N/+\ (D/+)}$**
190 Next, to directly test the impact of an inflammatory stimulus on Ripk1-mediated
191 necroptosis and bone marrow function in the setting of *Tet2* loss, we evaluated *VavTet2*$^{-/-}$ *and*
192 *VavTet2*$^{-/-}$ *Ripk1*$^{D138N/+\ (D/+)}$ mice (Polykratis *et al.,* 2014). Immunoblot examination of the bone
193 marrow revealed no difference in necroptotic protein levels between untreated WT and
194 *VavTet2*$^{-/-}$ mice. However, upon acute inflammatory stimulation with one dose of LPS (1.5
195 mg/kg), we observed an increase in Ripk1, Ripk3, TNFα, and anti-inflammatory ROS proteins
196 glutathione peroxidase 4 (GPX4) and peroxiredoxin II (PRXII) in the bone marrow, but not the
197 spleen, of *VavTet2*$^{-/-}$ mice. This inflammatory signaling was diminished in *VavTet2*$^{-/-}$*Ripk1*$^{D/+}$ (Fig.
198 3 A and Fig. S2 A), suggesting that inflammation in Tet2 loss is driven at least in part by Ripk1
199 kinase activity.
200 We further observed that early committed erythroid progenitors, including
201 proerythroblasts (ProE) and basophilic blasts (Baso), were significantly reduced with LPS in

VavTet2$^{-/-}$ mice, but not WT or *VavTet2*$^{-/-}$*Ripk1*$^{D/+}$ mice, indicating sensitivity of early erythrocytes to inflammation in the absence of *Tet2* (Fig. 3, B-D). We also observed a significant decrease in Orthoblasts (Ortho) and reticulocytes (Retics) in WT and *VavTet2*$^{-/-}$ but not *VavTet2*$^{-/-}$*Ripk1*$^{D/+}$ while the mature RBCs were relatively unaffected (Fig. 3, E-G and Fig. S2 B). These results indicate that Tet2 loss impairs the erythroid compartment at least in part through Ripk1-mediated necroptosis and may explain in part how inflammatory conditions contribute to anemia in individuals with TET2 mutations.

To understand the impact of inflammation on the microenvironment, we evaluated generation of reactive oxygen species (ROS), which occurs downstream of TLR stimulation with LPS (Hsu and Wen, 2002). *VavTet2*$^{-/-}$ but not *VavTet2*$^{-/-}$*Ripk1*$^{D/+}$ displayed increased cellular superoxide, as indicated by DHE, (Fig. 3 H and Fig. S2 C), consistent with the expression of antioxidant proteins (Fig. 3 A). Immunofluorescence analysis of FFPE sternum marrow for TNFα and Ripk1 before (Fig. S2, D and E) and after (Fig. 3 I) acute LPS injection followed by CellProfiler^{TM} analysis (Carpenter *et al.*, 2006) revealed a significant decrease in the percentage of Ter119 cells in the marrow of *VavTet2*$^{-/-}$ but not *VavTet2*$^{-/-}$*Ripk1*$^{D/+}$ mice (Fig. 3 J and Fig. S2 F) (See Methods). Importantly, there was no difference in the total number of nucleated cells in either untreated or treated mice (Fig. S2 G). Furthermore, we analyzed the percentage of TNFα positive cells that were erythrocytes and found that *VavTet2*$^{-/-}$ mice had a significant decrease in the overall number of TNFα positive erythroblasts, indicating enhanced sensitivity of *Tet2-/-* erythroblasts to inflammation (Fig. 3 J). This finding is intriguing as it suggests erythrocytes themselves may be a source of TNFα (Straat *et al.*, 2015; Karsten, Breen and Herbert, 2018).

We next examined erythroid colonies by methylcellulose in both the bone marrow and the spleen. *VavTet2*$^{-/-}$ but not *VavTet2*$^{-/-}$*Ripk1*$^{D/D}$ mice displayed expanded CFU-E colonies but not BFU-E or CFU-GEMM (Fig. 3 K and Fig. S2, H and I). This result suggests that the compensatory expansion of CFU-E colonies in *VavTet2*$^{-/-}$ bone marrow (Qu *et al.*, 2018) due to stress erythropoiesis can be alleviated by inhibiting Ripk1 activity within the bone marrow microenvironment.

Chronic necroptosis in TKO mice results in decreased RBC precursors and increased extramedullary hematopoiesis partially rescued by crossing to *Ripk1+/-* or *Ripk1*$^{D/D}$ mice

VavCre $^{+}$*Bax* $^{F/F}$*Bak* $^{-/-}$*Bid* $^{-/-}$ (TKO) mice develop bone marrow failure driven by necroptosis-mediated inflammation (Wagner *et al.,* 2018). Using TKO mice as a well as mice crossed to haploinsufficient *Ripk1* (TKO*Ripk1+/-*) (Berger *et al.*, 2014) and TKO mice crossed to *Ripk1*$^{D138N/D138N\ (D/D)}$ (Polykratis *et al.*, 2014) to specifically target Ripk1 kinase function, we evaluated erythropoiesis.

We found that TKO mice have significantly decreased cellularity in the bone marrow and increased splenic weights, indicative of extramedullary hematopoiesis. Both cellularity and spleen weights could be restored by crossing TKO mice to either *Ripk1+/-* or *Ripk1*$^{(D/D)}$ (Fig. 4, A and B). It is important to note the decreased cellularity observed here, but not by Wagner et al., is due to the fact that these numbers reflect marrow that has not had red cells removed by lysis. This suggests that erythrocytes are substantially decreased in these mice.

We then evaluated erythropoiesis in the bone marrow and spleen of WT, TKO, TKO*Ripk1+/-*, and TKO*Ripk1*$^{(D/D)}$ mice. TKO mice showed significantly decreased numbers of Ter119^{+} cells compared to WT mice. Both TKO*Ripk1+/-* and TKO*Ripk1*$^{(D/D)}$ mice had significantly

restored populations. We also observed a compensatory increase in extramedullary Ter119^{+} cells in the spleen, however this was not significantly reduced in either TKO*Ripk1+/-* and TKO*Ripk1*$^{(D/D)}$ mice, reflecting the unique, highly necroptotic microenvironment of marrow compared to the spleen (Fig. 4, C and D).

We observed significantly decreased RBC count and reticulocytes in *VavTKO* which could be increased in TKO*Ripk1+/-* and TKO*Ripk1*$^{(D/D)}$ mice (Fig. 4, E and F). TKO mice also displayed significantly decreased numbers of all populations of erythroid precursors. TKO*Ripk1*$^{(D/D)}$ mice were able to restore both the Baso and Ortho populations in the marrow, but not the spleen. Immature erythroid precursors evaluated by methylcellulose were also significantly decreased in TKO mice (Fig. 4 G and Fig. S3, A-C). These results suggest that in settings of necroptosis, there is not a defect in red cell maturation, but rather a broader impact on the bone marrow microenvironment that is particularly detrimental to early nucleated, erythroid blasts.

As with *VavTet2* mice, we evaluated sternum marrow by immunofluorescence. We found, similarly, that the percentage of TNFα positive cells that are erythrocytes was significantly reduced in TKO mice while there was no difference in overall nucleated cell numbers (Fig. 4, H- J).

A risk reduction model reveals that targeted TNFα biologics reduce MDS risk in approved use patient groups

Our data suggest that modulating inflammation by targeting underlying necroptosis may be beneficial to anemia and MDS. TKO mice also benefited from a short course of the anti-TNFα biologic, Enbrel (Wagner *et al.,* 2018). To test this hypothesis in humans, we developed a risk reduction model using the Vanderbilt's SD to evaluate approved-use drugs (to induce "rescue"),

267 including the targeted TNFα biologics Enbrel and Humira (Fig. 5, A and B, and Fig. S3, D-F). We
268 also tested a first-line immunosuppressive drug methotrexate, common non-steroidal anti-
269 inflammatory drugs (NSAID) Celebrex and naproxen, as well the analgesic, acetaminophen.
270 Compared to disease groups alone (not sub-categorized by medication), we found the
271 associated OR for MDS and disease groups 1 and 2 were significantly reduced in individuals
272 taking either Enbrel or Humira (OR=3.5, 95% CI [3.90-5.51] versus OR=3.0 , 95% CI [2.04-5.64]
273 and OR 3.6, 95% CI [4.28-5.73] versus OR=2.1, 95% CI [1.43-3.83]). Additionally, there was no
274 benefit for methotrexate, common NSAIDs, (ibuprofen, Celebrex, naproxen), or acetaminophen
275 (Fig. 5 C).

276 This data suggests that targeted anti-inflammatory biologics may warrant further study
277 as therapy for MDS patients with chronic inflammation. When used in combination with EPO,
278 the negative impact of TNFα on EPO may be lessened, resulting in better overall response to
279 therapy (Rusten LS *et al.,* 1995). These drugs are desirable, as they are already widely clinically
280 used and would be strong candidates for repurposing.

281 Overall, our results from human phenomic, human genetic, and mouse studies highlight
282 the detrimental impact of inflammation on the erythroid compartment. We propose this can
283 be due in part to genetic predisposition, such as loss of TET2 or increased RIPK1 genetically-
284 determined expression. Phenome-wide association study of SNPs in the RIPK1 locus using the
285 UK Biobank reveals significant effect on multiple inflammatory phenotypes, including
286 endocarditis and MDS. TET2 also associates with inflammatory phenotypes. BioVU analysis
287 shows interaction between TET2 and RIPK1, suggesting altered phenotypic effect of the gene
288 expression of one by the gene expression of the other. In individuals with the lowest TET2

289 expression, we find increased RIPK1 expression in hemolytic anemia. ATAC-Seq analysis also
290 reveals altered chromatin accessibility in *Ripk1* in the absence of *Tet2* relative to wildtype in
291 three replicates, indicating the impact of *Tet2* on open chromatin and transcription-factor
292 binding at *Ripk1*.

293 We propose that genetic predisposition in combination with an additional inflammatory
294 trigger such as infection, will cause stress within the marrow that is particularly damaging to the
295 erythroid compartment and promotes anemia and potentially over time, bone marrow failure.
296 Our data confirms and extends previous reports in small populations that autoimmune and
297 inflammatory syndromes associate with MDS (Wolach *et al.*, 2016). Inflammation is known to
298 impair the erythropoietic compartment (ACD) (Weiss *et al,,* 2005). Our findings now add Ripk1
299 and necroptosis to the critical pathways that modulate erythropoiesis.

300 Our mouse models also confirm the association between inflammation and bone
301 marrow failure in the setting of *Tet2* loss. We find that loss of *Tet2* primes the bone marrow
302 environment for increased sensitivity to LPS resulting in necroptotic death and impaired early
303 erythroid precursors. Overwhelming death in the TKO marrow is also detrimental to all
304 erythroid progenitors and loss of Ripk1 only partially restores these precursors. The differences
305 between these models suggest a continuum of disease progression. While few CHIP patients
306 actually progress to MDS, the majority of MDS patients present with mutations in one or more
307 of these genes. Our results begin to elucidate factors that may cooperate with CHIP mutations
308 to promote MDS. Loss of Tet2 function may increase sensitivity of the marrow to inflammatory
309 insults, particularly latent viral infections such as EBV. A recent study that suggests that LPS-
310 treated *Tet2-/-* donor marrow had increased capacity for clonal expansion in recipient mice,

311 which could be partially reduced by targeting inflammatory pathways (Chen *et al.*, 2018).
312 Targeting inflammation with TNFα biologics or, alternatively, Ripk1 specific kinase inhibitors
313 such as necrostatin drugs (Degterev *et al.*, 2005) warrant further study as potential therapeutic
314 targets in MDS.
315
316 **Materials and Methods**
317 Mice
318 *VavCreBaxBakBid* (TKO mice) were made as previously described (Wagner et al., 2018).
319 TKO mice were crossed to *Ripk1*^{K45A} mice, which harbor loxP sites flanking exon 4 of *Ripk1*
320 (obtained as a kind gift from Peter Gough (Berger *et al.*, 2014)) to achieve TKO*Ripk1+/-* mice.
321 TKO mice were also crossed to transgenic *Ripk1*$^{D138N/D138N}$ mice (obtained as kind gift from
322 Michelle Kelliher (Polykratis A et al., 2014)). To achieve TKO*Ripk1*$^{D/D}$ mice, *Tet2*$^{F/F}$ mice
323 (obtained as a kind gift from Omar Abdel-Wahab (Moran-Crusio *et al.*, 2011)) were crossed with
324 mice harboring both *VavCre+ and Ripk1*$^{D138N/D138N}$. Mice were backcrossed at least 9
325 generations with C57BL/6J mice from The Jackson Laboratory. Mice were also rederived into a
326 C57BL/6 background from Jackson Laboratories (Stock No. 000664, RRID: IMSR_JAX:000664) in
327 order to move them into the Vanderbilt Barrier Facility. The Vanderbilt University Institutional
328 Animal Care and Use Committee approved all experiments (IACUC # M1900021, V18/00188).
329
330 LPS injection of mice
331 Mice were intraperitoneally injected with 1.5 mg/kg LPS (L4391; Millipore-Sigma) and
332 monitored for at least 6 hours following injection and provided with IP-saline when needed to
333 prevent dehydration. Animals were sacrificed 18 hours later, and bone marrow, spleen and

sternums were harvested for flow cytometry and immunofluorescence analysis respectively, described below.

Flow cytometry

Single cell suspension of isolated bone marrow and spleens were obtained by flushing both femurs and tibias with media or 3% FBS. Cells were filtered, counted, diluted, and stained on ice at 1:200 with CD16/CD32 (Fc Block) (553142; BD Biosciences, RRID:AB_394657). Red blood cell surface makers were then added at 1:200 for 30 minutes on ice in the dark. Samples were washed two times and flow was run (without fixation) within approximately an hour of staining. The following antibodies were used: APC Rat anti-mouse CD44 (IM7) (559250; BD Biosciences, RRID:AB_398661), FITC Rat anti-mouse CD71 (C2) (561936; BD Biosciences, RRID:AB_11153845), PE Rat anti-mouse TER-119 (553673; BD Biosciences, RRID:AB_394986). Immediately prior to analysis, samples were stained with Propidium Iodide (P4864; Millipore-Sigma) for viability. Samples were run on a BD LSRFortessa flow cytometer with FACSDiva software and analyzed using FlowJo software (RRID:SCR_008520), gating on viable cells. At least 50,000 events per sample were collected.

For ROS staining, bone marrow and spleen (without RBC lysis) was incubated with 5 μm of dihydroethidium (DHE) (Cat#D11347, ThermoFisher Scientific (Invitrogen)) for 30 minutes in complete IMDM. Cells were harvested, washed in 1x PBS and immediately run for flow cytometry using a BD FACSCalibur (BD Biosciences) and CellQuest Pro acquisition software

(RRID:SCR_014489). Samples were analyzed using FlowJo software (RRID:SCR_008520) and minimum of 20,000 events per sample were collected.

Immunofluorescence

Sternums were harvested, fixed in 10% formalin for at least 24 hours, and decalcified with 13% formic acid for 1 hour. Samples were then paraffin-embedded and sectioned approximately 3 μm thick. For TNFα staining, samples were deparaffinized in Xylene overnight, blocked for 1 hour at room temperature (Blocking buffer: 1% BSA, 10% Normal goat serum, and 0.3% Triton X-100), and incubated with anti-TNFα antibody overnight at 4°C (ab9739; Abcam, RRID:AB_308774) at 7.5 μg/ml followed by anti-mouse AlexaFluor 546 secondary (Cat# A-11030, Invitrogen, RRID:AB_144695) (1:1500) for 1 hour at room temperature. All staining was done in combination with Ter119 (550565; BD Biosciences, RRID:AB_393756) at 1:50 primary overnight and 1:200 secondary AlexaFluor 488 (Cat# A32723, Invitrogen, RRID:AB_2633275) followed by DAPI (D1306; Thermo Fisher Scientific (Invitrogen)) and mounted with ProLong™ Gold Antifade reagent (P10144; Life Technologies, USA). Sternums were imaged with a 40X water objective on an LSM 710 Meta inverted scanning confocal microscope located within Vanderbilt University's Cell Imaging Shared Resource (CISR) core. Images were viewed and scale bars were added with Zeiss ZEN imaging software (RRID:SCR_013672). Images in all figures are representative of a single z-plane.

Image analysis

CellProfiler™ Software (v3.1.8, Broad Institute, Cambridge, MA, USA, RRID:SCR_007358) was used to determine the number of cells (nuclei per field), percentage of Ter119 positive nucleated cells (erythroid progenitors), and percentage of TNFα positive cells expressing Ter119. Briefly, a pipeline was created to analyze confocal images (czi files). Primary objects including nuclei, Ter119 positive cells and TNFα positive cells were identified using global thresholding. Images were then masked using nuclei as objects to identify nucleated Ter119 cells and nucleated TNFα positive cells. Nucleated TNFα positive cells were further masked with nucleated Ter119 positive cells. Primary objects from all masking steps were then identified. Percent Ter119 positive was calculated as: (Ter119+ nuclei/all nuclei) X 100 and Percent TNFα positive with Ter119 was calculated as: (TNFα positive nucleated cells with Ter119/TNFα positive nucleated cells) X 100. A minimum of at least 5 images per sternum per mouse were analyzed from a single z-plane of a 40X confocal image (approximately 20,000 cells total per mouse). An example pipeline has been provided in Fig. S2E.

Colony forming unit assays

Bone marrow and splenocytes were harvested as previously described, and single cell suspensions were lysed for red blood cells and counted. A 10X concentration of $3x10^5$ bone marrow cells and $5x10^5$ splenocytes were resuspended in MethoCult™ M3134 (03134; Stem Cell Technologies) supplemented with FBS (16000044; Gibco (ThermoFisher Scientific)), BSA (BP1600-100; Fisher Scientific), SCF (255SC010; R&D Systems), IL-3 (403ML010CF, R&D Systems), IL-6 (406ML005CF; R&D Systems), EPO (287TC500; R&D Systems), Apo-transferrin (T1428; Millipore-Sigma), and insulin (16634; Millipore-Sigma). Samples were plate in triplicate

in 35 mm dishes and incubated at 37°C in 5% CO_2. Plates were counted 48-72 hours after plating to evaluate CFU-E colonies and 10 days after plating to evaluate BFU-E and CFU-GEMM.

Western blot

Bone marrow and splenic tissue were harvested and made into a single cell suspension followed by lysis in HEPES protein buffer (25mM HEPES pH 7.5, 250mM Sodium Chloride, 2mM EDTA, 0.5% NP-40, 10% Glycerol, 1X Complete Mini Protease Inhibitor, EDTA free (Roche (Millipore-Sigma)) and 1x Complete Mini Phosphatase Inhibitor (Roche (Millipore-Sigma)). Samples were denatured by boiling in Laemmli Buffer (containing β-mercaptoethanol), and then run by SDS-PAGE. The following antibodies were used: Ripk1 (610459; BD Biosciences, RRID:AB_397832), Ripk3 (NBP1-77299; Novus Biologicals, RRID:AB_11040928), TNFα (ab9739; Abcam, RRID:AB_308774), GPx-4 (sc-166570; Santa Cruz Biotechnology, RRID:AB_2112427), PRX II (sc-515428; Santa Cruz Biotechnology), and β-Actin (A5441; Sigma, RRID:AB_476744).

Human comorbidity analysis

Comorbidity analysis was performed using the Vanderbilt University Medical Center Synthetic Derivative (SD). The SD consists of approximately 2.8 million de-identified records that contain basic clinical and demographic information of individuals seen at Vanderbilt University Medical Center. Analysis was done as previously described. (Salisbury-Ruf et al., 2018) For a pair of disease traits, we tested for departure from the null hypothesis of independence using Pearson's Chi-squared test. Summary of results can be found in the corresponding figure and supplemental figures. European-ancestry subjects (all ages and all

genders) were used to create a 2 x 2 contingency table to determine the odds ratio (OR), which was presented in the heat map. Importantly, the results are not driven by sample size or patient age as there was no trend between patient numbers or age and OR. For results presented in Supplemental Figure 3 G-I, we also tested each drug individually compared to MDS. Interestingly, prednisone (steroidal anti-inflammatory) and methotrexate alone substantially increased MDS risk. This result may be due to steroid-induced lymphopenia and immunosuppression, respectively and thus increased infection risk.

Human genetic analyses

We performed systematic analyses of the effect of RIPK1 on inflammation and erythropoiesis. We integrated two large-scale biobank resources with extensive human phenome data.

First, we leveraged the UK Biobank (Neale mega-GWAS) to analyze SNP-level effects on a broad spectrum of inflammatory and hematologic disorders. We performed a phenome-wide association study and identified the top SNP association in the RIPK1 locus (within 1 Mb, consistent with the gene's local regulatory region used in the PrediXcan analysis (Gamazon *et al.,* 2015) for each tested phenotype in the UK Biobank. We tested 9,122 variants in the locus and all 2,419 phenotypes, of which only a subset is involved in inflammation and erythropoiesis. We applied Bonferroni correction based on the total number of SNP-phenotype pairs tested and define significance as $p<2.26e-09$; this approach is highly conservative since not all phenotypes are related to inflammation or erythropoiesis and some phenotypes are not independent.

Next, we estimated the genetically-determined component of gene expression for downstream association analysis with disease. The genetic component of gene expression is estimated from an imputation model (Elastic Net (Gamazon *et al.*, 2015)) with mixing parameter a = 0.5) trained on a reference transcriptome data set (the Genotype-Tissue Expression (GTEx) project v6p (Consortium *et al.*, 2015; Gamazon, Eric R., Ayellet V. Segrè, 2018). Imputation performance for a gene in a tissue is evaluated using 10-fold cross-validation (between imputed expression and directly measured expression), as previously described (Gamazon *et al.*, 2015).

We applied PrediXcan to whole-genome genetic data from BioVU (n=29,366), a Vanderbilt University resource that links human DNA samples and genetic data to de-identified electronic health records (EHRs). BioVU has been previously described (Roden *et al.*, 2008). We estimated the genetic component of RIPK1 and TET2 in the BioVU samples and tested each gene's effect on hemolytic anemia and inflammatory disorders. We performed logistic regression with disease status as the response variable, the inferred genetic component of gene expression as predictor, and genomic ancestry (first principal component), sex, and age as covariates. In secondary analyses, we also tested the phenotypic effect of the genetically determined expression of MLKL, RIPK3, BAX, and CASP8.

To replicate the association between IBD and RIPK1 expression, we leveraged two additional GWAS. One included 1,963 individuals (Rioux *et al.*, 2007) as well as a second GWAS of IBD or ulcerative colitis (UC) of 86,640 European ancestry individuals (Liu *et al.*, 2015). We applied summary-statistics based PrediXcan on these data to test for non-zero effect of RIPK1 expression on the inflammatory disorder.

To determine whether RIPK1 is associated with impaired erythropoiesis in TET2 deficient humans, we evaluated the BioVU subjects with the lowest genetically determined TET2 expression, that is, in the bottom ~12.5% of the distribution, for association of RIPK1 with hemolytic anemia. Our methodology identifies individuals in the EHR closest to the gene (TET2) knockout. Briefly, from a reference panel of n samples with directly measured expression levels $y_1, y_2, \ldots, y_n$, we build a model that solves the following optimization problem:

$$\hat{\beta} = \arg\min_{\beta} \ (1/2)\sum_{i=1}^{n}(y_i - x_i^T\beta)^2 + \ \lambda\left(\left(\frac{1-\alpha}{2}\right)\|\beta\|_2^2 + \alpha\|\beta\|_1\right) \qquad (*)$$

Here $\alpha = 0.50$. The prediction of *y* on new genotype data X_{new} from an individual in the EHR is given by:

$$\widehat{y_{new}} = X_{new}\hat{\beta}$$

A reference human population panel such as the 1000 Genomes project can be used to generate the sampling distribution in a specific ancestry. Here we leveraged the EHR data and the extensive phenotype information available in it for any subsample. The bottom of the distribution (e.g., Fig. 1 F) can be used to identify the individuals, and their phenome, closest to a 'human knockout' in the population.

Given the RIPK1 association among TET2 deficient individuals, we tested explicitly for the presence of gene-gene interaction (statistical epistasis) between the RIPK1 and TET2 to determine whether the effect of either gene on hemolytic anemia and inflammatory traits is modified by the other gene. We used the following logistic model:

$$\log\left(\frac{P[Y=1|x_1,x_2]}{1-P[Y=1|x_1,x_2]}\right) = \beta_0 + \beta_1 x_1 + \beta_2 x_2 + \beta_3 x_1 x_2$$

where Y is the disease status and x_1 and x_2 are the genetically determined expression of TET2 and RIPK1 with effect sizes β_1 and β_2, respectively. The interaction effect β_3 can be estimated by maximizing the likelihood function and its standard error calculated through the inverse of the Hessian of the likelihood. We used the *glm* implementation in R. A test of the null hypothesis of no interaction can be performed by testing whether $\beta_3 = 0$. We performed permutation analysis (n=1000), using the proportion of permuted (null) datasets with at least as many associations ($p<0.05$) with inflammatory diseases to estimate the significance of enrichment for interaction effects on these phenotypes.

Statistical analysis of mouse models

Unless specified above, all additional analyses were completed using GraphPad Prism (GraphPad Software). Data was analyzed with either one-way or two-way ANOVA and all pairwise comparisons were made with Student's t-test as indicated in the figure. The following denote statistical significance: ns = not significant, *p<0.05, **p<0.01,***p<0.005,****p<0.001. For Pearson's Chi-squared, a p-value of 0 was reported as < 1.0×10^{-300}. All error bars indicate SEM (standard error of the mean).

Online Supplemental Material

All data in Fig. S1 corresponds to analysis in Figs. 1 and 2. Fig. S1 A is a table of hematological disorders, ICD 9 and 10 codes, Odds Ratio (OR), 95% Confidence Interval (CI), number of subjects within the Vanderbilt University Medical Center Synthetic Derivative (SD), and Pearson's Chi-

506 squared statistical analysis corresponding to Fig. 1 B. Fig. S1 B is a scatter plot of patient number
507 versus OR for the indicated disorder. Fig. S1 C is a table of all diseases included within the super-
508 inflammatory cohort, and Fig. S1, D and E correspond to comorbidity analysis in Fig. 1 C as
509 described. Fig. S1, F and G correspond to comorbidity analysis between MDS and infections in
510 Fig. 1 D. Fig. S1, H and I are additional PrediXcan results showing increased RIPK1 expression in a
511 BioVU cohort as well as two additional cohorts including the European IBD GWAS and a GWAS
512 for Crohn's disease as indicated in Methods.
513
514 Data in Fig. S2 corresponds to analysis of *VavTet2*$^{-/-}$ mice as in Fig. 3. Fig. S2 A shows western blot
515 analysis of untreated and LPS treated spleens harvested from WT, *VavTet2*$^{-/-}$, and *VavTet2*$^{-/-}$*Ripk1*
516 $^{D/+}$ mice corresponding to Fig. 3 A. Fig. S2 B is flow cytometry data of all Ter119+ bone marrow
517 cells with and without LPS. Fig. S2 C is flow analysis for superoxide indicator DHE in all splenocytes
518 from indicated mice. Fig. S2 D is an example CellProfiler™ Pipeline (as described in the methods)
519 and Fig. S2 E are additional images from untreated sternums as indicated. Fig. S2 F is analysis of
520 the number of Ter119+ cells quantified by CellProfiler™ for the indicated genotypes with and
521 without LPS. Fig. S2 G corresponds to the overall number of nuclei per field without LPS (no
522 treatment=NT) and with LPS as indicated. Fig. S2, H and I are the number of BFU-E and CFU-
523 GEMM colonies in the bone marrow and spleen corresponding to Fig. 3 K.
524
525 Data in Fig. S3 corresponds to analysis in Fig 4. Flow cytometry of splenic erythrocytes in WT,
526 TKO, *Vav*TKO*Ripk1* (*+/-*) and *Vav*TKO*Ripk1*$^{D/D}$ mice in Fig. S3 A corresponds to Fig. 4 C-G. Fig. S3,
527 B and C are colonies numbers from methylcellulose assay from bone marrow and spleen,

respectively corresponding to CFU-E, BFU-E, and CFU-GEMM from mice indicated above. Fig. S3 D is a table of ICD9 and ICD10 codes corresponding to disease groups shown in Fig. 5 B. Fig. S3 E-F correspond to Fig. 5 C including a table with statistical analysis of disease groups with MDS and a scatter plot of number of cases versus OR for the indicated disease groups. Fig. S3 G-I is comorbidity analysis between MDS and drugs alone with statistics (table) as well as number of patients plotted against OR values.

Acknowledgements

The authors thank Dr. Michelle Kelliher for the Ripk1^{D138N} mice and Dr. Omar Abdel-Wahab for the Tet2$^{F/F}$ mice, the following core resources at Vanderbilt University Medical Center: The Flow Cytometry Shared Resource and Translational Pathology Shared Resource Core (TPSR). Experiments were performed in part using the Vanderbilt Cell Imaging Shared Resource (supported by NIH grants CA68485, DK20593, DK58404, DK59637 and EY08126) at Vanderbilt University.

This research was supported by the following grants and awards: National Institutes of Health, National Heart, Lung, and Blood Institute grant 1R01HL133559 (SSZ), I01 BX002250 VA MERIT review (SSZ), CDMRP W81XWH-16-1-0057 (SSZ).

E.R.G. is supported by the National Human Genome Research Institute of the National Institutes of Health under Award Number R35HG010718. The content is solely the responsibility of the

authors and does not necessarily represent the official views of the National Institutes of Health.

E.R.G. receives an honorarium from the journal *Circulation Research*, as a member of the Editorial Board. He also performs consulting on pharmacogenetic analysis with the City of Hope / Beckman Research Institute.

Author contributions: Salisbury-Ruf CT, Gamazon ER, and Zinkel SS conceived of the project, designed, performed, and analyzed experiments, created figures and wrote the manuscript. Dugger, TC performed and analyzed experiments and assisted with the manuscript

Figure Legends

Figure 1. **MDS and anemia associate with inflammatory diseases and infections, corresponding to increased RIPK1 expression. (A)** Experimental approach and workflow schematic indicating a phenomic approach using de-identified electronic health records (EHRs) within Vanderbilt University's Synthetic Derivative (SD), SNP associations in the UK Biobank, and analysis of genetically determined gene expression (PrediXcan) analysis to identify associations between inflammatory diseases and anemias, including Myelodysplastic syndrome (MDS). These findings are supported by experimental analysis of the erythroid compartment in *VavCreTet2* and *VavCre*TKO mouse models and supported by additional phenomic results using a risk reduction model. **(B)** Phenomic analysis of comorbidity between the indicated diseases known to be associated with MDS (all ages, all sexes, European ancestry). Odds ratio (OR), denoted in the heat maps, was calculated using 2x2 contingency tables using patient numbers

derived from the Vanderbilt SD. **(C)** Phenomic analysis as in (B) of a "super-inflammatory" cohort (>300,000 subjects) with control diseases compared to indicated anemias. **(D)** Phenomic analysis as in (B) of an MDS patient cohort with infectious diseases subcategorized by etiology of infection as acute or latent.

Figure 2. **PrediXcan reveals increased RIPK1 and decreased TET2 expression associated with inflammation and epistatic interaction between these two genes**.
(A) The most significant SNP association with the inflammatory trait "I38 Endocarditis" within RIPK1 in the UK Biobank (with 7637 cases) is rs114183703 (p=1.9e-13). Locus zoom plot shows the -log10 transformed p-value (y-axis) and the position (x-axis) of local association results at RIPK1. The r^2 represents the linkage disequilibrium of nearby SNPs with rs114183703. **(B)** Several SNPs at the RIPK1 locus were found to be highly significantly associated with inflammatory traits and MDS in the UK Biobank. The red dash indicates the conventional GWAS threshold for significance (p=5e-08). **(C)** PrediXcan analysis methodology using common variants to predict the direction of genetically determined gene expression associated with disease. **(D)** PrediXcan analysis results for hereditary anemia (Phecode=282) in a BioVU cohort (n=13409) assessed for expression of RIPK1 in primary analysis and CASP8, MLKL, BAX, and RIPK3 in a secondary analysis. Direction of genetically determined gene expression is indicated by the arrow and plotted against -log10 p-value. **(E)** PrediXcan analysis of a BioVU cohort for inflammatory diseases associated with decreased TET2 expression (n=13409). **(F)** Schematic of TET2 gene expression among 23,000 BioVU individuals. The lowest 12.5% of TET2 expressers comprised 2,898 individuals. **(G)** These individuals were analyzed for disease association of

RIPK1 expression, which was significantly higher among non-autoimmune hemolytic anemia cases than controls (Mann-Whitney U test $p<2.2x10^{-16}$). **(H)** Diseases which show epistatic interaction between RIPK1 and TET2. **(I)** ATAC-Seq data track reveals altered chromatin accessibility across the *Ripk1* locus in *Tet2*$^{-/-}$, relative to WT, embryonic stem cells in three independent replicates. Visualization was generated using IGV. Areas highlighted in blue correspond to regions of distinct chromatin accessibility in WT compared to *Tet2*$^{-/-}$ across all replicates. Genomic coordinates used the mm10 genome build.

Figure 3. **Erythrocytes from *VavCreTet2* mice are highly sensitive to LPS due increased necrotic cell death in the bone marrow. (A)** Immunoblot analysis of bone marrow (and spleen Fig. S2 A) from WT, *VavTet2*$^{-/-}$, and *VavTet2Ripk1*$^{D/+}$ mice without and with acute LPS (IP injection of 1.5 mg/kg, 18 hours) for Ripk1, truncated Ripk1 (tRipk1) and Ripk3, as well as TNFα and anti-oxidants glutathione peroxidase 4 (GPX4) and peroxiredoxin II (PRXII). Blots are representative of three independent replicates. **(B-H)** Flow cytometry analysis of erythrocyte precursors in the bone marrow with and without LPS. Erythroid cells were gated by $PI^{neg}Ter119^{+}CD44^{+}FSC$ and numbers of cells were calculated for the indicated populations including **(B)** proerythroblasts, **(C)** basophilic erythroblasts, **(D)** poly erythroblasts, **(E)** ortho erythroblasts, **(F)** reticulocytes, and **(G)** mature RBCs, n= 5, 5, 6, for WT, *VavTet2*$^{-/-}$, and *VavTet2Ripk1*$^{D/+}$ mice without LPS and n= 7, 12, 4 with LPS, respectively. **(H)** Total bone marrow treated with LPS as in (A) and analyzed by flow for percent positivity of the superoxide indicator dihydroethidium (DHE). n=7, 12, 4 for the indicated genotypes. **(I)** Representative confocal images of immunofluorescence staining of sternum bone marrow from mice treated with LPS as

in (A) (See Fig. S2 E for images of untreated mice). TNFα = AlexaFluor546 (Red), Ter119= AlexaFluor488 (green) and nuclear stain with DAPI. Zoomed in images correspond to indicated boxes in the overlay. **(J)** Cell Profiler analysis of confocal images for the indicated mice for percent of nucleated Ter119 positive cells (top) and percent of TNFα cells positive for Ter119 (bottom). A minimum of 5 fields (40x) were analyzed per sternum per mouse. n=4,4,3 for WT, *VavTet2*$^{-/-}$, and *VavTet2Ripk1*$^{D/+}$ mice respectively. (**K)** Methylcellulose assay for fold change of colony forming unit-erythroid (CFU-E) populations from the bone marrow and spleen from the indicated mice. n=5,5,3 for WT, *VavTet2*$^{-/-}$, and *VavTet2Ripk1*$^{D/D}$ mice respectively. Data was analyzed by two-way ANOVA with student's t-test for B-G and one-way ANOVA with for student's t-test for H, J, and K. ns = not significant, *p<0.05, **p<0.01, ***p<0.005, ****p<0.001.

Figure 4. **TKO mice have increased extramedullary hematopoiesis which can be partially rescued by crossing to *Ripk1+/-* or *Ripk1*$^{D/D}$ mice. (A)** Number of cells in the bone marrow (all four long bones) **(B)** and total spleen weights (mg) from WT, *Vav*TKO, *Vav*TKO *Ripk1 (+/-)* and *Vav*TKO*Ripk1* $^{D/D}$ mice. n=11, 9, 7, and 7 for the indicated genotypes. (C,D)Flow cytometry analysis of bone marrow and spleen for total number of all Ter119+ positive cells. **(E)** Representative flow cytometry plots of bone marrow for the indicated genotypes. Cells were first gated as PI^{neg}Ter119^{+} and then gated based on FSC v CD44^{+} as shown. ProE=proerythroblasts, Baso=basophilic erythroblast, Poly=poly erythroblasts, Ortho=Ortho erythroblasts, Retic=reticulocytes and RBC=red blood cells. **(F)** Number of RBCs and reticulocytes for mice gated in E. n=11, 9, 7, and 7 for the indicated genotypes. **(G)** Number of

red cell precursors for the indicated genotypes as in (F). **(H)** Representative confocal images of immunofluorescence staining of sternum bone marrow. TNFα = AlexaFluor546 (Red), Ter119= AlexaFluor488 (green) and nuclear stain with DAPI. Zoomed in images correspond to indicated boxes in the overlay. **(I)** Cell Profiler™ analysis of confocal images for the percent of TNFα cells positive for Ter119. **(J)** the average number of cells within a field. A minimum of 5 fields (40x) were analyzed per sternum per mouse. Data was analyzed by one-way ANOVA with student's t-test for A-D, F, I, and J and two-way ANOVA with for student's t-test for G. ns = not significant, *p<0.05, **p<0.01, ****p<0.001.

Figure 5. **Phenomic analysis using a risk reduction model reveals targeted TNFα biologics reduce MDS risk in multiple patient groups.**

(A) Schematic of workflow used to develop risk reduction model for MDS. **(B)** Table indicating patient groups (1-4) corresponding to diseases with approved therapeutic use of the indicated drugs including methotrexate, TNFα biologics (Enbrel and Humira), non-steroidal anti-inflammatories (NSAID) including ibuprofen, Celebrex and naproxen, as well as the analgesic acetaminophen. **(C)** Comorbidity analysis of MDS with each group indicated in (B) further subcategorized by individuals prescribed the indicated drug. Odds ratio (OR) is indicated within the heat map, and all comparisons are statistically significant (Pearson's chi-squared analysis can be found in Fig. S3 E). OR are not driven by patient numbers as indicated in Fig. S3 F.

References

Banerjee, T. *et al.* (2019) 'Blood Reviews Flaming and fanning : The Spectrum of in fl ammatory

661 in fluences in myelodysplastic syndromes', 36, pp. 57–69. doi: 10.1016/j.blre.2019.04.004.
662 Berger, S. B. *et al.* (2014) 'Cutting Edge: RIP1 Kinase Activity Is Dispensable for Normal
663 Development but Is a Key Regulator of Inflammation in SHARPIN-Deficient Mice', *The Journal of*
664 *Immunology*, 192(12), pp. 5476–5480. doi: 10.4049/jimmunol.1400499.
665 Busque, L. *et al.* (2012) 'Recurrent somatic TET2 mutations in normal elderly individuals with
666 clonal hematopoiesis', *Nature Genetics*. Nature Publishing Group, 44(11), pp. 1179–1181. doi:
667 10.1038/ng.2413.
668 Bycroft, C. *et al.* (2018) 'The UK Biobank resource with deep phenotyping and genomic data',
669 *Nature*, 562(7726), pp. 203–209. doi: 10.1038/s41586-018-0579-z.
670 Carpenter, A. E. *et al.* (2006) 'CellProfiler: image analysis software for identifying and
671 quantifying cell phenotypes', *Genome Biology*, 7(10), p. R100.
672 Chen, S. *et al.* (2018) 'Inhibition of Inflammatory Signaling in Tet2 Mutant Preleukemic Cells
673 Mitigates Stress-Induced Abnormalities and Clonal Hematopoiesis', *Cell Stem Cell*. Elsevier Inc.,
674 23(6), pp. 833-849.e5. doi: 10.1016/j.stem.2018.10.013.
675 Cogle, C. R. (2015) 'Incidence and Burden of the Myelodysplastic Syndromes', *Current*
676 *Hematologic Malignancy Reports*, 10(3), pp. 272–281. doi: 10.1007/s11899-015-0269-y.
677 Consortium, T. Gte. *et al.* (2015) 'The Genotype-Tissue Expression (GTEx) pilot analysis:
678 Multitissue gene regulation in humans', *Science*, 348(6235), pp. 648–660. doi:
679 10.1126/science.1262110.
680 Dayyani, F. *et al.* (2010) 'Cause of Death in Patients with Lower-Risk Myelodysplastic
681 Syndrome', *Cancer*, 116(9), pp. 2174–2179. doi: 10.1002/cncr.24984.
682 Degterev, A. *et al.* (2005) 'Chemical inhibitor of nonapoptotic cell death with therapeutic

potential for ischemic brain injury', *Nature Chemical Biology*, 1(2), pp. 112–119. doi: 10.1038/nchembio711.

Gamazon, Eric R., Ayellet V. Segrè, M. van de B. (2018) 'Using an atlas of gene regulation across 44 human tissues to illuminate complex 2 disease- and trait-associated variation', *Nat Genet*. Springer US, 50(July). doi: 10.1038/s41588-018-0154-4.

Gamazon, E. R. *et al.* (2015) 'A gene-based association method for mapping traits using reference transcriptome data.', *Nature genetics*, 47(9), pp. 1091–1098. doi: 10.1038/ng.3367.

Ghoti, H. *et al.* (2007) 'Oxidative stress in red blood cells, platelets and polymorphonuclear leukocytes from patients with myelodysplastic syndrome', *European Journal of Haematology*, 79(6), pp. 463–467. doi: 10.1111/j.1600-0609.2007.00972.x.

Higgins, J. M. *et al.* (2014) 'Age-Related Clonal Hematopoiesis Associated with Adverse Outcomes', *New England Journal of Medicine*, 371(26), pp. 2488–2498. doi: 10.1056/nejmoa1408617.

Hotz, M. J. *et al.* (2018) 'Red blood cells homeostatically bind mitochondrial DNA through TLR9 to maintain quiescence and to prevent lung injury', *American Journal of Respiratory and Critical Care Medicine*, 197(4), pp. 470–480. doi: 10.1164/rccm.201706-1161OC.

Hsu, H. Y. and Wen, M. H. (2002) 'Lipopolysaccharide-mediated reactive oxygen species and signal transduction in the regulation of interleukin-1 gene expression', *Journal of Biological Chemistry*, 277(25), pp. 22131–22139. doi: 10.1074/jbc.M111883200.

Karsten, E., Breen, E. and Herbert, B. R. (2018) 'Red blood cells are dynamic reservoirs of cytokines', *Scientific Reports*. Springer US, 8(1), pp. 1–12. doi: 10.1038/s41598-018-21387-w.

Kim, S. Y. *et al.* (2014) 'Myelodysplastic syndrome evolving from aplastic anemia treated with

immunosuppressive therapy: Efficacy of hematopoietic stem cell transplantation',
Haematologica, 99(12), pp. 1868–1875. doi: 10.3324/haematol.2014.108977.
Kulasekararaj, A. G. *et al.* (2019) 'Somatic mutations identify a subgroup of aplastic anemia patients who progress to myelodysplastic syndrome', 124(17), pp. 2698–2705. doi: 10.1182/blood-2014-05-574889.A.G.K.
Li, W. *et al.* (2016) 'Thrombocytopenia in MDS : epidemiology , mechanisms , clinical consequences and novel therapeutic strategies', (November 2015), pp. 536–544. doi: 10.1038/leu.2015.297.
Libby, P. and Ebert, B. L. (2018) 'CHIP (Clonal Hematopoiesis of Indeterminate Potential)', *Circulation*, 138(7), pp. 666–668. doi: 10.1161/circulationaha.118.034392.
Locke, A. E. *et al.* (2015) 'Genetic studies of body mass index yield new insights for obesity biology', *Nature*, 518(7538), pp. 197–206. doi: 10.1038/nature14177.
Majumder, D. *et al.* (2006) 'Red cell morphology in leukemia, hypoplastic anemia and myelodysplastic syndrome', *Pathophysiology*, 13(4), pp. 217–225. doi: 10.1016/j.pathophys.2006.06.002.
Marisavljevic, D. *et al.* (2004) 'Myelofibrosis in Primary Myelodysplastic Syndromes', *Medical Oncology*, 21(4), pp. 325–331.
Montoro, J. *et al.* (2018) 'Autoimmune disorders are common in myelodysplastic syndrome patients and confer an adverse impact on outcomes', *Annals of Hematology*. Annals of Hematology, 97(8), pp. 1349–1356. doi: 10.1007/s00277-018-3302-0.
Moran-Crusio, K. *et al.* (2011) 'Tet2 Loss Leads to Increased Hematopoietic Stem Cell Self-Renewal and Myeloid Transformation', *Cancer Cell*. Elsevier Inc., 20(1), pp. 11–24. doi:

10.1016/j.ccr.2011.06.001.

Pfeilstocker, M. *et al.* (2016) 'Time-dependent changes in mortality and transformation risk in MDS', 128(7), pp. 902–911. doi: 10.1182/blood-2016-02-700054.The.

Polykratis, A. *et al.* (2014) 'Cutting Edge: RIPK1 Kinase Inactive Mice Are Viable and Protected from TNF-Induced Necroptosis In Vivo', *The Journal of Immunology*, 193(4), pp. 1539–1543. doi: 10.4049/jimmunol.1400590.

Qu, X. *et al.* (2018) 'TET2 deficiency leads to stem cell factor–dependent clonal expansion of dysfunctional erythroid progenitors', *Blood*, 132(22), pp. 2406–2417. doi: 10.1182/blood-2018-05-853291.

Rasmussen, K. D. *et al.* (2019) 'TET2 binding to enhancers facilitates transcription factor recruitment in hematopoietic cells', *Genome Research*, 29(4), pp. 564–575. doi: 10.1101/gr.239277.118.

Rauh, M. J. *et al.* (2017) 'Tet2 restrains inflammatory gene expression in macrophages', *Experimental Hematology*. Elsevier Inc., 55, pp. 56-70.e13. doi: 10.1016/j.exphem.2017.08.001.

Rioux, J. D. *et al.* (2007) 'Genome-wide association study identifies new susceptibility loci for Crohn disease and implicates autophagy in disease pathogenesis', *Nature Genetics*, 39(5), pp. 596–604. doi: 10.1038/ng2032.

Roden, D. M. *et al.* (2008) 'Development of a large-scale de-identified DNA biobank to enable personalized medicine.', *Clinical pharmacology and therapeutics*, 84(3), pp. 362–9. doi: 10.1038/clpt.2008.89.

Rusten, L. S. and Eirik, S. (1995) 'Tumor Necrosis Factor (TNF)-a Directly Inhibits Human Erythropoiesis In Vitro: Role', *Journal of Biological Chemistry*, 85(4), pp. 989–996.

749 Rusten LS, J. S. (1995) ‘Necrosis Factor (TNF)-alpha directly inhibits human erythropoiesis in
750 vitro: Role of p55 and p75 TNF Receptors’, *Blood*, 85(4), pp. 989–996.
751 Saleheen, D. *et al.* (2017) ‘Clonal Hematopoiesis and Risk of Atherosclerotic Cardiovascular
752 Disease’, *New England Journal of Medicine*, 377(2), pp. 111–121. doi: 10.1056/nejmoa1701719.
753 Salisbury-Ruf, C. T. *et al.* (2018) ‘Bid maintains mitochondrial cristae structure and function and
754 protects against cardiac disease in an integrative genomics study’, *eLife*, 7(Imm), pp. 1–36. doi:
755 10.7554/elife.40907.
756 Sallman, D. A. and List, A. (2019) ‘The central role of inflammatory signaling in the pathogenesis
757 of myelodysplastic syndromes’, 133(10), pp. 1039–1049. doi: 10.1182/blood-2018-10-844654.
758 Sano, S. *et al.* (2018) ‘Tet2-Mediated Clonal Hematopoiesis Accelerates Heart Failure Through a
759 Mechanism Involving the IL-1β/NLRP3 Inflammasome’, *Journal of the American College of*
760 *Cardiology*, 71(8), pp. 875–886. doi: 10.1016/j.jacc.2017.12.037.
761 Smatti, M. K. *et al.* (2018) ‘Epstein – Barr Virus Epidemiology , Serology , and Genetic Variability
762 of LMP-1 Oncogene Among Healthy Population : An Update’, 8(June). doi:
763 10.3389/fonc.2018.00211.
764 Straat, M. *et al.* (2015) ‘Extracellular Vesicles from Red Blood Cell Products Induce a Strong Pro-
765 Inflammatory Host Response, Dependent on Both Numbers and Storage Duration’, *Transfusion*
766 *Medicine and Hemotherapy*, 43(4), pp. 302–305. doi: 10.1159/000442681.
767 Tanyong, D. I. *et al.* (2015) ‘Effect of Tumor Necrosis Factor-Alpha on Erythropoietinand
768 Erythropoietin Receptor-Induced Erythroid Progenitor Cell Proliferation in β
769 Thalassemia/Hemoglobin E Patients’, *Turkish Journal of Hematology*, 32(4), pp. 304–310. doi:
770 10.4274/tjh.2014.0079.

771 Vlantis, K. *et al.* (2016) 'NEMO Prevents RIP Kinase 1-Mediated Epithelial Cell Death and Chronic
772 Intestinal Inflammation by Article NEMO Prevents RIP Kinase 1-Mediated Epithelial Cell Death
773 and Chronic Intestinal Inflammation by NF- k B-Dependent and -Independent Functions',
774 *Immunity*. The Authors, 44(3), pp. 553–567. doi: 10.1016/j.immuni.2016.02.020.
775 Waisbren, J. *et al.* (2017) 'Disease characteristics and prognosis of myelodysplastic syndrome
776 presenting with isolated thrombocytopenia', *International Journal of Hematology*. Springer
777 Japan, 105(1), pp. 44–51. doi: 10.1007/s12185-016-2081-4.
778 Weiss, G. and Goodnough, L. T. (2005) 'Anemia of Chronic Disease', *New England Journal of*
779 *Medicine*, 352(10), pp. 1011–1023. doi: 10.1056/NEJMra041809.
780 Wolach, O. and Stone, R. (2016) 'Autoimmunity and inflammation in myelodysplastic
781 syndromes', *Acta Haematologica*, 136(2), pp. 108–117. doi: 10.1159/000446062.
782 Yan, H. *et al.* (2017) 'Distinct roles for TET family proteins in regulating human erythropoiesis',
783 *Blood*, 129(14), pp. 2002–2012. doi: 10.1182/blood-2016-08-736587.
784 Yuan, J., Amin, P. and Ofengeim, D. (2019) 'Necroptosis and RIPK1-mediated
785 neuroinflammation in CNS diseases', *Nature Reviews Neuroscience*. Springer US, 20(January).
786 doi: 10.1038/s41583-018-0093-1.
787 Zhang, Q. *et al.* (2015) 'Tet2 is required to resolve inflammation by recruiting Hdac2 to
788 specifically repress IL-6', *Nature*, 525(7569), pp. 389–393. doi: 10.1038/nature15252.
789 Zinkel, S. S. *et al.* (2018) 'Increased Ripk1-mediated bone marrow necroptosis leads to
790 myelodysplasia and bone marrow failure in mice', *Blood*, 133(2), pp. 107–120. doi:
791 10.1182/blood-2018-05-847335.
792 Zou J, Shi Q, Chen H, Juskevicius R, Z. S. (2019) 'Programmed Necrosis is Upregulated in Low-

793 grade Myelodysplastic Syndromes and May Play a Role in the Pathogenesis', *Haematologica*, p.
794 In revision.
795

Figure 1

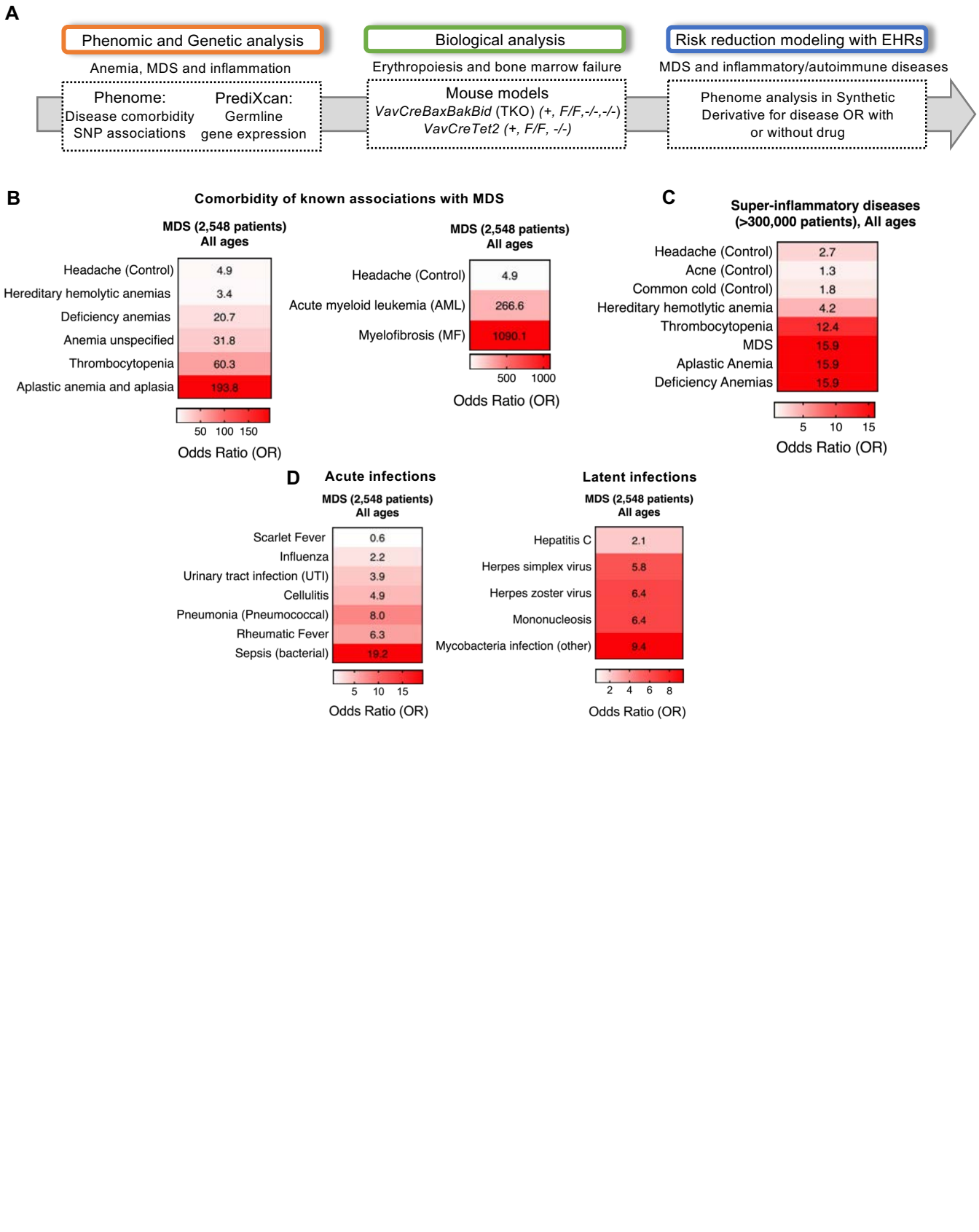
A
Phenomic and Genetic analysis
Anemia, MDS and inflammation
Phenome:
Disease comorbidity
SNP associations
PrediXcan:
Germline
gene expression
Biological analysis
Erythropoiesis and bone marrow failure
Mouse models
VavCreBaxBakBid (TKO) (+, F/F,-/-,-/-)
VavCreTet2 (+, F/F, -/-)
Risk reduction modeling with EHRs
MDS and inflammatory/autoimmune diseases
Phenome analysis in Synthetic Derivative for disease OR with or without drug
B
Comorbidity of known associations with MDS
MDS (2,548 patients)
All ages
Headache (Control) 4.9
Hereditary hemolytic anemias 3.4
Deficiency anemias 20.7
Anemia unspecified 31.8
Thrombocytopenia 60.3
Aplastic anemia and aplasia 193.8
50 100 150
Odds Ratio (OR)
MDS (2,548 patients)
All ages
Headache (Control) 4.9
Acute myeloid leukemia (AML) 266.6
Myelofibrosis (MF) 1090.1
500 1000
Odds Ratio (OR)
C
Super-inflammatory diseases
(>300,000 patients), All ages
Headache (Control) 2.7
Acne (Control) 1.3
Common cold (Control) 1.8
Hereditary hemotlytic anemia 4.2
Thrombocytopenia 12.4
MDS 15.9
Aplastic Anemia 15.9
Deficiency Anemias 15.9
5 10 15
Odds Ratio (OR)
D
Acute infections
MDS (2,548 patients)
All ages
Scarlet Fever 0.6
Influenza 2.2
Urinary tract infection (UTI) 3.9
Cellulitis 4.9
Pneumonia (Pneumococcal) 8.0
Rheumatic Fever 6.3
Sepsis (bacterial) 19.2
5 10 15
Odds Ratio (OR)
Latent infections
MDS (2,548 patients)
All ages
Hepatitis C 2.1
Herpes simplex virus 5.8
Herpes zoster virus 6.4
Mononucleosis 6.4
Mycobacteria infection (other) 9.4
2 4 6 8
Odds Ratio (OR)

Figure 2

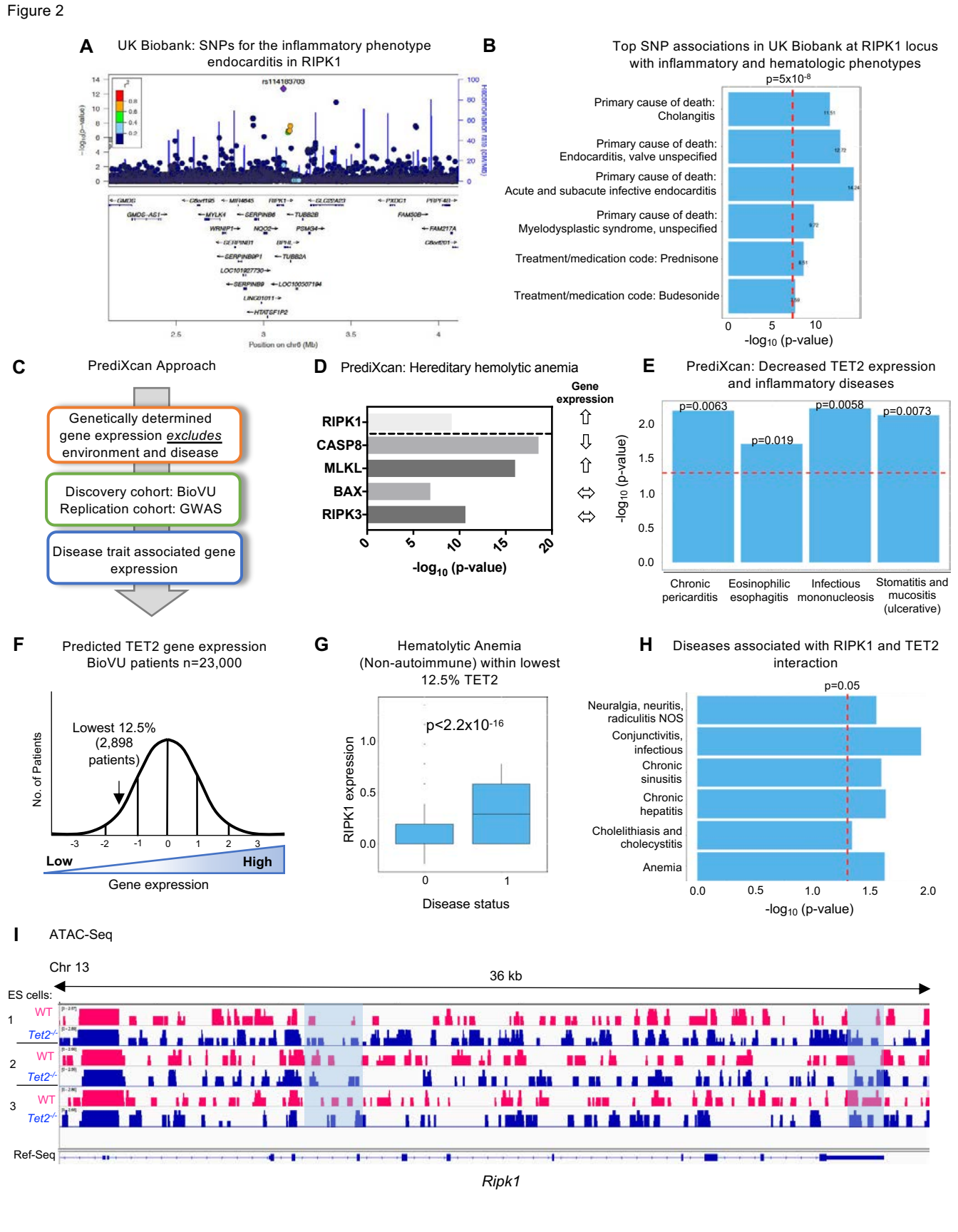
A
UK Biobank: SNPs for the inflammatory phenotype endocarditis in RIPK1
rs114183703
-log10(p-value)
Position on chr6 (Mb)
B
Top SNP associations in UK Biobank at RIPK1 locus with inflammatory and hematologic phenotypes
p=5x10-8
Primary cause of death: Cholangitis
Primary cause of death: Endocarditis, valve unspecified
Primary cause of death: Acute and subacute infective endocarditis
Primary cause of death: Myelodysplastic syndrome, unspecified
Treatment/medication code: Prednisone
Treatment/medication code: Budesonide
-log10 (p-value)
C
PrediXcan Approach
Genetically determined gene expression excludes environment and disease
Discovery cohort: BioVU Replication cohort: GWAS
Disease trait associated gene expression
D
PrediXcan: Hereditary hemolytic anemia
Gene expression
RIPK1
CASP8
MLKL
BAX
RIPK3
-log10 (p-value)
E
PrediXcan: Decreased TET2 expression and inflammatory diseases
p=0.0063
p=0.019
p=0.0058
p=0.0073
-log10 (p-value)
Chronic pericarditis
Eosinophilic esophagitis
Infectious mononucleosis
Stomatitis and mucositis (ulcerative)
F
Predicted TET2 gene expression BioVU patients n=23,000
Lowest 12.5% (2,898 patients)
No. of Patients
Low
High
Gene expression
G
Hematolytic Anemia (Non-autoimmune) within lowest 12.5% TET2
p<2.2x10-16
RIPK1 expression
Disease status
H
Diseases associated with RIPK1 and TET2 interaction
p=0.05
Neuralgia, neuritis, radiculitis NOS
Conjunctivitis, infectious
Chronic sinusitis
Chronic hepatitis
Cholelithiasis and cholecystitis
Anemia
-log10 (p-value)
I
ATAC-Seq
Chr 13
36 kb
ES cells:
1
2
3
WT
Tet2-/-
Ref-Seq
Ripk1

Supplementary Figure 1

A

Heme disorders and MDS	ICD9, ICD10 codes	Odds Ratio	95% CI (-/+)	SD Patients	Chi-squared	P-value
Myelodysplastic Syndrome (MDS)	238.72, 238.73, 238.74, 238.75, D46	NA	NA	2548	NA	NA
Headache (control)	784, G44	4.9	4.74-5.65	525	1111.1	1.30E-243
Hereditary hemolytic anemias	282, D56-58	3.4	2.40-4.94	30	48.408	3.46E-12
Deficiency anemias	281, D51-53,D55	20.7	18.36-23.71	270	4401.6	<1.0E-300
Anemia, unspecified	285.9, D64.9	31.8	25.72-46.04	1585	1337	1.05E-292
Thrombocytopenia	287.5, D69.6	60.3	56.74-66.39	1267	35599	<1.0E-300
Aplastic anemia and aplasia	284, D61	193.8	180.21-211.67	1451	107000	<1.0E-300
Acute myeloid leukemia (AML)	205.0-205.02, C92	266.6	245.54-291.23	984	129410	<1.0E-300
Myelofibrosis (MF)	289.83,238,76,D75.81	1090.1	937.1269-1269.27	417	164420	<1.0E-300

B

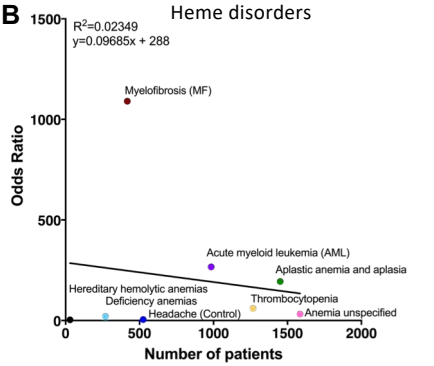

C

Super-inflammatory group	ICD9, ICD10 codes	SD Patients
Diabetes mellitus	250, E10,E11,E13	122840
Anemia, unspecified	285.9, D64.9	85572
Atherosclerosis	440, I70	28158
Multiple sclerosis	340, G35	8194
Psoriasis	696, L40.8,L40.9	3923
Rheumatoid arthritis	714.0, M06.9	16381
Crohn's disease	560.89, K50	7518
Ulcerative colitis	556, K51	8179
Asthma	493.9, J45	30439
Sarcoidosis	135, D86	2346
Myasthenia gravis	358.0, G70.0	934
Vasculitis	447.6, I77.6	2193
Autoimmune thyroiditis	245.2, E06.3	8653
Psoriatic arthritis	696.0, L40.52	2901
Systemic lupus	710.0, M32.9	5327

D

Heme disorders and Super-inflammatory group	ICD9, ICD10 codes	Odds Ratio	SD Patients	95% CI (-/+)	Chi-squared	P-value
Headache (control)	784, G44	2.7	29,797	2.81-2.89	19433	<1.0E-300
Acne (control)	706.1, L70	1.3	4,070	1.29-1.39	252.7	6.68E-57
Common cold (control)	460, J00	1.8	2,579	1.69-1.85	643.55	5.65E-142
Hereditary hemolytic anemia	282, D56-58	4.2	2,592	4.02-4.45	3658.4	<1.0E-300
Thrombocytopenia	287.5, D69.6	12.4	20,156	12.34-12.96	65612	<1.0E-300
MDS	238.72, 238.73, 238.74, 238.75, D46	15.9	1,862	14.61-17.40	6960.1	<1.0E-300
Aplastic Anemia and aplasia	284, D61	15.9	9,820	15.43-16.65	36353	<1.0E-300
Deficiency Anemias	281, D51-53,D55	15.9	7,551	15.24-16.62	28185	<1.0E-300

E

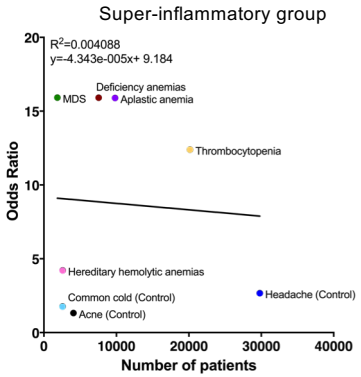

F

Infectious disease and MDS	ICD9, ICD10 codes	Odds Ratios	95% CI (-/+)	SD Patients	Chi-squared	P-value
Acute infections						
Scarlet Fever	34.1, A38.9	0.60	0.42-0.86	30	2.0912	7.4893
Influenza	487,488, J090-J11	2.2	1.81-2.71	98	61.194	5.17E-15
Urinary tract infection (UTI)	599, N39.0	3.9	1.46-3.00	513	877.03	9.68E-193
Cellulitis	682, L03.9	4.9	4.40-5.43	413		
Pneumonia (Pneumococcal)	481, 482, J13, J15	8.0	6.84-9.31	175	976.08	2.84E-214
Rheumatic Fever (bacteria)	390, 391, I00,I01,I05,I06,I07	6.3	5.00-8.01	69	290.95	3.08E-65
Sepsis (bacterial)	995.91, 995.92, A41	19.2	17.45-21.23	503	6805.3	<1.0E-300
Chronic/Latent infections						
Hepatitis C	070.54,070.7, B18.2	2.1	1.46-3.00	30	15.666	7.56E-05
Herpes simplex virus	054, B00.9	5.8	4.75-7.06	102	379.69	1.45E-84
Herpes zoster virus	53.9, B02.9	6.4	5.31-7.80	111	476.43	1.28E-105
Mononucleosis	75, B27.90	6.4	4.62-8.88	37	159.32	1.59E-36
Mycobacteria infection (other)	31, A31	9.4	6.02-14.61	20	138.49	2.2E-16

G

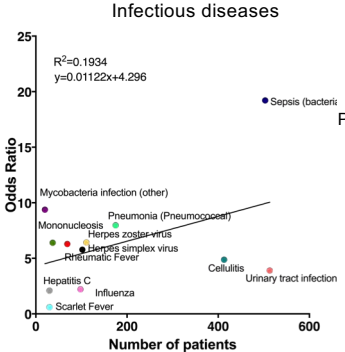

H

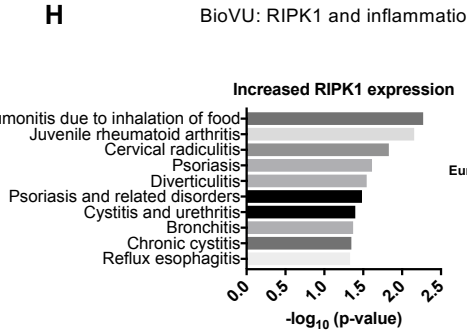

I

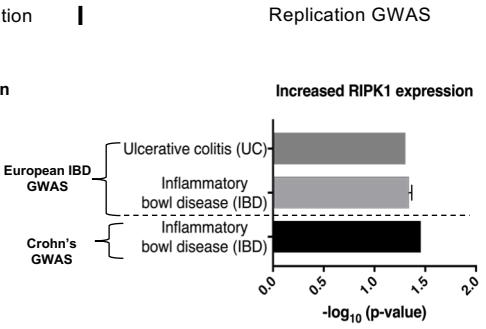

Figure 3

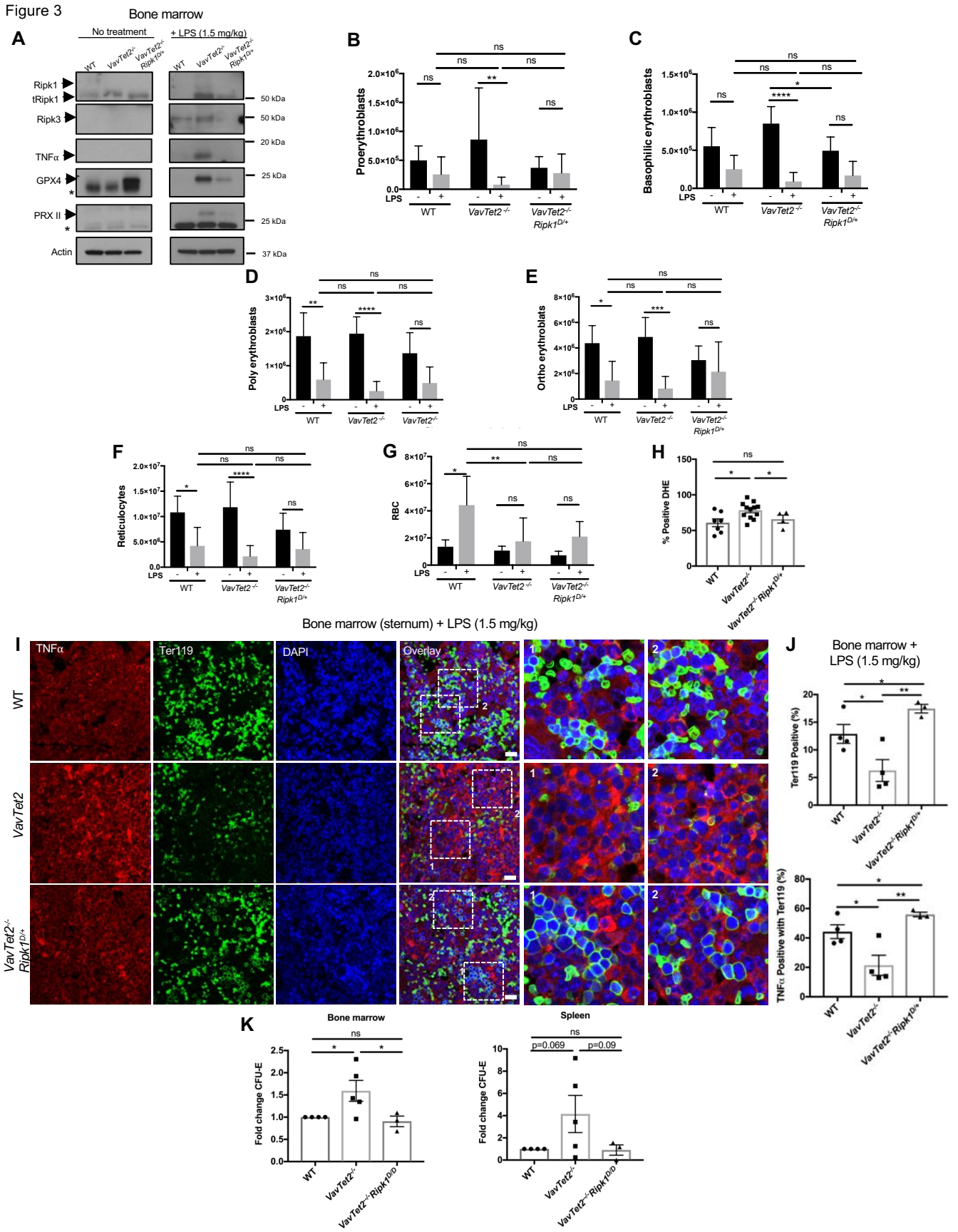
Bone marrow
A
No treatment
+ LPS (1.5 mg/kg)
WT
VavTet2-/-
VavTet2-/- Ripk1D/+
Ripk1
tRipk1
Ripk3
TNFα
GPX4
PRX II
Actin
50 kDa
50 kDa
20 kDa
25 kDa
25 kDa
37 kDa
B
Proerythroblasts
C
Basophilic erythroblasts
D
Poly erythroblasts
E
Ortho erythroblasts
F
Reticulocytes
G
RBC
H
% Positive DHE
LPS
ns
Bone marrow (sternum) + LPS (1.5 mg/kg)
I
TNFα
Ter119
DAPI
Overlay
VavTet2
VavTet2-/- Ripk1D/+
J
Bone marrow + LPS (1.5 mg/kg)
Ter119 Positive (%)
TNFα Positive with Ter119 (%)
K
Bone marrow
Spleen
Fold change CFU-E
p=0.069
p=0.09
VavTet2-/- Ripk1D/D

Supplemental Figure 2

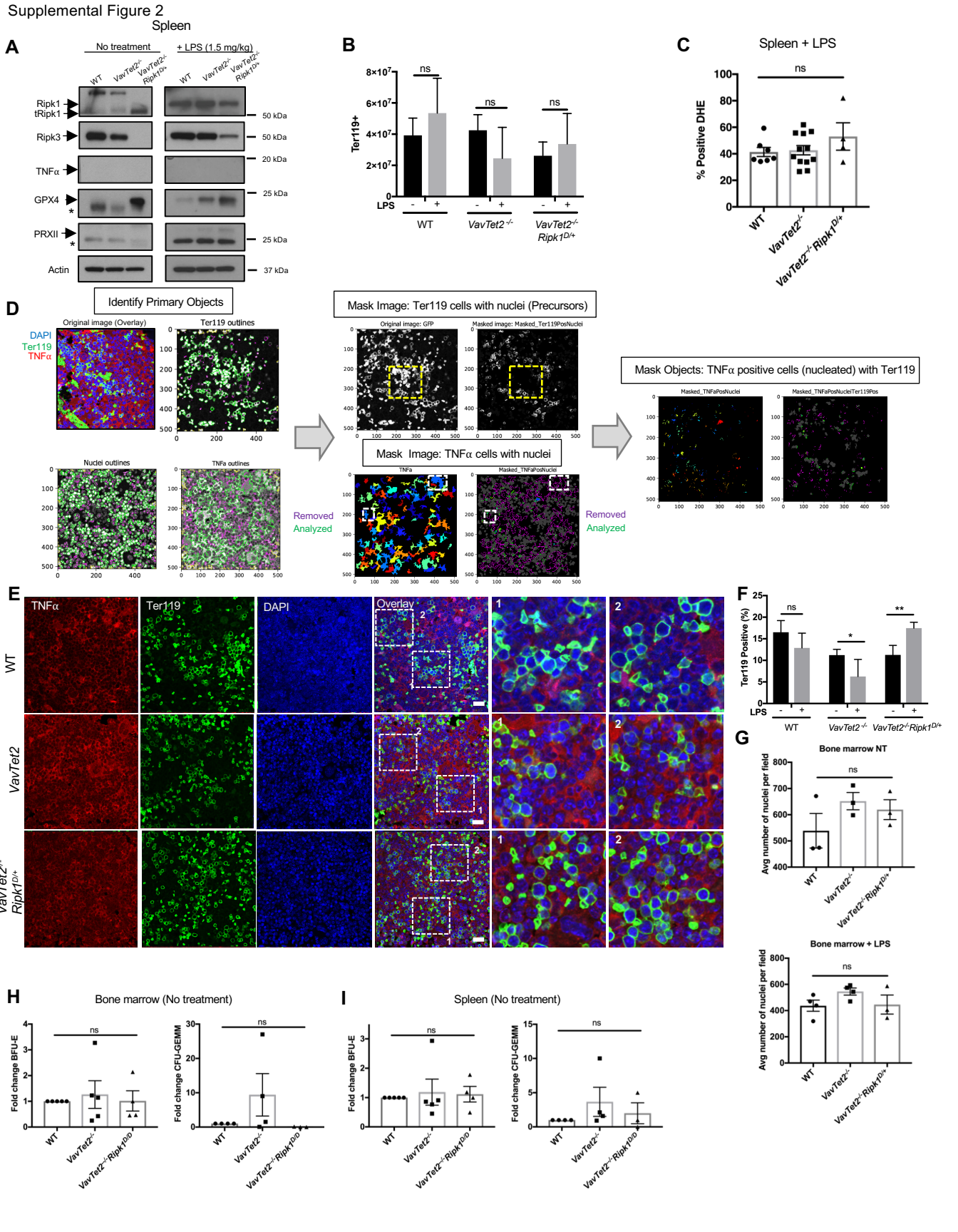

Figure 4

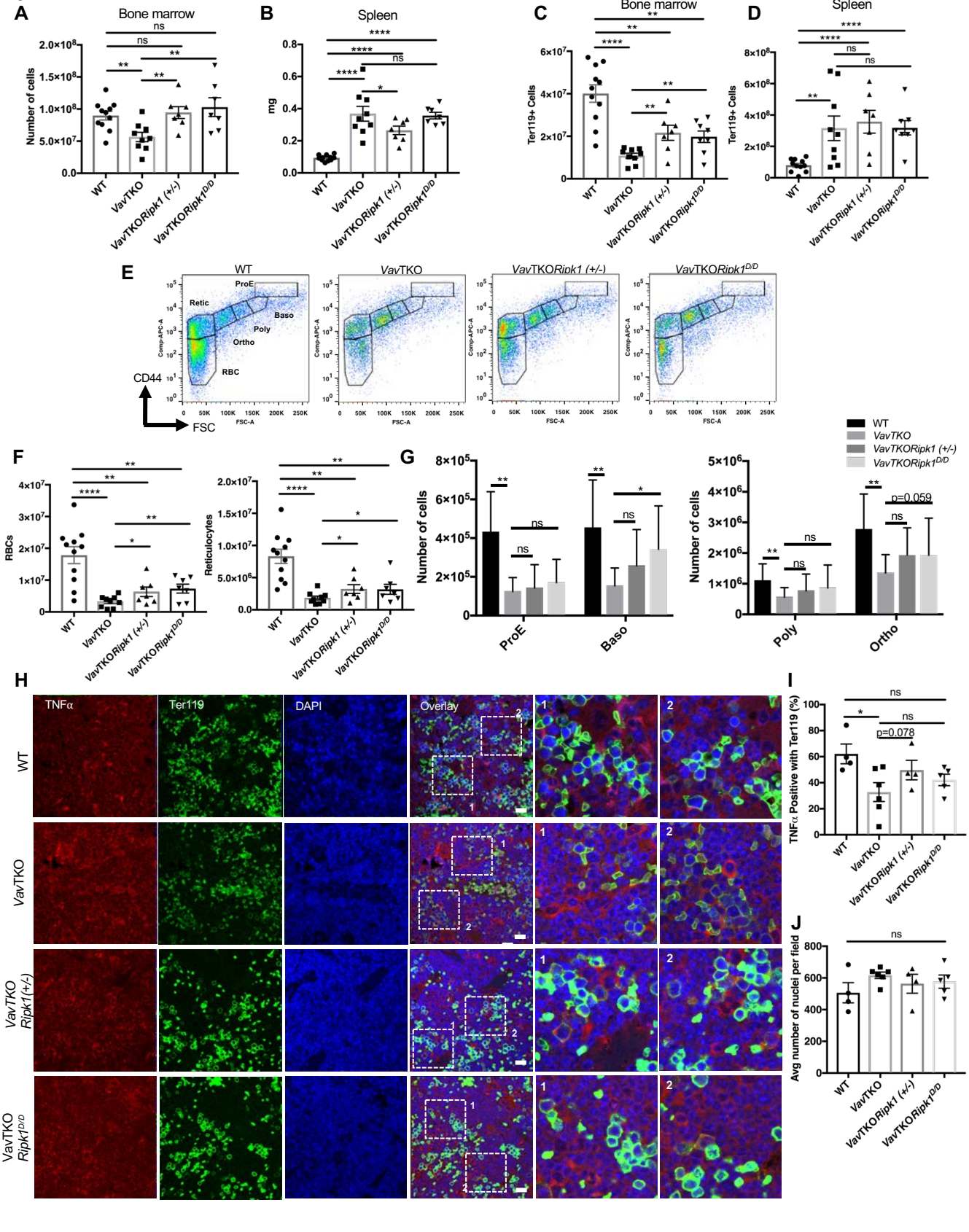
A
Bone marrow
Number of cells
WT
VavTKO
VavTKORipk1 (+/-)
VavTKORipk1D/D
B
Spleen
mg
C
Bone marrow
Ter119+ Cells
D
Spleen
Ter119+ Cells
E
WT
VavTKO
VavTKORipk1 (+/-)
VavTKORipk1D/D
ProE
Retic
Baso
Poly
Ortho
RBC
CD44
FSC
Comp-APC-A
FSC-A
F
RBCs
Reticulocytes
G
Number of cells
ProE
Baso
Poly
Ortho
p=0.059
H
TNFα
Ter119
DAPI
Overlay
VavTKO
VavTKO Ripk1(+/-)
VavTKO Ripk1D/D
I
TNFα Positive with Ter119 (%)
p=0.078
J
Avg number of nuclei per field
ns

Figure 5

A

Risk reduction model using EHRs

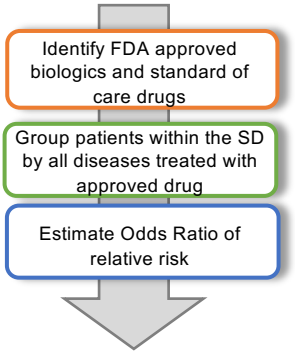

B

Group	Diseases	Drugs
1	Rheumatoid Arthritis (RA), Plaque Psoriasis, Psoriatic Arthritis, Ankylosing Spondylitis (AS)	Enbrel (Etanercept) or Methotrexate (Rheumatrex)
2	Psoriatic Arthritis, Rheumatoid Arthritis, Crohn's, Ulcerative Colitis, Ankylosing Spondylitis, Hidradenitis Suppurativa, Non-infectious Uveitis	Humira (Adalimumab)
3	Osteoarthritis, Rheumatoid Arthritis, Ankylosing Spondylitis	Celebrex (Celecoxib)
4	Rheumatoid Arthritis, Systemic lupus erythematosus, Psoriasis, Psoriatic arthritis, Multiple Sclerosis, Crohn's, vasculitis, sarcoidosis, Asthma, Myasthenia Gravis, autoimmune thyroiditis, Ulcerative colitis	Prednisone Ibuprofen Acetaminophen Naproxen

C

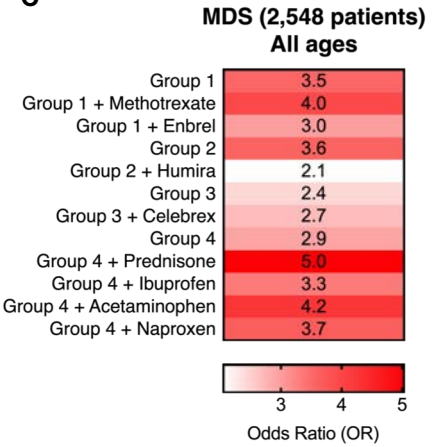

Supplementary Figure 3

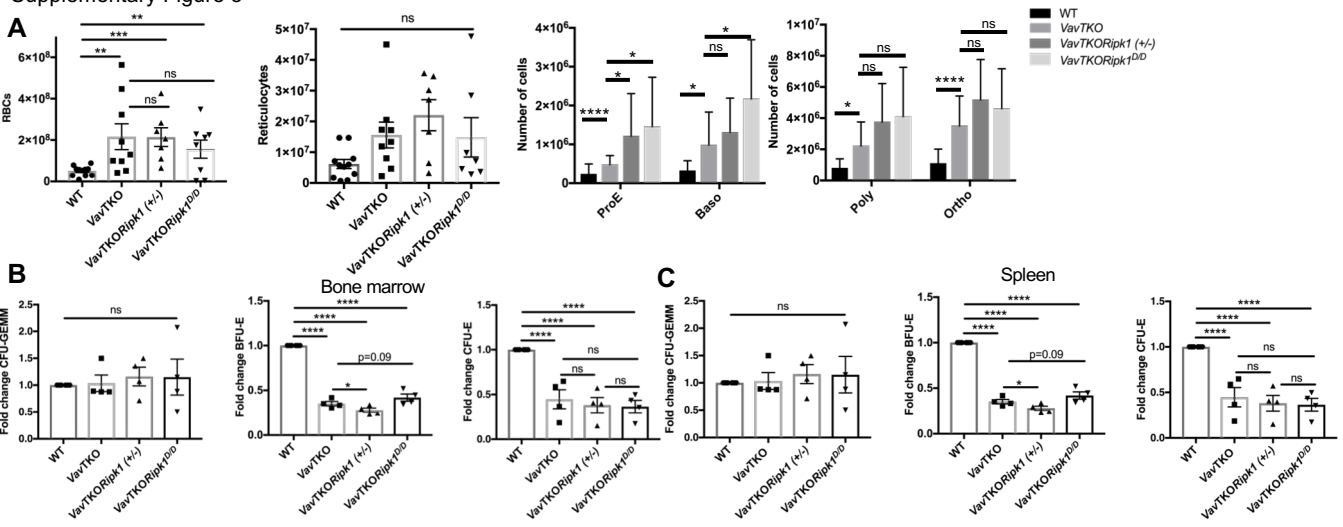

D

Diseases	ICD9, ICD10 codes
Rheumatoid Arthritis (RA)	714.0, M06.9
Plaque Psoriasis	696, L40.8,L40.9
Psoriatic arthritis	696.0, L40.52
Ankylosing Spondylitis (AS)	720, M45.X6-M45.X9
Crohn's disease	560.89, K50
Ulcerative Colitis	556, K51
Hidradenitis Suppurativa	705.93, L73.2
Non-infectious Uveitis	364, H20.043
Osteoarthritis	715.3, M19.9
Systemic lupus	710.0, M32.9
Multiple sclerosis	340, G35
Vasculitis	447.6, I77.6
Sarcoidosis	135, D86
Autoimmune thyroiditis	245.2, E06.3
Asthma	493.9, J45
Myasthenia gravis	358.0, G70.0

E

Group	Diseases	Drug	Odds Ratio	95% CI (-/+)	SD Patients	Chi-squared	P-value
1	Rheumatoid Arthritis (RA), Plaque Psoriasis, Psoriatic Arthritis, Ankylosing Spondylitis (AS)	None	3.5	3.90-5.51	112	190.18	2.90E-43
		Methotrexate (Rheumatrex)	4.0	2.97-4.58	42	87.782	7.31E-21
		Enbrel (Etanercept)	3.0	2.04-5.64	15	17.64	2.67E-05
2	Psoriatic Arthritis, Rheumatoid Arthritis, Crohn's, Ulcerative Colitis, Psoriatic arthritis, Ankylosing Spondylitis, Hidradenitis Suppurativa, Non-infectious Uveitis	None	3.6	4.28-5.73	151	258.16	4.32E-58
		Humira (Adalimumab)	2.1	1.43-3.83	16	7.52	0.0060907
3	Osteoarthritis, Rheumatoid Arthritis, Ankylosing Spondylitis	None	2.4	3.12-4.20	140	109.91	1.03E-25
		Celebrex (Celecoxib)	2.7	3.19-6.01	27	26.59	2.51E-07
4	Rheumatoid Arthritis, Systemic lupus erythematosus, Psoriasis, Psoriatic arthritis, Multiple Sclerosis, Crohn's, vasculitis, sarcoidosis, Asthma, Myasthenia Gravis, autoimmune thyroiditis, Ulcerative colitis	None	2.9	3.37-4.13	348	375.68	1.09E-83
		Prednisone	5.0	5.64-7.07	270	769.69	2.10E-169
		Ibuprofen	3.3	3.54-4.69	162	243.35	7.32E-55
		Acetaminophen	4.2	5.02-6.16	333	707.4	7.36E-156
		Naproxen	3.7	4.22-6.13	85	154.95	1.44E-35

F

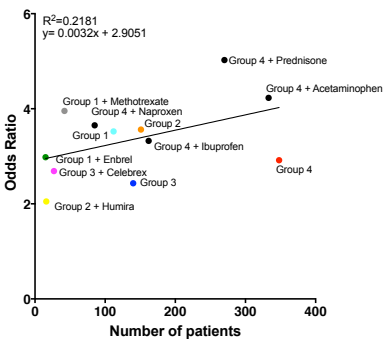

G

Drugs and MDS	Odds Ratio	95% CI (-/+)	SD Patients	Chi-squared	P-value
Methotrexate	11.4	10.20-12.79	352	2835.2	<1.0E-300
Enbrel	3.7	2.55-5.25	30	54.33	1.69E-13
Humira	2.5	1.73-3.55	30	24.53	7.32E-07
Celebrex	2.5	2.17-2.99	161	139.52	3.39E-32
Prednisone	7.8	7.26-8.48	1170	3745.90	<1.0E-300
Ibuprofen	1.4	1.28-1.54	631	54.23	1.78E-13
Acetaminophen	4.9	4.53-5.39	1846	1589.70	<1.0E-300
Naproxen	1.9	1.64-2.10	281	96.94	7.16E-23

H

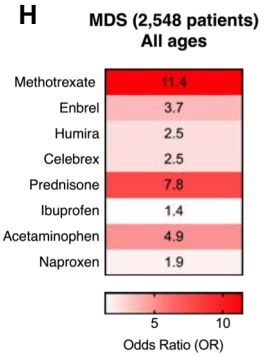

I

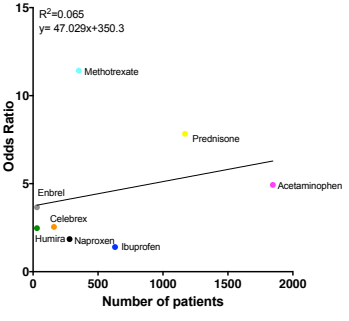

VANDERBILT UNIVERSITY
Center for Technology Transfer and Commercialization

Disclosure ID: IPD807093019
Technology ID: VU20042
Title: Targeting the necroptosis pathway in anemias and other hematologic disorders
Type: Invention Disclosure
Submitted By: Sandra Zinkel
Updated Date: 10/1/2019
Stage: Approved
Status: Active

Contacts

Primary Contact
Which inventor will be the PRIMARY contact between CTTC and the inventors?

Sandra Zinkel

CTTC Licensing Officer Contacted
If you have been in contact with a CTTC Licensing Officer regarding this Invention please select their name from the list below or select none.

Clarissa Muere

Invention Specifics

DETAILED Description (Required)
Provide a DETAILED description below of the Invention being disclosed. Attach any SUPPORTING DOCUMENTS such as a summary, PowerPoint, grant applications, draft manuscripts or abstracts to the documents field at the end of this form.

We have demonstrated, using multiple complimentary approaches, that the necroptosis pathway of programmed cell death is activated in hematopoietic disorders such as hereditary hemolytic anemia and the bone marrow failure disorder, Myelodysplastic syndrome (MDS). We first identified an association between inflammatory conditions and MDS and anemias by phenomic analysis of the synthetic derivative of BioVU. We identified increased necroptosis in hereditary hemolytic anemia using a PrediXcan analysis of BioVU. We further show an epistatic interaction between RIPK1 (a driver of necroptosis) and TET2 (a gene commonly mutated in clonal hematopoiesis, MDS, and myeloid leukemias) using phenomic and genetic analysis. We validate these findings in genetically modified mouse models in which TET2 is conditionally deleted and RIPK1 kinase activity or expression are conditionally deleted in hematopoiesis where we improve defects in erythropoiesis (red blood cell development) by inhibiting RIPK1.
See attached document for further details.

Practical Application
Briefly describe any uses of the Invention or problems this Invention overcomes. List the most likely potential products or applications.

The approach- using phenomic analysis, in combination with gene level (prediXcan) analysis allows identificatino of important gene pathways associated with disease. In addition, by broadly querying the phenome, common pathophysiologic features between diseases can be revealed. Finally, using mouse models, we validate associations, and important first step in demonstrating feasibility of targeting signaling pathways in disease.

New or Novel Elements
List any elements of the Invention that you believe to be unique state of the art.

The integrative approach of electronic health record queries and mouse model validation is unique and state of the art. Vanderbilt has one of the largest Biobanks linked to eletronic health records.

Level of Development
Describe the current developmental stage of the Invention e.g. proof of concept, experiments completed, benchtop development, preliminary results obtained, in-vivo/in-vitro data...

We have completed our first study (manuscript has been supplied) and are now moving toward pharmacologic inhibition of inflammatory pathways (TNF, IL1) as well as necroptosis (RIPK1) in mouse models.

Plans for Ongoing Development
List any experiments/development work that will be performed in the next 6-12 months.

We are planning to complete the inhibition studies in the next 6-12 months

Potential Licensees
List any companies you believe are interested in the Invention.

Glaxosmithkline (GSK) is developing RIPK1 inhibitors for use in autoimmune diseases and may have an interest in expanding into anemias.
Abbvie has developed Humira, a TNF inhibitor for autoimmune disease and may have an interest in expanding into anemias (the patent for Humira will expire in the near future).

Comparable Technology Approaches
List any current competitive or compatible technologies/works/products available, and describe the advantages of this Invention over those.

To our knowledge, we are the only group undertaking this integrative approach. Our approach has an advantage over the more widely used GWAS approach in that we have increased power to detect signaling pathways, and we can move beyond simple associations by probing mechanism in mouse models.

Publishing/Public Disclosure

Relevant Publications
List any literature or information that you are aware of that is similar to this invention e.g. submitted manuscripts/posters either from your lab or other places.

We are planning submission of a manuscript.
We described the finding that RIPK1 is increased in MDS by immunofluorescence in a publication (that contains no genetic data).
Wagner et al. Blood 133: 107-120 (2019)., and a poster at ASH (Zou et al., 2018)
We described the mouse findings but not the therapeutic implications in an oral abstract at the CSHL cell death meeting in August

Inventor Publications (Required)
Has this Invention been described in either a publication or verbally to Non-Vanderbilt Individuals?

No

Public Disclosure Details
Select the "Add Row" button at right to add each disclosure. List where, when and how you disclosed or plan to disclose your Invention (e.g. abstract, poster, publication, presentation, website, Power Point, etc.) Attach any of these files that contain the disclosure to the documents field at the end of this form.

Where	When (date critical)	How
Journal of Experimental Medicine	Tuesday	Journal article submission

Funding

Funding Information (Required) *
All federal agencies and most others require complete funding information to be compliant. All funding used as full or partial support during any stage of the research resulting in THIS invention OR if you plan to acknowledge a funding source in a publication or grant progress report in which you describe this invention, should be listed below.

Federal

Y

Federal Funding

Funding Source	Grant/Contract/Award Numbers/IDs
NHLBI- NIH	R01 HL133559
DOD-CDMRP bone marrow failure	W81XWH-16-1-0057
VA MERIT AWARD	I01BX002250

Foundation

N

Industry

N

Internal

N

Other

N

State

N

None

N

Compliance

Third Party Material (Required)
Was any material, equipment , software code, or content provided by a third party?

Yes

Third Party Material Details
Provide details about the material or equipment and its source (contact and location).

TET2 conditional KO mouse OMar Abdel-Wahab MSKCC - no MTA signed, collaboration
RIPK kinase inactive mouse Michelle Kelliher University of Massachusetts- no MTA signed, collaboration
GSK- RIPK1 conditional knockout mouse, RIPK1 inhibitor- MTA signed

Third Party MTA Signed
Was a material transfer agreement signed?

Yes

Export Control (Required)
Does the research or project involve information, technology, software, source code, hardware or other materials that have export control sensitivity?

Example

- **Pathogenic biological materials including bacteria, virus or fungus, reverse genetics systems encoding viruses, toxin, or a protein or DNA encoding one of these materials**
- **Chemicals that could be used to cause or protect against chemical warfare, including precursors for toxic chemical agents and medical countermeasures to protect against defense-related chemical or biological agents**
- **Sensors and lasers**
- **Navigation, avionics and flight controls**
- **Telecommunication, cryptography, encryption software**
- **Spacecraft systems, satellites and radar**
- **Defense weaponry, vehicles or explosives**
- **Military software and electronics**

List is not all inclusive. Contact Vanderbilt Export Compliance (vec@vanderbilt.edu) or VUMC Export Compliance (vumc.export@vumc.org), as applicable, if you are unsure or require assistance. For a link to representative lists go to https://www.vanderbilt.edu/exportcompliance/controlled_tech.

No

Inventors

Documents

Remarks

Inventors

First Name	MI	Last Name	Contribution
Sandra		Zinkel	50.00 %
Eric	R	Gamazon	50.00 %

Documents

File Name	Created By	Date Created
Salisbury-Ruf_Fig. S3.tiff	Sandra Zinkel	10/1/2019
Salisbury-Ruf_Fig. S2.tiff	Sandra Zinkel	10/1/2019
Salisbury-Ruf_Fig.5.tiff	Sandra Zinkel	10/1/2019
Salisbury-Ruf_Fig.4.tiff	Sandra Zinkel	10/1/2019
Salisbury-Ruf_Fig.3.tiff	Sandra Zinkel	10/1/2019
Salisbury-Ruf_Fig.2.tiff	Sandra Zinkel	10/1/2019
Salisbury-Ruf_Fig.1.tiff	Sandra Zinkel	10/1/2019
anemia manuscript draft v7.gamazoncsrrefssz.v7-6-3 copyb copy copy-2.docx	Sandra Zinkel	10/1/2019
Salisbury-Ruf_Fig. S1.tiff	Sandra Zinkel	10/1/2019

To be signed by Vanderbilt contributors only.
For good and valuable consideration, as set forth in the Policy on Technology and Literary and Artistic Works in the Vanderbilt University Faculty Manual or, as applicable, the Policy on Technology and Literary and Artistic Works in the Vanderbilt University Medical Center Employment Manual, as such policies may be amended from time to time, the sufficiency and adequacy of which are hereby acknowledged, I agree to assign and hereby do assign, sell, and transfer unto VANDERBILT UNIVERSITY, whose post-office address is 305 Kirkland Hall, 2201 West End Ave., Nashville, TN 37240, U.S.A., my entire right, title and interest in and to any invention(s), software, creative work(s), or material(s) disclosed herein and related thereto, including but not limited to any associated intellectual property rights. I hereby agree to execute without further consideration any and all applications, petitions, oaths and assignments or other papers and instruments which may be necessary in order to carry into full force and effect, the sale, assignment, transfer and conveyance hereby made or intended to be made. I hereby agree that no assignment, sale, agreement or encumbrance has been or will be made or entered into which would conflict with this assignment. I further represent that to the best of my knowledge, the information provided herein and in the body of this Disclosure, is true and accurate, and I agree to promptly disclose to the Center for Technology Transfer and Commercialization any updated or new information relating to the disclosed technology hereunder.
I have read and reviewed the information contained in the Disclosure Form and this Assignment of Rights and agree that all information, including contributor information and royalty sharing allocation, is acceptable and accurate to the best of my knowledge.

Sandra Zinkel (Lead Inventor 50.00 %) Date

Eric R Gamazon (Co-Inventor 50.00 %) Date